FABRICATION OF NANOPARTICLE AND PROTEIN NANOSTRUCTURES USING NANOIMPRINT LITHOGRAPHY

This research has been financially supported by the Council for Chemical Sciences of the Netherlands Organization for Scientific Research (NWO-CW) in the Vernieuwingsimpuls programme (Vidi grant 700.52.423). The research was carried out at the Supramolecular Chemistry and Technology & Molecular Nanofabrication groups, MESA$^+$ Institute for Nanotechnology, University of Twente.

Publisher: Print Partners Ipskamp, Postbus 333, 7500 AH Enschede, the Netherlands,

http://www.ppi.nl

University of Twente, Enschede, The Netherlands.

ISBN: 90-9021448-8

FABRICATION OF NANOPARTICLE AND PROTEIN NANOSTRUCTURES USING NANOIMPRINT LITHOGRAPHY

PROEFSCHRIFT

ter verkrijging van
de graad van doctor aan de Universiteit Twente,
op gezag van de rector magnificus,
prof. dr. W. H. M. Zijm,
volgens besluit van het College voor Promoties
in het openbaar te verdedigen
op vrijdag 26 januari 2007 om 13.15 uur

door

Pascale Anne Maury

geboren op 18 maart 1976
te Marmande, Frankrijk

Dit proefschrift is goedgekeurd door:

Promotoren: prof. dr. ir. J. Huskens
prof. dr. ir. D. N. Reinhoudt

Citation

To my parenst

Contents

Chapter 1

General Introduction

The traditional disciplines of physics, chemistry, and biology look at the properties of molecules or materials from different perspectives, while nanotechnology combines these fields. Nanotechnology is the art and science of manipulating matter at the nanoscale or even at the atomic or molecular level.[1] One of the primary objectives of nanotechnology is to study the properties of single objects such as biomolecules[2,3] and nanoparticles.[4] At the nano level, materials show amazing properties compared to the bulk as witnessed by various analytical techniques applied in the nanosciences. The techniques of nanofabrication comprehend top-down and bottom-up approaches. In the top-down approach, a bulk material is patterned laterally while in the bottom-up approach, molecules or particles self-assemble on a surface.

The research presented in this thesis was focused on the combination of top-down and bottom-up techniques in order to create high-resolution structures. Nanoimprint lithography has been used as the top-down technique because of its high resolution, high throughput, and low cost. The formation of self-assembled monolayers (SAMs) was used as a bottom-up approach because of its versatility with respect to the end-groups that can be used and their relatively simple modification. Objects such as nanoparticles, layer-by-layer assemblies and proteins have been anchored to SAMs.

Electrostatic as well as supramolecular interactions have been investigated. The advantages of supramolecular interactions are the control of the binding strength, the specificity, and the reversibility of the attachment allowing the regeneration of the substrate.

Chapter 2 is a review of different combinations of top-down and bottom-up techniques. It describes how top-down techniques can be used to confine bottom-up assemblies to a pattern. Application of top-down and bottom-up techniques to create functional devices is also reviewed. The devices treated in this chapter, 3D photonic crystals and protein assays, may lead to applications based on experiments that are described in this thesis.

In Chapter 3, the use of nanoimprint lithography as a method to pattern SAMs on silicon oxide with high resolution is described. Two types of templates have been investigated: (i) topographical templates with chemical functionalization and (ii) chemically patterned, topographically flat substrates. Both types of substrate were tested for the directed assembly of nanoparticles using electrostatic interactions.

Chapter 4 deals with the use of vertical deposition, or meniscus method, in order to attach nanoparticles with high order. Nanoparticles were attached on topographical templates with a chemical functionalization and on chemically patterned substrates using a vertical deposition apparatus. Attachment of nanoparticles was performed on patterns of various sizes and shapes. The confinement of the nanoparticles was characterized using scanning electron microscopy (SEM).

In Chapter 5, the patterning of β-cyclodextrin (CD) host monolayers on silicon oxide is described. The characterization was performed by atomic force microscopy and X-ray photoelectron spectroscopy. The patterned host monolayer was used to attach molecules functionalized with a guest functionality using supramolecular interactions.

Both topographical, with a cyclodextrin functionalization, and chemical templates were fabricated for attachment of molecules.

Chapter 6 presents the patterning of supramolecular layer-by-layer assemblies. Topographical templates with patterned CD layers were used as a host for directing the supramolecular layer-by-layer assembly of guest-functionalized dendrimers and CD-functionalized nanoparticles. Two types of layer-by-layer assemblies were patterned consisting of 2.8 nm CD-functionalized Au nanoparticles and 60 nm silica CD-functionalized nanoparticles. For the latter, vertical deposition was used to attach the silica nanoparticles with dense packing. The polymer template was removed by lift-off to reveal the LBL pattern. Layer-by-layer assemblies were patterned down to 50 nm lateral size.

In Chapter 7, the patterning of proteins using electrostatic and NiNTA-histidine interactions is shown. Proteins were directed onto topographical templates with chemical functionalization and on chemically patterned templates. NTA attachment and patterning were characterized with various techniques. These tagged-proteins were attached onto the NTA patterns. One of the advantages of using NiNTA-histidine interactions is that the proteins can be released from the substrate leading to regeneration of the substrate. Successive protein attachment on the same substrate, after regeneration, has been studied.

1.1 References

[1] Ozin, G. A.; Manners, I.; Fournier-Bidoz, S.; Arsenault, A. *Adv. Mater.* **2005**, *171* 3001.
[2] Pellegrino, T.; Kudera, S.; Liedl, T.;Javier, A. M.; Manna, L.; Parak, W. J. *Small*, **2005**, *1*, 48.
[3] Klefenz, H. *Eng. Life Sci.* **2004,** *4*, 211.
[4] Antonietti, M.; Ozin, G. A. *Chem. Eur. J.* **2004**, *10*, 29.

Chapter 2

Combinations of Top-Down and Bottom-Up Nanofabrication Techniques and Their Application to Create Functional Devices

2.1 Introduction

Lithography techniques are used to create patterns on substrates. Thanks to lithography, a wide variety of devices can be made. Nanotechnology requires lithography techniques with improved resolution down to the sub-100 nm scale. In microelectronics, lithography techniques have improved over time in such a way that the transistor density of integrated circuits doubles every 1.5 years, following what is called Moore's law. On the other hand, in a new trend of microelectronic applications, integration of components that classically have not been integrated, instead of miniaturizations is of key importance. These types of devices are comprised in what is called "more than Moore" applications and include, for instance, sensing, actuating and processing for wireless device applications.

Two approaches exist for the creation of structures: (i) the top-down approach, where a bulk material is directly patterned using irradiation or molding,[1] and (ii) the bottom-up techniques using self-assembly of molecules or compounds on a surface. The top-down approach is currently used in microelectronics while the bottom- up approach has been developed in chemistry and biology. The main top-down and bottom-up techniques that are used in nanofabrication will be presented in section 2.2. Since the emphasis lies here on the combined methodologies, these descriptions will only be brief. Mixed techniques that make use of a combination of both approaches will constitute the core of this chapter. First, confining a bottom-up assembly in a pattern created by a top-down technique will be shown as a strategy to obtain high-resolution features. Then examples of devices created by the combination of top-down and bottom-up techniques will be shown. Photonic devices fabricated by the patterned assembly of particles and biological assays formed by controlling the protein position will be demonstrated, as they are also topics described in other chapters of this thesis.

2.2 Top-down and bottom-up techniques

2.2.1 Top-down techniques

Decreasingly smaller patterns are created by photolithography following Moore's law. The latest microelectronic production equipment has a resolution of 45 nm with a throughput of around 130 (300 mm diameter) wafers per hour and development of 32 nm resolution equipment is on the way. In addition to high resolution, other important parameters for silicon technologies are overlay and ability of multistep and multilayer patterning, needed to create integrated circuits.

2.2.1.1 Patterning a polymer template

Lithography techniques based on patterning a polymer spin-coated on a substrate are presented first. The resulting polymer template is used as a mask to transfer the pattern onto the substrate, by additive techniques such as lift-off or by subtractive techniques such as etching or by modifying the substrate properties by ion implantation or diffusion.

Photolithography makes use of a light-sensitive resist that is exposed with a light source through a mask applied on the substrate. After development, the irradiated photoresist is removed when using a positive tone resist, or the non-irradiated photoresist is removed when a negative tone resist is used. The resolution (d) is related to the wavelength (λ) by $d = k_1 l / NA$ (Rayleigh criterion), where NA is the numerical aperture of the projection lens system and k_1 the process factor that depends on the process. Photolithography is a parallel technique with high throughput that allows overlay for multistep processes. A limitation at high resolution is the proximity effect that consists of degradation of the shape of the pattern features because of the unintentional exposure of the resist in high density patterns. This effect can be reduced by using resolution enhancement techniques that consist of compensating the effect by modifying the mask design.

The concept of photolithography is used with some changes in order to achieve a higher resolution. In a technique called immersion lithography, a liquid is used between the lens and the substrate in order to reduce the NA and increase the depth of focus. In this way, a resolution down to 45 nm is obtained with production class equipment. Another technique to obtain higher resolution than photolithography makes use of extreme ultra- violet (EUV) radiation.[2] Smaller features can be obtained by using shorter wavelengths.

Features down to 32 nm have been obtained with this method. This technique has not yet reached production level and one of the challenges is the low power of the EUV sources and the need of vacuum chambers.

In Laser Interference Lithography (LIL) or holographic lithography, the photoresist is irradiated directly by a laser beam without using a mask. The pattern is given by an interference pattern created by splitting and recombining a laser beam. The advantage of this technique is that high resolution can be obtained on large areas. Resolution is on the order of 100 nm. The disadvantage is that the pattern choice is limited to periodic patterns obtained by interference.

Electron Beam Lithography (EBL) makes use of an electron beam to expose an electron sensitive resist. The resist is usually a polymer, the molecules of which are broken or cross-linked upon electron irradiation. The resolution of EBL goes down to 1 nm. The throughput of this technique is relatively low because of its serial nature. In industry EBL is used, for instance, for the fabrication of masks for photolithography.

Nanoimprint Lithography (NIL) is a nanofabrication technique which employs physical deformation of a polymer film by using a hard stamp. Chou discovered NIL in 1995 obtaining for the first time sub-micron features (25 nm) on poly(methylmethacrylate) (PMMA) polymer films using a SiO_2 stamp.[3] NIL has had a growing success in research laboratories for its simplicity and lowcost.[4] Its application requires only a press with heating capability. Stamps are elaborated by traditional lithography techniques (photolithography or EBL lithography, followed by RIE). Stamps can be made of silicon, silica, metal or glass.

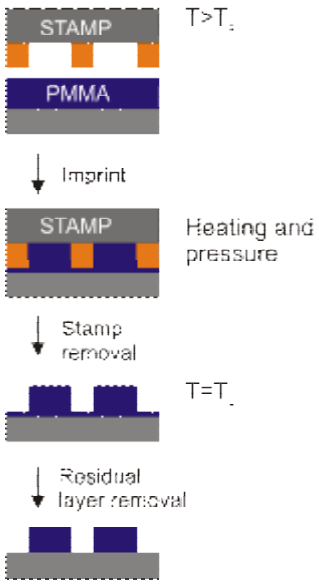

Scheme 1. *The nanoimprint lithography process.*

The sample to be patterned is composed of a substrate covered with a uniform polymer thin film. The stamp is applied on the sample and both are placed in the press. The temperature is increased and pressure is applied for a certain time (Scheme 1). Then the pressure is released and the sample is cooled down to below the glass transition temperature of the polymer. At that point stamp and imprint are separated. UV-NIL and step-and-flash lithography have been developed because of the need for overlay. In that case, a transparent mold is used to pattern a monomer which is polymerized after irradiation.

2.2.1.2 Direct patterning

Nanostencil lithography can be used to produce patterns by means of a shadow mask and the evaporation of material in a vacuum.[5] The method consists of placing a mask between a source and a substrate, the evaporated material being deposited only in the non-shadowed area as can be seen in Scheme 2. It is a one-step technique because a lift-off step is not necessary. The advantages of this method can be summarized as follows: a) it can be used on fragile substrates (like sol-gels, hydrogels, biological macromolecules and organometallic molecules) because it does not need chemical or thermal treatment; b) it can be used *in situ* for high-vacuum experiments; c) it allows patterning on non-flat substrates such as microelectromechanical systems (MEMS) and atomic force microscopy (AFM) cantilevers.

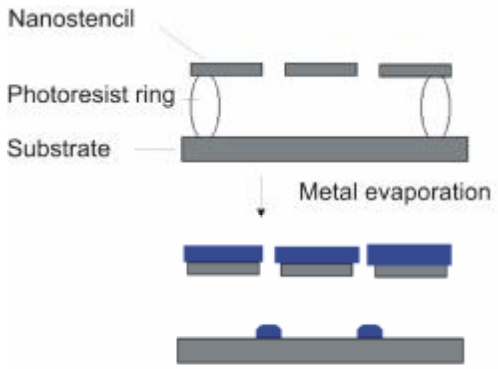

***Scheme 2**. Shadow mask evaporation using a nanostencil. The nanostencil behaves as a mask for patterning a metal on a substrate.*

Focused ion beam (FIB) lithography consists of direct writing with an ion beam on a substrate such as Si.[6,7] Direct writing on silicon is possible because ions are able to etch silicon. The resolution limit of the method is about 20 nm. It is a low throughput technique because the features are written or milled directly by the ion beam. It is used mainly in industry for mask repair and sample preparation for characterization.

2.2.2 Bottom-up techniques

Self-assembly is the spontaneous organization of molecules or objects into stable, well-defined structures by non-covalent forces. The final structure is close to or at thermodynamic equilibrium; it therefore tends to form spontaneously and to self-repair defects. Bottom-up nanofabrication makes use of self-assembly of components to create structures on the nanometer scale. The advantage of bottom-up techniques is the straightforward application of the associated self-assembly processes such as immersion, drop-casting, spin-coating, dip-coating, etc. It also allows large area processing but the choice of patterns is limited to periodic structures with homogeneous sizes.

A self-assembled monolayer (SAM) is an ordered molecular assembly that is formed spontaneously by adsorption of a surfactant with a specific affinity of its headgroup to the surface. It consists of a two-dimensional film, one molecule thick, covalently organized or non covalently assembled at an interface. Molecules used to form SAMs have an anchoring part that attaches to the substrate, an alkyl chain and a functional end-group. These molecules have the property to self-assemble on the surface with high order. The most widely used types of SAMs are thiols on Au and silanes on SiO_2 surfaces. SAMs can be used to anchor functional components or as etch barriers.

Block-copolymers consist of molecules containing two polymer chains of different nature. The chains have the property to rearrange in order to form spheres, cylinders (orthogonal or parallel), and lamellae spontaneously after heating. The ability to rearrange is controlled by the nature and the length of the two polymer chains and can be tuned easily.[8] These blocks can be either periodic, alternating or random.[9]

The advantage of using block-copolymers is that the range of feature sizes that can be created is between 1 and 100 nm, making them particularly interesting for high-resolution patterning.[10] In order to transfer the patterns to the substrate, one of the polymer chains can be modified to behave as an etch barrier.[11]

Colloidal lithography consists of using nanoparticles arranged in a hexagonal fashion on a substrate. The highly ordered colloidal arrangement is usually obtained using immersion in a suspension or procedures based on capillary forces exerted on the nanoparticles.[4, 16] The nanoparticles patterns are then used as a mask for lift-off or etching. The inter-nanoparticle distance dictates the resolution of the pattern that is related to the size of the nanoparticles. A resolution of 50 nm has been obtained.[12]

Layer-by-layer (LBL) assembly consists of building up multilayered films by alternatingly depositing components held together owing to attractive forces such as electrostatic interactions (Scheme 3).[13] The advantage of this technique is that the height of the LBL assemblies is accurately controlled by the total number of deposited layers. Moreover, LBL assembly allows to create composite films by applying layers with different properties. The properties of the LBL assembly can be modified by changing pH and ionic strength, for instance.

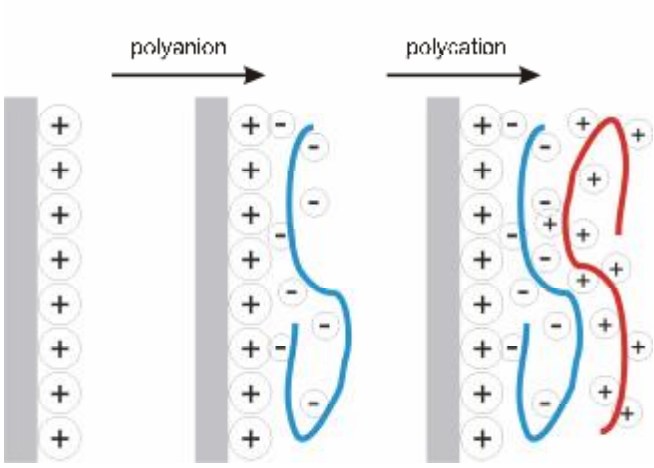

Scheme 3. *Representation of layer-by-layer assembly.*

2.2.3 Mixed techniques

Many research groups do not have access to cleanroom facilities and many university cleanrooms lack lithographic equipment capable of high-resolution patterning. Therefore, several alternative and low cost methods have been developed that give access to high resolution patterning while keeping the research interests in mind, i.e. with a focus on versatility and fundamental science rather than mass-scale production. Additionally, there are special applications where alternative lithography techniques are more efficient or the only possibility.

Microcontact printing (μCP) consists of depositing an ink that forms a SAM on a substrate with the help of a soft stamp by simple contact.[14] It is a direct patterning method that permits working on non-flat surfaces. As the deposited ink molecules are highly ordered, they allow controlling the surface chemistry of substrates, and they can be used to form resist masks for etching. Using this technique, surfaces can be functionalized with small molecules (thiols on gold), precursors (catalyst, functionalized polymers) as well as biological molecules (proteins, DNA, spacers).[15] An advantage of μCP is that it is possible to print on flexible substrates. The resolution is limited by the size of the stamp features, the stability of the flexible stamp structures and ink diffusion. The usual feature sizes produced by μCP are on the micrometer scale, but sub-micrometer features, down to about 100 nm, have been created by using fine-tuned processes.[16]

Printing with PDMS stamps is not limited to thiol inks. The low surface energy of PDMS stamps, which makes them inert towards chemical and metallic compounds, allows the printing of elements such as metals, e.g. Au, or molecules used for LBL assembly. After the application of the stamp to the substrate, only the material in contact with the substrate is transferred, creating a pattern (Scheme 4).

This application, known as nanotransfer printing (nTP), is important for processes where solvents need to be avoided.[17] For example, in nanoelectronics, nTP of Au was used to create Au pads on a material that would be damaged by the usual Au lift-off technique normally used to create electrodes.

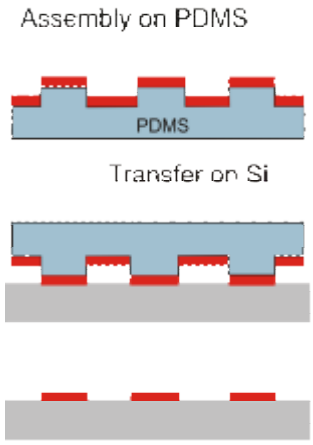

Scheme 4. *Representation of nanotransfer printing.*

Dip-pen nanolithography (DPN) is a direct-write lithographic technique that uses an AFM to build a pattern on the substrate material.[18] The tip is inked with molecules, and then used to write on the substrate. The resolution is related to the size of the AFM tip and to the diffusion of the molecule used as an ink, typically down to 40 nm.[19]

2.3 Combining top-down and bottom-up techniques for high-resolution patterning

In recent years, there has been an increasing number of reports on techniques to pattern bottom-up assemblies based on the use of physical or chemical patterns produced by means of top-down techniques. In the physical patterning techniques, topographical patterns are created on Si or polymer substrates using top-down lithography techniques such as photolithography or EBL (Scheme 5 A). The pattern defines the lateral resolution and provides the confinement needed to obtain the desired structures and ordering. In addition, the polymer pattern acts as a mask to prevent unwanted adsorption. After lift-off of the polymer mask the pattern is revealed. The disadvantage of this technique is that the solvent needed to remove the polymer during the lift-off step may induce disorder into the attached nanostructures.

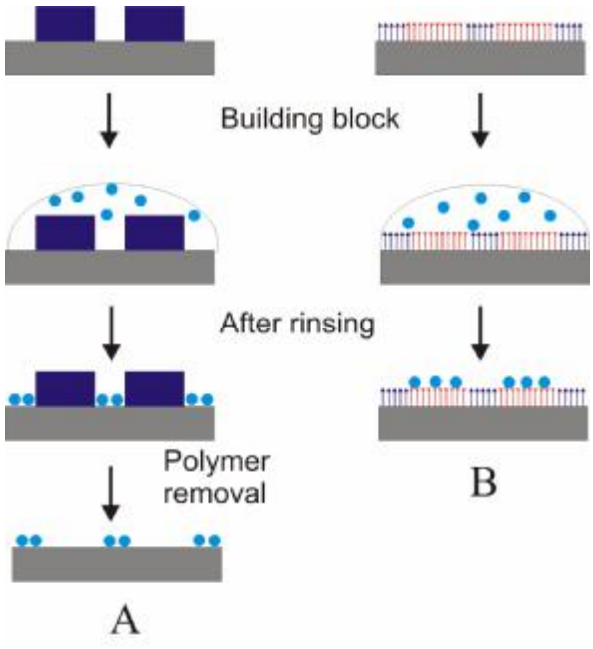

Scheme 5. *Utilization of topographical (A) and chemical templates (B) to pattern building blocks.*

On the other hand, chemical patterning consists of using substrates having regions of different properties or composition. Examples of chemical patterns include molecular patterns of dissimilar nature, such as SAMs with different functionalities, alternating charges on the substrate surface, and metallic patterns on Si (Scheme 5 B). The functionalization can lead to differences in wettability, hydrophobicity, charge, or surface composition (e.g. Si/Au). A usual way of creating chemical patterns is to use mixed techniques such as μCP or DPN. Patterning methods for SAMs on Au[16] or SiO_2[20] have been reviewed elsewhere. The elements to be patterned attach selectively to one component of the pattern. The advantage of this approach is that the lift-off step is avoided because the compound is deposited directly on the pattern and adsorbs only on the desired areas, without further processing steps. The disadvantage is the risk of non-specific adsorption due to the lack of physical barriers and reduced ordering due to the absence of physical confinement.

Another way to create a pattern is to use irradiation, e.g. photolithography after the bottom-up assembly of components such as block-copolymer,[21,22] NPs,[23,24] and LBL assembly.[25] The irradiated part is removed in solvent. The use of topographical and chemical patterns for the confinement of bottom-up assembly in order to increase the pattern resolution is treated in this section. Confinement of surface-initiated polymerization, micelles, block-copolymers, nanoparticles (NPs) and LBL assemblies will be introduced.

2.3.1 Top-down nanofabrication and polymerization

Surface-initiated polymerization is a technique that makes use of a surface initiator to graft polymers. When the surface initiator is patterned, polymerization is induced locally on the predefined sites. This technique can be used to amplify a pattern. The advantage is that the thickness and polymer graft density can be controlled, in contrast to other methods to produce grafted polymers.

Surface initiators can be selectively attached on chemical patterns created by μCP,[26-29] irradiation,[30] by metal evaporation by nanoshaving.[31, 32] The polymer is grown from the surface initiator by immersion in a monomer solution. The polymer brushes that have been used are polystyrene (PS), other olefins, and caprolactone. The typical height obtained after polymerization varied from 6 to 30 nm, which is high enough to be useful as a pattern enhancement technique. Additionally, polymers can be patterned at high resolution by coating an AFM tip with monomers. An applied voltage polymerizes the monomers, and polymer lines down to 30 nm in width have been created in this way.[33] STM tips can also be used to control chain polymerization.[34, 35] Zauscher studied the formation of long polymer sizes up to 200 nm. Under the same conditions as for the micrometer features, a smaller height of 170 nm was measured for sub-micrometer features. They explained this lower height by considering the effective initiator surface density and chain crowding. Polymerization occurred vertically and also laterally on the Au features, and appears to be anisotropic (lateral 220 nm/ vertical 250 nm). In an experiment inspired by the molecular ruler, which is treated in Section 2.3.5, the controlled lateral growth of polymer brushes was used as a way to reduce the interfeature distance on a polymer substrate. The measured (isotropic) height increase of 15 nm on the polymer structure caused the reduction of the interfeature distance to 30 nm.[36]

2.3.2 Top-down nanofabrication and micelles

A beautiful integration of top-down and bottom-up techniques using micelles has been shown by Spatz.[37, 38] EBL and attachment of 7 nm Au clusters loaded in 300 nm micelles was combined in this approach towards ultrahigh resolution. Micelles are spherical aggregates formed dynamically from surfactants. Au NPs were homogeneously confined in the polymer pattern because the micelles behave as spacers controlling the spatial orientation and avoiding aggregation of the Au NPs. Oxygen plasma etching was performed to remove the micelle envelopes after polymer lift-off. Single Au clusters of 7 nm with a periodicity of 2 μm as well as 60 nm lines were obtained, see Figure 1.

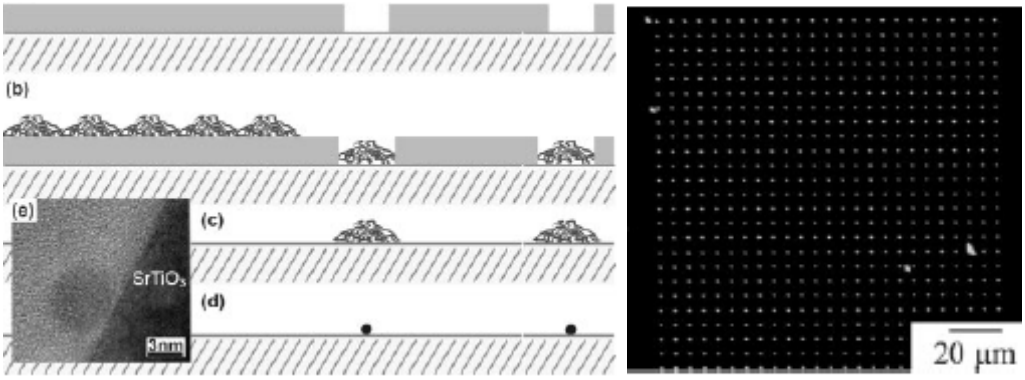

Figure 1. *(a) Scheme showing Au clusters inserted in 300 nm micelles deposited on a polymer pattern created using EBL. Polymer was removed afterwards. (b)Dark-field microscopy image of the Au clusters after deposition, removal of the polymer template and removal of micelles by O_2 plasma. (Courtesy of J. Spatz et al)*[38]

2.3.3 Top-down nanofabrication and block-copolymer assembly

When non-patterned, block-copolymers have no preferred orientation and films formed from them contain defects in their arrangement on large areas. Confinement in a physical pattern directs the orientation of the block-copolymers and diminishes the defects in self-assembly by introducing geometric substrate anisotropy. Additionally, this technique allows integrating block-copolymers in device applications.

As a first example of this technique, 1D designs or lines will be discussed.[39] PS-*b*-poly(ethylenepropylene) (PEP) block-copolymers, the chosen material, forms hexagonally packed cylinders in bulk (L = 23 nm, p = 26.6 nm, where L is the diameter of the cylinder and p its period). When the block-copolymer is spin-coated into grooves made in Si, PS chains wetted the sidewalls preferentially and aligned along them, forming cylinders. The linewidth and the periodicity were controlled by the size of the chains of the block-copolymer. The usual range of the chains is between 10 and 50 nm with a filling factor of 50 %. The width of the grooves determined the number of lines, while the edge roughness of the sidewalls influenced the rectilinearity of the adjacent PS cylinders as they closely followed the geometry of the edges. Lines in the middle of the pattern were not influenced. Defect-free areas were larger than on non-confined block-copolymers and corresponded to regions of about 100 μm^2. The thickness of the spin-coated film determined the number of layers. For a thickness smaller than one cylinder, no patterning was obtained. For a thickness corresponding to three layers, a multilayer of ordered cylinders was obtained.

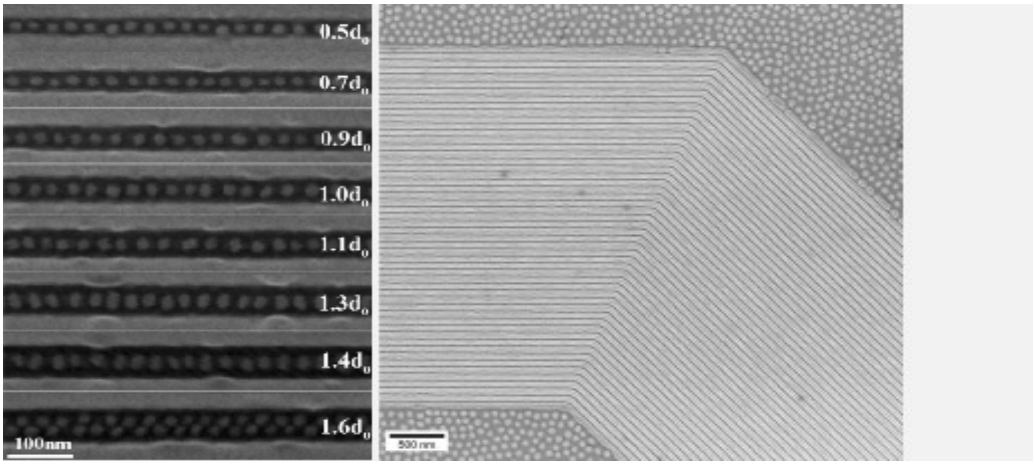

Figure 2. *(a) Spherical block-copolymer assembly confined in a physical template consisting of lines (Courtesy of C. Ross et al.)*[40] *and (b) cylindrical block-copolymer assembly on a chemical pattern consisting of lines. (Courtesy of P. Nealey et al.)*[41]

In a second example, 2D designs such as dots were targeted.[40] In this case 2D PS-*block*-polyferrocenyldimethylsilane (PFS) block-copolymers with a spherical morphology were used. Polymer patterns were made using EBL on hydrogen silsesquioxane (HSQ) resist. PS wets the sidewalls and after curing the PFS phase arranged as spheres. The spheres aligned inside the grooves in a hexagonal configuration. In this example two degrees of freedom are involved, which caused the assemblies to have more defects than the cylinders of PS-*b*-PEP. Similar to 1D patterning, edge roughness influenced the homogeneity and arrangement on the adjacent spheres. Domains in the middle of the templates were not influenced by edge roughness. Nevertheless, block-copolymers could be confined successfully in a cavity formed by walls at a 60º angle and the dots were aligned according to this angle. Confinement of a single line of spheres of block-copolymers (of a diameter d) was obtained when the line width (W) was narrowed (Figure 2a).[42]

For $W/d < 1$, spheres were elongated parallel to the sidewalls in order to fit inside the line while for $W/d > 1$, they are elongated perpendicular to them. For $W/d > 1.5$, two lines of spheres were obtained in a zigzag configuration. Two layers of spheres were also prepared with block-copolymers. The phases of the block-copolymers are deformable in contrast to the rigid colloids or metallic nanoparticles. Block-copolymers adapt their configuration to the shape of the confining features following the roughness of the sidewalls or assuming elongated shapes if necessary. The attractiveness of this approach is the homogeneity of the obtained high resolution structures, the usual range being 10 to 50 nm. In contrast, this high-resolution and homogeneity can be difficult to obtain with NPs because of their polydispersity at this scale. A new and interesting approach has been developed by Huck who uses NIL to pattern block-copolymers.[43] In this method, patterning and annealing (assembly) are performed simultaneously. The mold features provided the physical confinement that allowed the block-copolymers to rearrange following the borders of the sidewalls while being annealed at the same time. At the end of the process, the mold was removed. It is important to note that the resulting patterned block-copolymer structures that consist of substrate areas covered with polymer and others free of polymer can be used directly as a resist. Even though the results are still preliminary, the concept seems very promising.

In addition to physical templates, chemical patterns have also been used to align and orient lamellar domains of symmetric PS-*b*-PMMA block-copolymer films perpendicularly to the surface.[44, 45] For monodomain ordering, the chemical pattern needs to have the same dimensions as the block-copolymer patterns which are on the 50 nm scale.

EBL or EUVL were used to create a polymer pattern that was used as a mask for SAM formation in order to create chemical patterns, e.g. OTS/SiO_2[45] or PS brush/SiO_2.[41,46] The aim was to create a hydrophobic/hydrophilic pattern that is wetted preferentially by one of the chains of the block-copolymer. PMMA wets SiO_2 and PS wets OTS or PS brush. L_s represents the periodicity of the chemical pattern and L_o the lamellar period of the block-copolymer. When $L_s = L_o$, defect-free lines were obtained because each part of the block-copolymer is commensurate to the corresponding chemical area (e.g. L_s = 47.5 nm, L_o = 48 nm). For $L_s < L_o$, (L_s = 45 nm, L_o = 48 nm), dislocations appeared and for $L_s > L_o$, (L_s = 50 nm, L_o = 48 nm) lamellae were undulated and tilted out of plane. The thickness appeared to be important as well. Above a certain thickness (60 nm), lamellae went out of plane with a tilt angle q, for which $\cos q = L_o/L_s$.[47] In order to increase the range of defect-free areas, a significant improvement was made by increasing the contrast in interfacial energy or wetting behavior between adjacent chemically patterned regions.[48] Defect-free areas were obtained for 40 nm < L_s < 52.5 nm. Owing to this improved process, continuous patterns of non-regular structures could be created with angles from 30 to 135° (Figure 2b).[41]

2.3.4 Top-down nanofabrication and NP assembly

Interesting effects can be observed when creating NP patterns depending on the relation between particle size and the pattern feature size, shape of the confining features and type of confinement. Unlike block-copolymers, nanoparticles can be confined on any shape of pattern. When using topographical templates, capillary forces play an important role in the ordering process especially with respect to pattern design and the continuity of the features.

In a striking example, Xia used templates made of Si (photolithography and RIE) to confine particles inside the patterns by means of the meniscus method.[49,50] In the meniscus method, capillary forces push the particles inside the pattern. Xia studied the different configurations obtained with particles confined in holes of various shapes such as circles, squares, rectangles (lines), triangles, and rings. Expressions for the geometrical requirements in order to obtain a given cluster configuration taking into account the diameter of the particle *d*, and the dimension of the pattern, a hole diameter *D* or width of a line *w* were deducted and explained the observed results (Figure 3). Moreover, zigzag confinement in helicoidal shape was shown by using V grooves.[50]

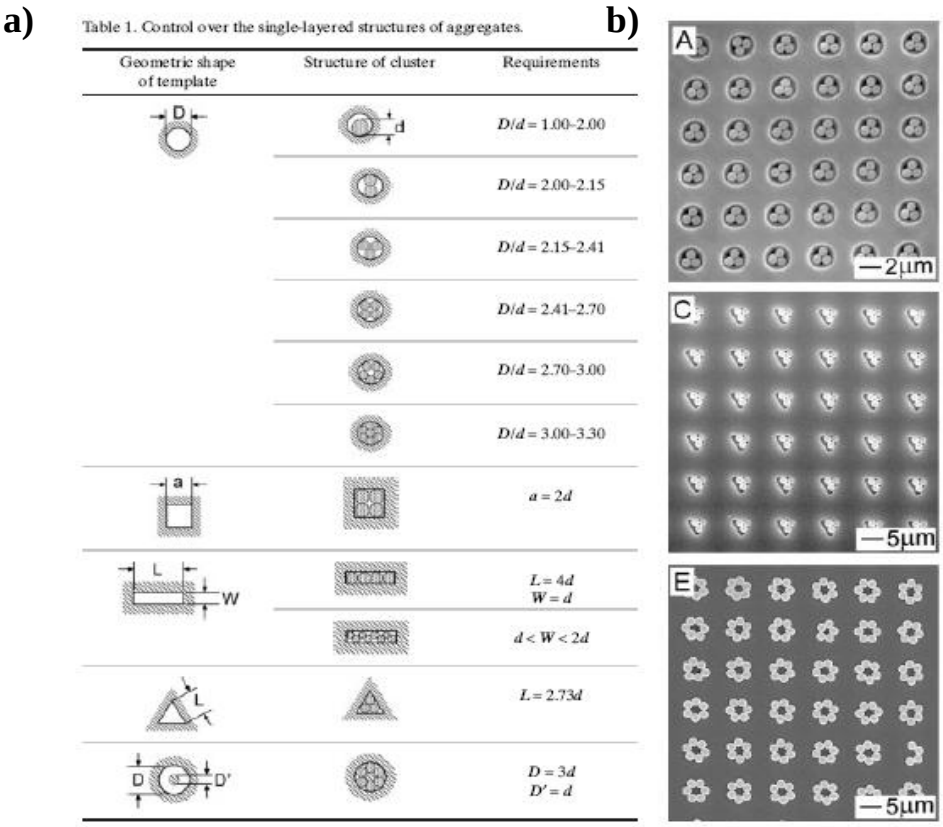

Figure 3. *(a) Library of the different geometric configurations that particles can take when confined in a physical template of the same range of dimensions as their diameter. (b) SEM images of PS particles confined in silicon holes of different diameters. (Courtesy of Y. Xia et al)* [49,50]

Kumacheva studied nanoparticles confined in micrometer grooves in which, by tuning the width of the grooves, perfect ordering or defect zones were seen, showing the importance of the *d/W* ratio on ordering.[51, 52] Two states of the arrays of particles could be distinguished: highly ordered hexagonal packing and random dense packing corresponding to the configuration where NPs have too much free space inside the pattern. It was predicted that hexagonal packing of NPs could be obtained when the width of the grooves (D_c) and the radius of the NPs used (R) was given by the expression: $D_c = 2R[(n-1)\cos 30^\circ+1]$.

Following these examples, intense research efforts were devoted to confine NPs in nanopatterns on SiO_2 using different patterning techniques such as FIB[53] and EBL,[54] and on other substrates.[55-57] Ozin made use of microfluidics to pattern particles inside V grooves closed by a PDMS flat stamp.[58] Colloids were patterned in diverse, non-regular and non-rectilinear, patterns.[54] Kim showed one-dimensional groove patterns with single particle attachment in the shape of a necklace.[50] At the nanometer scale, Alivisatos noticed that particles smaller than 8 nm could not be physically confined.[54]

After using a topographical pattern for confining particles, the physical barrier can be removed. Xia demonstrated confinement on the sub-200 nm scale by spin-coating NPs into polymer grooves made by LIL.[1] The polymer pattern was removed afterwards. Capillary forces pushed NPs inside the grooves, but confining particles in closed patterns such as holes was not so efficient. Using the same process, Koo demonstrated the confinement of 8 and 20 nm NPs in a polymer pattern created by EBL.[59] In both cases, NPs were annealed in order to improve their attachment to the substrate and to remove the polymer. Alternatively, to avoid this harsh process, a chemical functionalization can be made on the non-covered areas of the substrate to anchor NPs with the appropriate functionalization (Chapter 4).

Pattern confinement has been used to control lattice and superlattice symmetry by modeling the periodicity (*p)* and height (*h)* of the pattern. This technique is called colloidal epitaxy. Van Blaaderen was the first to demonstrate epitaxial assembly of NPs using topographically patterned square arrays of holes, creating a 2D square microarray.[60] The directing pattern is underneath and the size of the features is smaller than the NPs in order to direct their ordering.[52,61-63] Kim showed that for *h/D* (*D* being the diameter of the colloid) > 0.35, mulitlayer square array patterns were obtained.[50] For 0.28 < *h/D* < 0.35, pseudo-{110} structures are obtained and for *h/D* < 0.28 no 3D crystallization was observed, but tetragonal or hexagonal clusters.

Manipulation of individual NPs to create a pattern has also been demonstrated. Van Blaaderen made use of optical tweezers in order to arrange particles one by one in the desired shape.[64-66] With the use of a nanorobot,[67] Lopez constructed a multilayer of particles with a diamond-type structure on a patterned silicon substrate that directed the lattice formation.

Chemical templates can be used to pattern particles usually composed of polymer (PS or PMMA), SiO_2, or magnetic material.[68] The generally functionalized particles are attached selectively to one area of the pattern. One of the advantages of this process is that the substrate is not modified topographically and can be used after particle attachment for further processing. The most popular chemical pattern for NP attachment is a hydrophobic/hydrophilic contrast made in SAMs patterned by e.g. photolithography [69, 70] or μCP.[71, 72] NP suspensions do not wet the hydrophobic areas and NPs remain on the hydrophilic areas. Various shapes, periodic and non-periodic, have been made using NPs commensurate to the chemical pattern.[73] Jonas and Koumoto studied the effect of chemical confinement while using the meniscus method.[73,74]

The attachment of the particles was governed by wetting properties and the shape of the meniscus. The discontinuity of the wetting properties at the interface on the chemical pattern made well- defined edges difficult to obtain. Moreover, the shape of the meniscus, that was higher on the center of the pattern than on the edges, led to the formation of a multilayer in the center.[75] Ordered single particle attachment along a continuous line was obtained by Koumoto using a chemical pattern made by a liquid mold and its drying process.[73] These studies were made on the micrometer scale. The process of attachment on chemical templates is more sensitive to wetting than on physical templates because attachment occurs along the meniscus (the meniscus needs to be homogeneous across the sample in order for the method to produce homogeneous linewidths).

Another popular technique for patterning NPs consists of making chemical patterns with positively/negatively charged and positively/uncharged areas by using patterned SAMs,[63,71] LBL of polyelectrolytes,[76] and xenography.[77] Charged particles, usually negatively charged by means of carboxylate functionalization, are used. This method presents the advantage that the negatively charged NPs slightly repel each other, which avoids particle aggregation and improves ordering. The NPs are attached using the meniscus method or immersion. Various geometries have been obtained and NPs attach with high selectivity and commensurate to the appropriate chemical pattern. NPs can be patterned with hexagonal packing, except on the edges of the pattern.

Confinement in clusters where the NPs need to take a certain configuration are more difficult to obtain with chemical patterns than with physical patterns because of the lack of a physical confinement effect that would add capillary forces. Nevertheless, confinement has been shown in 1D and 2D on the micrometer scale.

The quality of the features was comparable to the one obtained with physical confinement. Particles were shown to attach with a zigzag configuration[72, 73, 78] or on a single line.[79]

Confinement in 2D features is more difficult to obtain than in 1D as reported in several papers[71,79-81]. It should be noted that most of these studies deal with electrostatic attachment. Hammond produced confined clusters of NPs with shapes similar to the ones obtained with physical confinement with the difference that the *D/d* value is slightly higher for the chemical pattern.[76, 81] This is due to the fact that for chemical patterns, particles can adsorb on patterns smaller than their size because it is the contact area of the colloids that needs to fit the pattern (see Figure 4, case *D/d* < 1.0). In contrast, in the case of physical patterns, the whole NP has to fit inside the pattern in order to be attached.

a)

Colloidal cluster		*D/d* (Theoretical)	*D/d* (Experimental)
monomer		< 1.0	0.43 (0.36–0.50)
dimer		1.00–1.15	1.02 (0.89–1.17)
trimer		1.15–1.41	1.36 (1.21–1.54)
regular quatramer		1.41–1.70	1.71 (1.48–1.95)
regular pentamer		1.70–2.00	2.05 (1.78–2.34)
regular hexagomer	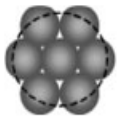	2.00–2.30	2.39 (2.09–2.72)

b)

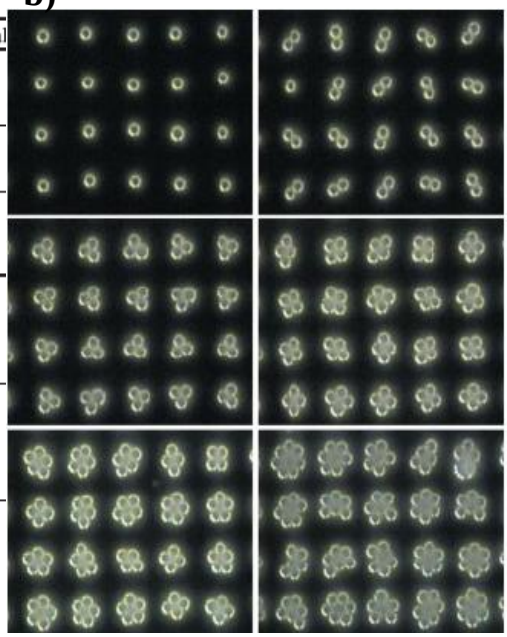

Figure 4. *(a) Library of the different geometric configurations that particles can take when confined on a chemical template of the same size as its diameter. (b) Optical microscopy images of PS particles confined on a chemical pattern created by positively charged dots. (Courtesy of P. Hammond et al.)*[76, 81]

Therefore, physical patterns need to be slightly larger than the NP size. Single particle attachment on a chemical array was obtained by Shinya.[53]

Less effort has been devoted to study chemical confinement on the sub-200 nm scale as compared to physical confinement, because chemical templates in that range are difficult to prepare and the resulting templates are difficult to image. Nevertheless, NPs have been selectively attached on chemical patterns down to 200 nm[71] made using LIL, 90 nm[82] using edge lithography, 40 nm[83, 84] and 30 nm[85] using DPN. Sagiv showed the attachment of 17 nm Au NPs densely packed and with a degree of order similar to the one obtained by physical confinement.

A new approach consists of using ordered NPs to be transported to another substrate using a PDMS stamp, which might be patterned or not. The key to this process is to play with the surface energy of the particles on the surface. When the surface energy is low, particles can be picked up from the substrate provided their interaction with the stamp is higher than with the source substrate. They are then deposited on a target substrate with an even higher interaction with the colloids. This is a clear example of how the integration of top-down and bottom-up to control the surface energy, allows control of building blocks such as NPs. In a first example of this approach, the meniscus method was used to attach and pattern NPs by means of physical confinement.[86] The height of the template was smaller than the size of the NPs in order to have the NPs protruding from the pattern. The substrate was treated in advance with a fluoroalkyl SAM to minimize the adhesion between the surface and the NPs. A flat PDMS stamp was used to pick up the patterned NPs to subsequently deposit them on a Si substrate, having a higher adhesion with the NPs than PDMS. In this way, patterns of single NPs could be obtained at 5 μm period and multilayer colloidal slabs could be transported.

Additionally, NPs could also be applied on top of another layer of NPs. In another experiment, a patterned PDMS stamp was applied on ordered NPs from a substrate to pick them up.[87, 88]

By deposition on another substrate the NPs were patterned and remained ordered. In this way, multilayers and patterned multilayers could be fabricated by printing one layer on top of another keeping the original orientation or orthogonal to the previous one. Yang took advantage of the swelling (using solvent) and stretching properties of PDMS used as the transporting material.[89] In this way, the PDMS stamp can be deformed after picking up the NPs thus changing the periodicity of the NPs that can be deposited on the substrate (enlarged in general). These experiments were done on the micrometer scale.

Choi used ordered NPs in order to pattern PDMS stamps on the sub-micrometer scale.[90] NPs were first ordered in the grooves of a PDMS stamp using the meniscus method. These colloids arranged in typical shapes given by the physical confinement and the design was made such that they protrude from the PDMS stamp. Then this hybrid stamp was used to emboss a substrate coated with polyurethane polymer. Therefore, a mold with features in two size ranges was obtained. Similar experiments were performed using two types of NPs with different sizes.[91-93]

2.3.5 Top-down nanofabrication and layer-by-layer assembly

Layer-by-layer assembly is a technique that allows controlling the thickness and composition of multilayered films. LBL assemblies are usually formed by alternating immersion of a substrate in solutions of the different components. Patterning LBL assemblies allows the creation of 3D nanostructures. A review by Hammond describes the different ways of patterning LBL assemblies.[94, 95]

Therefore, the different techniques to pattern LBL assemblies will be only briefly mentioned here and the emphasis will be on the confinement issues in patterned LBL assemblies.

In contrast to the section on block-copolymers and NPs, the crucial issue here is not ordering of the building blocks but control over the selective attachment of one layer on top of the other in order to have an accurate control over the height of the assembly.

In the template-assisted method, a polymer template is made usually by photolithography, EBL, or NIL (Scheme 6 A). In some experiments, a chemical functionalization is also made on the non-protected areas of the substrate. LBL assembly is formed on the template usually by immersion. After the desired number of layers, the polymer is removed, revealing the LBL pattern. Lift-off is a crucial step, as the solvent should not induce disorder in the LBL assembly that is usually held together by electrostatic, hydrogen bonding or hydrophobic interactions. Ultrasonication, which is normally used during lift-off can also affect the stability of the structures built in 3D. The advantage of this approach is that finding a chemical pattern to fit the requirements to attach the LBL assembly is not necessary because the LBL assembly is started directly on the substrate. The polymer pattern prevents non-specific adsorption and helps to obtain sharp edges after lift-off.

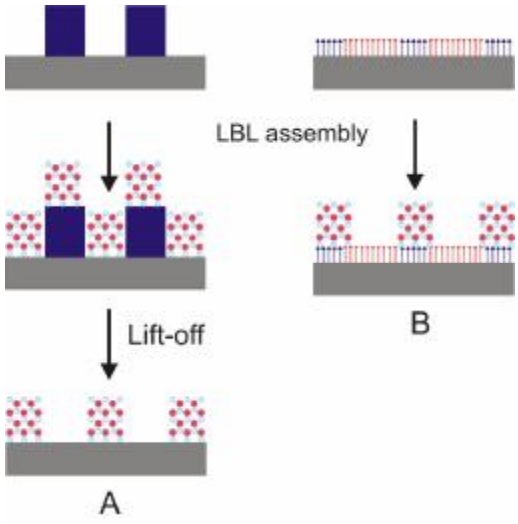

Scheme 6. *Utilization of polymer topographical (A) and chemical templates (B) to pattern layer-by-layer assembly.*

The usual criterion to check that the patterned LBL assembly was not damaged by the lift-off process is to measure the height of the LBL assembly after lift-off and to compare it to the corresponding height of the non-patterned LBL assemblies. Nevertheless, it has to be taken into account that different techniques are used to measure layer thickness on patterned substrates, typically AFM or cross-section SEM, and on non-patterned samples, typically ellipsometry.

Chemical patterning of LBL assemblies is based on a chemical contrast with a functionalization that attracts the first layer of the LBL assembly, usually a charged SAM such as with NH_3^+ or COO^- groups, and an anti-adherent functionalization for the LBL (alkyl or PEG, for instance, scheme 6 B).[29, 96, 97] A large number of layers can usually be attached while maintaining a good match with the chemical pattern that determines the lateral resolution. Patterning LBL assemblies on the micrometer scale has been widely studied but few attempts have been made on the sub-micrometer scale.[98, 99]

Mirkin was able to construct patterned LBL assemblies up to 19 nm height on 200 nm COOH-terminated thiol lines, and 16.3 nm height on 80 nm COOH-terminated thiol dots, using six bilayers. Jonas made a chemical pattern smaller than the length of the polyelectrolyte polymer, in which case the LBL assembly changed its configuration to fit the chemical pattern, resulting in a higher LBL height than for non-confined LBL assemblies.[100] Generally, high selectivity of the LBL assembly makes patterning an easy process but structures with high aspect ratios have not been obtained yet.

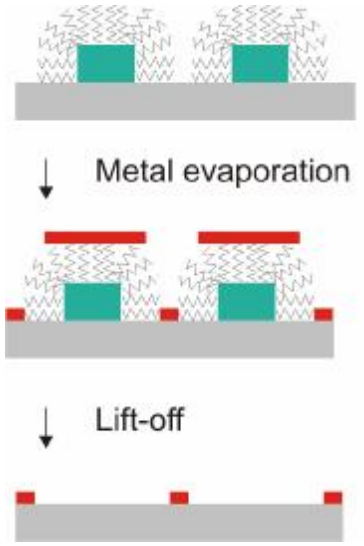

Scheme 7. *Use of the molecular rulers, created by LBL assembly on polymer structures, as a way to pattern high resolution metallic structures.*

In another experiment, a molecular ruler was created by LBL assembly on gold structures prepared using EBL and metal lift-off (Scheme 7).[101] The LBL assembly was anisotropically grown on Au features. The structure length was controlled by the number of deposited multilayers, one bilayer corresponding to 2 nm.

In this way, the interfeature distance was decreased and the patterned LBL assembly was used as a mask for Au deposition and lift-off, creating nanostructures of sizes down to 40 nm.

To avoid the rinsing step involved in lift-off, nanotransfer printing (nTP) can be used to transfer LBL assemblies. An LBL assembly was formed first on a patterned PDMS stamp.[102] The PDMS stamp was applied on a substrate and only the LBL areas that were in contact with the substrate were transferred.[103]

2.4 Applications of combined top-down and bottom-up nanofabrication for creating functional devices

2.4.1 Photonic crystal devices

Photonic crystals (PhCs) are periodic dielectric nanostructures designed to affect the propagation of light in the same way as the periodic potential in a semiconductor crystal affects the electron transport by defining allowed and forbidden electronic energy bands. The periodicity of the photonic crystal structure needs to be of the same order of magnitude than the wavelength of the light (in the 100 nanometer range). The photonic band gap (PBG) of a PhC is the range of wavelengths for which light does not propagate through the structure. An important parameter for PhCs is the difference in refractive index of the materials used (Δn) between the patterned material and the surroundings, generally air. A high Δn is desirable because it improves the light confinement and thus the band gap properties. Most of 1D and 2D PhCs are made using conventional lithography, such EBL and deep etching. 3D PhCs exhibit a PBG in all directions. The most popular method to create 3D PhCs is to make use of polymer or silica NP self-assembly because of the high order and low costs associated with this natural process. There exists a considerable number of reviews describing the performance of this type of PhCs.[58, 104-108]

Due to the low refractive index of the NPs, an interesting method to increase Δn is to create an inorganic matrix (generally made up of metal oxide such as TiO_2) around the colloidal assembly, and to burn away the NPs afterwards. In this way, a so-called inverted PhC is created.[109] In order to use these 3D photonic crystals as devices, they need to be structured, for example by creating intentional defects or defining waveguides, and integrated with other devices. Examples of devices that can be fabricated with PhCs are low-loss waveguides, filters and resonators.

The focus of this section is on the fabrication of 3D PhC devices by means of combinations of top-down and bottom-up techniques.

2.4.1.1 Patterning 3D photonic crystals

Colloidal epitaxy allows the controlled creation of 3D PhCs. The major drawback in colloidal self-assembly is the apparition of defects, usually cracks, which cause the NP domains to shrink. Cracks appear when the solvent used in the colloidal suspension evaporates. An effective method to overcome this problem is to add a slight interfeature distance between the colloids. This interfeature distance is obtained by creating a pattern underneath the colloids that directs the lattice or supperlattice parameters. This method is called colloidal epitaxy (see Section 2.2.1). In this way, patterned and defect-free areas of 800 × 800 μm^2 were made with ten layers of colloids.[110,111] An improvement of the quality of the PBG of the 3D PhCs fabricated in that way was observed.

In order to produce optical devices, the most ambitious being optical chips or light-driven computers, light needs to be processed analogous to the way electrons are in current electronic circuits.[87] For that purpose, 3D PhCs need to be integrated and patterned in circuits made with different 3D PhC channels.

A common method to pattern 3D PhCs is to grow or deposit NPs on patterned Si substrates using sedimentation, microfluidics,[112] the meniscus method,[113,114] or spin-coating.[55] The PhCs can be grown on various shapes, usually rectangular channels[113,115] but also V grooves or squares.[116,117] Multilayer NPs filling in closed patterns such as holes or rectangles is more difficult because the capillary forces are limited in those cases.[112] Sotomayor noticed that in the feature size range of 20 μm, cracks appeared along the sidewalls of the Si pattern.[118]

Metallic photonic crystals can be patterned as well using gold nanoparticles confined in photoresist channels.[55] In that case, the waveguide properties can be coupled to particle plasmon resonance.

A method to construct integrated circuits of 3D PhCs is to transfer the patterned NPs onto a substrate and construct the photonic circuit by assembling channels of PhCs. Free-standing slabs of NPs can be made using various ways and later used as building blocks for PhC circuits. Sotomayor made use of cracks appearing along the sidewalls of the Si template in order to extract the patterned NPs by using adhesive tape leading to free standing colloidal slabs.[115] Ozin used the same method after growing NPs on rectangular or V grooves. In additional experiments, NPs were grown in the pattern into an inverted lattice and etching of silica was performed to remove the template.[117] Matsuo produced free-standing pyramids[119] and Parikh used a sandwich structure formed by glass and Si substrates patterned chemically with hydrophobic SAMs with NPs grown in between to assemble free-standing NP slabs.[120] By integration of top-down and bottom-up techniques, Chua created a woodpile structure made of NP slabs.[121] Photolithography was used in order to create a polymer pattern that was used to confine a multilayer assembly of NPs. On top of the first layer, a second lithography step was performed which was followed by filling with NPs.

After the desired number of layers, the polymer was removed, leading to a woodpile of colloidal slabs shown in Figure 5.

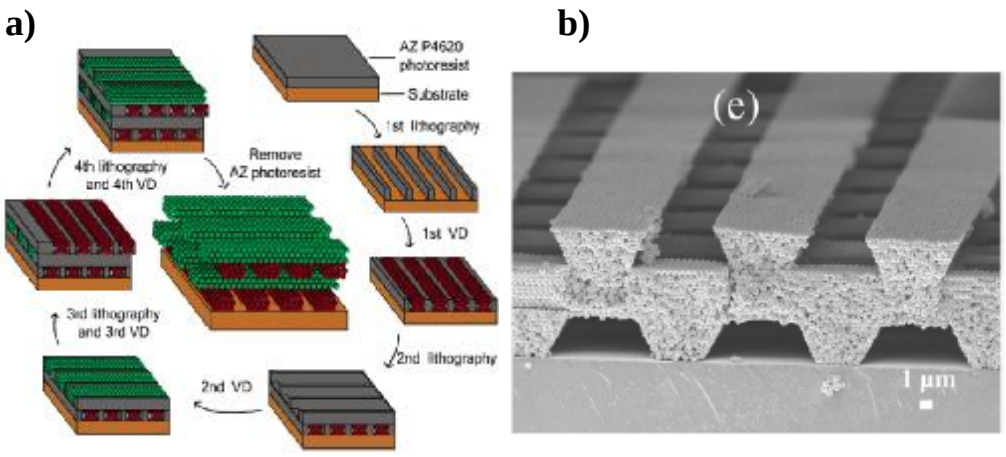

Figure 5. *(a) Scheme showing the multistep process of photolithography and colloidal assembly in order to create a colloidal woodpile. (b) SEM image of colloidal slab forming a woodpile.*[121]

2.4.1.2 Inserting defects in 3D photonic crystals

A review about the integration of defects in PhCs appeared recently.[105] Therefore, in this section, only the integration of defects in PhCs exclusively by using combinations of top-down and bottom-up lithographies is covered.

A method to propagate light along a given path inside a photonic crystal is via defects along the path, which is known as a waveguide. The challenge of this approach is the local integration of defects of the desired shape in an otherwise perfect NP assembly. When using PMMA NPs, defects can be created on surfaces, because this material is widely used as resist for e-beam lithography. By using NPs made of PMMA, grown into a PhC on a substrate, localized defects can be made by irradiating selectively some PMMA NPs and removing them (or parts of them) by developing in the appropriate solvent.[122,123]

Using this method, single NPs can be accurately removed and patterns of voids can be fabricated on top of the colloidal crystal.[124]

Trenches of the desired depth, up to the thickness of the assembly, were made inside the colloidal assembly by irradiating intensively the substrate. All irradiated NPs were dissolved during development, leading to trenches in the colloidal assembly.[115,122] In a similar experiment, Lopez infiltrated a SiO_2 matrix around the PMMA NP assembly. Then irradiation was performed, and the irradiated PMMA NPs were dissolved. The dissolved NPs led to a patterned inverted lattice.[123]

Another method to create defects is forming linear voids embedded inside the NP assembly. By using planar confinement,[125] a NP assembly was grown and then subjected to CVD infiltration.. Subsequently, a layer of silicon oxide was formed and the growth of the NP assembly was continued on top of it followed by CVD infiltration. At the end of the process, the silica was etched away and an inverted opal with a missing plane inside was obtained. Zhao used the same principle but instead of a silica layer, they employed a single layer of silica particles sandwiched between two layers of PS NPs.[126] At the end of the process, the substrate was infiltrated with silica and the PS NPs were removed by calcination to produce inverted opals with a planar defect in the center.

Chua used photoresist spin-coated on bulk silica NPs that was later patterned using photolithography.[127] NPs were assembled again around the polymer pattern. Then the polymer was removed in acetone leading to an empty rectangular line that was used as a waveguide. In a similar experiment, after removing the polymer pattern embedded inside the SiO_2 opals, the process was continued with CVD of Si or Ge, and wet etching was used to remove the silica opals and to fabricate an inverted lattice.[128]

An alternative method consists of embedding defects by using NPs of different sizes instead of creating voids. In that case, a bulk NP assembly was grown, on top of which photoresist was spin–coated and patterned by photolithography.[129]

This template was used to confine NPs of different sizes. The polymer was removed and the colloids of the first size were grown again around the patterned NPs of the second diameter, the process is similar to the one described in Figure 5. In this way, rows of the second type of NPs were embedded in bulk NPs. In a similar experiment but with a different patterning technique, NIL was performed on top of a silica opal assembly, and the polymer pattern was used to create a single layer of silica particles with a different diameter.[92] Then the previous silica opals were grown again. At the end of the process, the polymer pattern was removed using acetone. The aim of their experiment was to create point defects on the colloidal lattice.

Braun used multi-photon polymerization in order to write patterns of different shapes inside the bulk opals.[63] To that purpose, an opal assembly was grown to which a monomer was added as well as a photoinitiator. By using laser irradiation by a confocal microscope, the monomer was locally polymerized with the desired patterns, usually with a linear shape. Polymerization was induced inside the bulk using the property of a confocal microscope to focus the laser on different planes. Arbitrary features were written in this way, see Figure 6. After polymerization, wet etching was performed in order to create inverse opals and to remove the polymer pattern. At the end of the process, empty lines integrated in the bulk assembly of inverted opals were obtained. The empty line created in the bulk of the colloidal assembly was used as a waveguide.

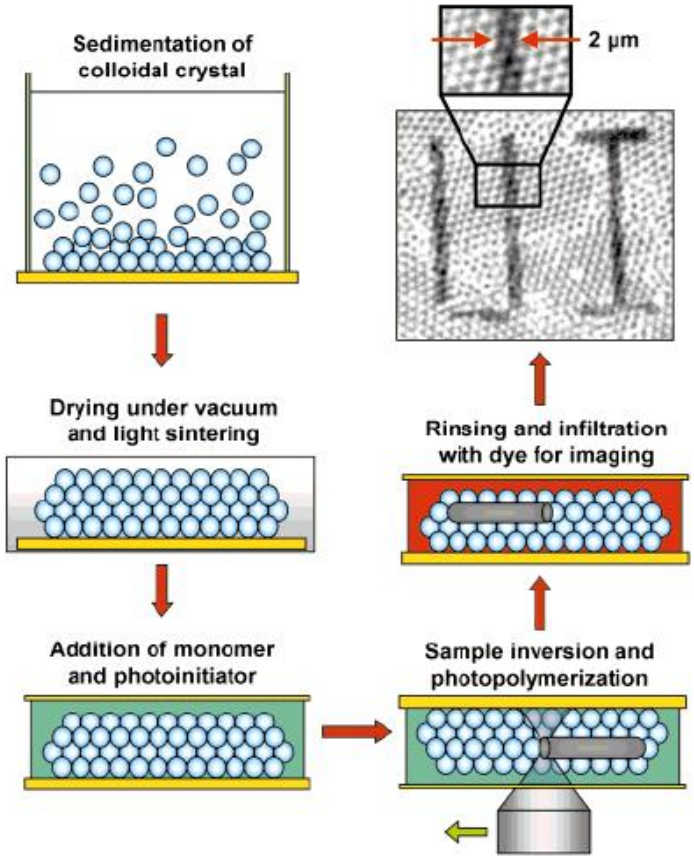

Figure 6. *Scheme showing the process of photopolymerisation on self-assembled NPs by using a laser of a confocal microscope.(Courtesy of P. Braun et al.)* [63]

Norris used a slight modification of this process to create an inverted lattice.[130,131] The colloidal assembly was infiltrated with a hybrid photoresist that stands high temperatures. After creating a line of defects using photopolymerization with a confocal microscope, the non-irradiated resist was removed and replaced by silicon. Colloids and irradiated resist were removed by wet etching. Embedded lines of 1 µm were created in that way.

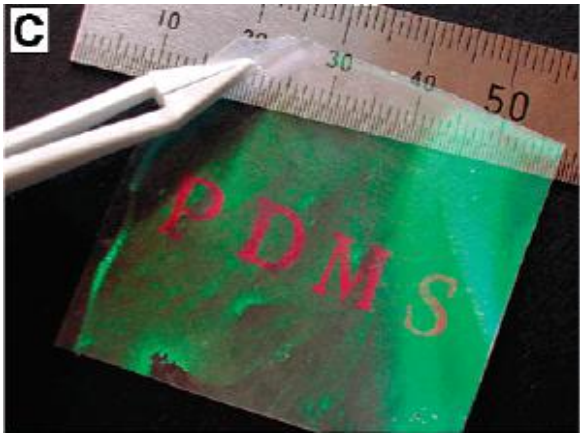

Figure 7. *Photograph of a 'photonic paper' consisting of particles embedded in a PDMS matrix, imprinted with a solvent by microcontact printing. The 'photonic paper' is illuminated with light.(Courtesy of Y. Xia et al.)* [132,133]

Xia used the swelling effect of PDMS when solvents such as silicon fluid, hexane or octane are applied on it.[132,133] NPs were assembled on a glass substrate integrated in a PDMS matrix, which was called 'photonic paper'. The solvent used as an ink was applied locally by means of ink-jet printing or μCP. The PDMS regions that were inked shrank locally causing the lattice parameter and thus the color of the colloidal assembly to change. After evaporation of the solvent the photonic paper went back to its initial state with uniform color.

2.4.2 Protein assays

Nanobiotechnology constitutes the interface between nanotechnology and biology. An extraordinary interest exists as a wide range of applications can be envisaged, ranging from biosensors, genomics, and proteomics. Several reviews deals with nanoparticles as biosensors,[134] protein chips,[135] transducers,[136] nanobiotechnology[137] in general, and bioengineering.[71]

A widely used method to pattern biological compounds such as proteins or DNA is ink-jet printing, where a drop of solution of the compound is delivered on a substrate. This technique allows the creation of arrays of different proteins on the millimeter scale.[138] In this chapter the focus is on the directed attachment of proteins on the micrometer and sub-micrometer scale using patterns made by combination of top-down lithography, as a way to create the lateral pattern, and bottom-up assembly to anchor selectively proteins through interactions such as physisorption, covalent attachment, and supramolecular interactions. Some requirements are needed in order to construct a suitable protein assay: (i) accurate spatial localization, (ii) specific adsorption of the selected protein, (iii) negligible non-specific adsorption of other components, (iv) controlled orientation of the proteins and (v) maintaining the functionality of the protein.

Common patterning methods are based on the adsorption of proteins, by using topographical templates with chemical functionalization, or chemical patterns. μCP and dip-pen nanolithography are widely use to create patterns for protein patterning. These will not be reviewed here. Molecular Assembly Patterning by Lift-off (MAPL) is used often to fabricate chemical patterns for protein adsorption on SiO_2.[139]

Nanosphere lithography is also popular as it allows easy access to sub-micrometer features over large areas.[140] The proteins are usually labeled with a fluorescent dye that allows characterization using fluorescence microscopy.

2.4.2.1 Patterned protein assembly using physisorption

The process of patterning proteins is simplified by the fact that proteins adsorb non-specifically on substrates. μCP has been used as a way to pattern a lipid membrane followed by filling the uncovered areas with proteins, or to pattern proteins followed by filling with a lipid membrane. In the first method, protein diffusion is limited by the lipid layer.[141] This technique provides a way to complex functionalized patterns that can be used both for protein and membrane studies. μCP was also used to pattern PEG layers that have protein-resistant properties for non-specific protein patterning directly on the SiO_2 areas.[142] Additionally, nanosphere lithography was used to create patterns of proteins.[143] The originality of this approach relies on the fact that both proteins and particles were present in the same suspension. When the suspension was allowed to dry on a mica surface, particles assembled with high order and confined the proteins at their interface. Due to the fact that particles were previously coated with a hydrophobic coating, they were removed by simple rinsing from the surface, revealing sub-micrometer protein patterns.

High resolution patterning of proteins down to 60 nm was performed by using a FIB to pattern GaAs on SiO_2.[144] Human Serum Albumin (HSA) was found to attach with high specificity on the patterned GaAs.

The full integration of proteins and DNA inside a microfabricated Si device has been achieved.[145] After preparation of the microstructures, proteins or DNA were inkjet printed on specific areas.

The structures were coated with gold to preserve their functionalities while further microfabrication processes were performed. At the end of the process, after gold removal, DNA molecules recovered their full functionality while proteins recovered only to about 50 %. This example offers good prospects for the future integration of proteins into devices.

When using proteins attached through hydrophobic interactions, a hydrophobic/hydrophilic chemical contrast is often created to direct their deposition. A way to create the chemical contrast is by patterning a polymer. Patterns have been obtained by printing (using μCP) a protein-resistant polymer such as poly(lactic acid) polyethylene glycol (PLA-PEG) on a hydrophobic PS surface, or by patterning Novolak resist using photolithography which becomes hydrophobic after irradiation.[146] Hydrophobic patterns can be created by irradiation of LBL assemblies.[147] On the sub-micrometer scale, nanosphere lithography was used indirectly to create Au patterns on SiO_2.[140] A hydrophobic thiol was attached to Au while PEG was formed on the SiO_2 areas with features down to 100 nm. Moreover, nanosphere lithography has been used directly to create a mask to form the chemical pattern.[148] PMMA-*b*-PS block-copolymer was used in order to obtain high-resolution patterning with sizes down to 45 nm easily.[149] Different proteins were adsorbed, and it was noticed that the protein height measured on the sub-50 nm patterned areas was smaller than the height of the protein when non-patterned. NIL was used to create chemical patterns down to 20 nm for protein adsorption. In these experiments, proteins attached with high specificity on the hydrophobic pattern and fluorescence microscopy was used to check the integrity of the protein.

Proteins can be attached through hydrophilic interactions. For instance, a Si surface was patterned with a carbohydrate-terminated monolayer using μCP which specifically attached carbohydrate-binding proteins.[150]

Electrostatic attachment is easy to use as proteins are usually charged. However, no specific orientation can be induced. Nanografting, that uses an AFM tip, was performed on a COOH-functionalized SAM to create a pattern. A hydrophobic SAM was formed on the uncovered areas to direct protein attachment through hydrophobic interactions. The aim of the process was to create a hydrophilic/hydrophobic pattern, but it was noticed that the proteins attached selectively on the negatively charged areas formed by the carboxylate groups. Proteins patterned down to 100 nm features were created.[151] Finally, nanosphere lithography was used to pattern proteins. The NPs were used as a mask for adsorption of a PEG SAM. After NP removal, the uncovered areas were filled with a negatively charged SAM. After protein deposition, pattern sizes down to 100 nm were obtained.[152]

2.4.2.2 Patterned protein assembly through covalent attachment

Covalent attachment is a good candidate when the protein needs to be firmly attached to the surface through specific functional groups. Covalent attachment can be achieved using a linker that binds to a conventional SAM and allows proteins to attach covalently via specific functional groups. A method for covalent attachment is based on photolithography, for which, after patterning a water-based resist, a SAM was formed on the unprotected areas.[153] Several functionalizations were performed allowing proteins or peptides to attach via their cystein sites. Lift-off was performed with water in order to avoid using organic solvents that could denature the proteins.

Another example is based on Au/Si patterns created using photolithography and Au lift-off.[154,155] A PEG SAM was attached specifically on SiO_2, while a carboxylic acid thiol was attached on the Au areas. A linker was attached to the thiol with the purpose to bind the proteins through their amino groups. The selective attachment of proteins was shown by fluorescence and also by infrared spectroscopy confirming the right composition. By resolving the protein shape with high resolution AFM imaging, it was confirmed that all proteins inside the pattern take a similar orientation, confirming the attachment at a specific site. Using the same type of covalent binding, photolithography was used to create a mask to chemically pattern amino and fluoro layers on a single crystal diamond surface.[55] DNA was attached covalently with high specificity on the chemical pattern.

In an experiment based on NP assembly, carboxylate-functionalized NPs were confined with hexagonal packing inside hole patterns created by photolithography.[156] Proteins were attached on the NPs through conjugation with carboxylic acid groups. The novelty consists of attaching proteins on curved surfaces in order to increase the surface area for protein attachment. This was inspired by the positive effect of surface curvature to retain the native structure and functionality of proteins compared to planar surfaces, but the quality of the proteins patterned in the former way was not investigated.[157, 158]

Nanosphere lithography was used to pattern a poly(acrylic acid) (PAA) layer with a COOH-terminated surface.[159] To fabricate this, a layer of PAA (130 nm thick) was deposited using plasma enhanced chemical vapor deposition, followed by attachment of PS beads on top using spin-coating. The dispersed PS beads were used as an etch mask for O_2 plasma to protect the PAA from etching. Finally the PS beads were removed in water and ultrasonication.

The resulting patterned PAA had the shape of a dome with a plateau in the center surrounded by an edge. BSA protein adsorption was performed. It was noticed that proteins attached preferentially in the center of the plateau and on the edges of the PAA domes.

2.4.2.3 Patterned protein assembly through supramolecular interactions

The advantage of using supramolecular interactions between the protein and the anchoring layer is that proteins can attach selectively via a specific binding site. The orientation of the protein can thus be directed. Another advantage is that the interaction can be reversed, allowing substrate regeneration. This effect has been studied mainly on non-patterned substrates.

Antibodies are Y-shaped proteins that attach specifically to antigens. Antibodies have been patterned by printing via physisorption,[160,161] or by covalent attachment on a silane layer.[159] Morhard found a higher quality by directed printing of the antibody compared to successive covalent binding, starting from printed alkyl thiols. Antibody patterns can also be formed starting from chemical patterns made by irradiation. A simple way to produce these patterns is to include the antibodies in a polymer matrix and subsequently imprint the polymer, as reviewed by Haupt.[162]

Physical confinement has been compared to chemical confinement for the guiding of microtubules attached on kinesin.[163] Topographical templates were created by a photoresist film patterned by photolithography which was subsequently functionalized with kinesin. The chemical template was formed by kinesin and a PEG SAM. The best directing quality was provided by the topographical pattern. It was found that microtubules remained fixed on the chemical edges when using chemical confinement.

An important issue for the development of protein chips is to pattern different types of proteins on the same area.

To achieve this, sequential patterning was performed using photolithography.[164] A pattern was prepared by photolithography, and the uncovered areas were filled with one type of protein using immersion. Then the same substrate was patterned for a second time using photolithography. Alignment marks allowed patterning in different areas than during the first lithographic step. This second pattern was filled with a different type of protein. Up to three different proteins were patterned in this way. The quality was checked by fluorescence microscopy, and inhomogeneous attachment was observed. The quality of the protein attachment was improved by antibody functionalization after UV patterning on the uncovered areas providing more homogeneous fluorescence images.

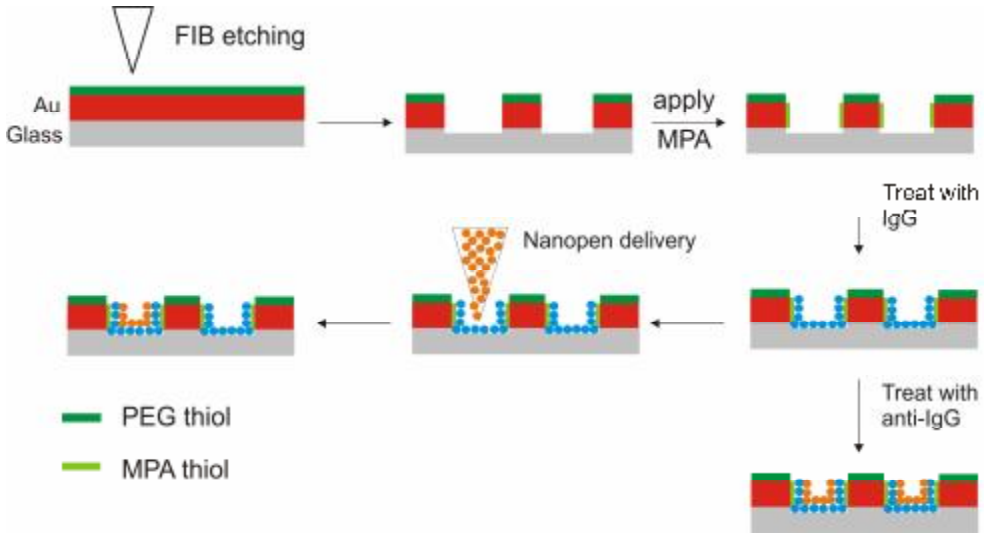

Scheme 7. *Scheme showing protein with a different label addressed using an AFM tip in an array of antibody functionalized holes.* [165] *Mercaptopropionic acid (MPA) is used to facilitate the immobilization of IgG antibodies.*

Bruckbauer proposed patterning on the sub-micrometer-scale of the same type of proteins functionalized with different fluorescent labels, in order to demonstrate a system in which biomolecules can be addressed.[165] The process consisted of fabricating an array of holes in which proteins with different labels were addressed, see Scheme 7. To achieve this, holes of 300 nm diameter were etched using FIB on a silicon substrate covered with gold. Au was functionalized with hexa(ethylene glycol) thiol to prevent non-specific adsorption, while the opening holes in silicon were functionalized with 3-mercaptopropionic acid to facilitate the immobilization of IgG antibodies trough electrostatic interactions. The IgG antibodies were deposited from solution. A nanopipet was used to address selectively an individual hole with a solution of anti-IgG protein. The size of the tip of the nanopipet corresponded to the diameter of the holes. IgG and anti-IgG were labeled with a different fluorescent label. To check their attachment, confocal microscopy was used, showing spots containing two fluorescent colors implying that both IgG and anti-IgG were present.

The biotin/streptavidin interaction is widely used in protein attachment applications. Streptavidin is a protein that contains four binding sites that interact specifically with biotin through supramolecular interactions. The biotin/streptavidin complex is very well-known and popular for its specificity and stability. Molecular Assembly Patterned by Lift-off (MAPL) was used to fabricate chemical patterns. First, a hydrophobic SAM was formed (fluoroalkyl or alkyl), and after removal of the patterned polymer, an aminoalkyl SAM was formed. Biotin was attached covalently on the aminoalkyl SAM to specifically direct streptavidin adsorption. The polymer patterns were made using photolithography,[139,166] EBL,[55,167] NIL,[168-170] and nanosphere lithography[171] with features of 100 nm, 75 nm and 50 nm, respectively.

Biotin-functionalized protein attached selectively to the streptavidin pattern.[166-168] Hoff demonstrated protein attachment on the micrometer scale by AFM and fluorescence, and in the sub-micrometer scale by AFM.[169,170] Zhang noticed a decrease of fluorescence intensity for dot diameters decreasing from 500 to 100 nm.[55] Huskens showed the use of the molecular printboard for binding streptavidin via an orthogonal linker and in particular the specificity, reversibility, and multivalency of this assembly scheme.[172]

Another approach consists of using PMMA-*b*-PS block-copolymers to provide a PS pattern template down to 15 nm.[173] The PMMA pattern was removed by acetone. PS provided the hydrophobic areas and an aminoalkyl SAM was formed in the uncovered areas. In this approach, the streptavidin functionalization was achieved by adsorption of streptavidin-functionalized Au NPs (10 nm) that attached selectively on the aminoalkyl SAM. This template was used for adsorption of biotin-functionalized molecules, followed by attachment of streptavidin. The protein attachment was demonstrated by cyclic voltammetry. In this example, regeneration of the substrate was shown using surface plasmon resonance (SPR). In another study, NP deposition was directed by patterning densely packed (sometimes hexagonal) streptavidin-functionalized 2 μm particles on chemical patterns.[171]

Chemical patterns made of amino/hydrophobic or PEG have also been made using irradiation through UV exposure,[166] EBL,[167] μCP,[59] and DPN.[174] Multilayers of proteins by alternating attachment of biotin and strepavidin have also been demonstrated.[167,173]

Doh has made use of aqueous photoresist to pattern successively two types of proteins.[175] After an initial biotin patterning followed by protein attachment, the areas protected by the resist were uncovered to be filled with biotin and followed by another protein adsorption step.

In another study, a transparent substrate was used which was covered on one side by a biotin, and UV irradiation was performed through the other side using a mask.[176] The biotin attachment was activated by the UV exposure. Subsequently, the biotin pattern was used to direct streptavidin attachment.

Several attachment steps can be performed using UV exposure through a mask and mask alignment to prevent overlaying, as the substrate does not need processing.

N-nitrilotriacetic acid (NTA) allows specific and reversible binding of His-tagged proteins through its Ni^{2+} complex. This technique is widely used to purify proteins. NTA, bound to a support, is complexed with a metal ion (Ni^{2+} or Co^{2+}) that allows binding of the proteins functionalized with a histidine group. Dissociation of the proteins attached by means of NiNTA-His-tag interactions can be induced by releasing the chelate complex (using EDTA) or by using a competitive agent such as histidine or imidazole.[177]Tampé et al. have further developed this approach on gold surfaces using μCP. The chemical pattern consisted of a hydrophobic SAM (alkyl thiol) and NTA thiols. A binding essay was created by ink-jet printing different types of proteins on the same array.[177,178] The hydrophobic areas prevented overflow and spillover between the spots. Other experiments were made using NTA thiols on Au.[179] Yu used an NTA-functionalized hydrogel surface patterned using a PDMS mold.[180] By varying the concentration of NTA, the quantity of bound proteins could be controlled. Montemagno used 80 nm Ni dots made by EBL and 50 nm Ni dots made by NIL to deposit a His-tag F_1-ATPase motor functionalized with a propeller.[181-183]

2.5 Concluding remarks

Top-down techniques have been successfully used as a way to pattern bottom-up assemblies such as SAMs, micelles, block-copolymers, nanoparticles and layer-by-layer assemblies. Some of the assemblies (block-copolymers, nanoparticles), when their dimensions are commensurate to the patterns, are confined and thus take on different configurations. These configurations are determined by the dimensions of the pattern and can be predicted. New elements are obtained, that could not be done by using only top-down or bottom-up techniques. The integration allows high-resolution patterning as well, and is more versatile and cheaper.

Functional devices, such as 3D photonic crystals, were fabricated by embedding a structure inside a colloidal assembly. Protein assays have been demonstrated by using top-down techniques to pattern with lateral resolution and bottom-up assemblies as a way to direct and anchor the protein adsorption, non-specifically or specifically.

2.6 References

[1] Geissler, M.; Xia, Y. N. *Adv. Mater.* **2004**, *16*, 1249.
[2] Alkaisi, M. M.; Blaikie, R. J.; McNab, S. J. *Adv. Mater.* **2001**, *13*, 877.
[3] Chou, S. Y.; Krauss, P. R.; Renstrom, P. J. *Science* **1996**, *272*, 85.
[4] Guo, L. J. *J. Phys. D, Appl. Phys.* **2004**, *37*, R123.
[5] Ludwig, A.; Cao, J.; Brugger, J.; Takeuchi, I. *Meas. Sci. Tech.* **2005**, *16*, 111.
[6] Tseng, A. A. *J. Micromech. Microeng.* **2004**, *14*, R15.
[7] Tseng, A. A. *Small* **2005**, *1*, 924.
[8] Krishnamoorthy, S.; Pugin, R.; Brugger, J.; Heinzelmann, H.; Hinderling, C. *Adv. Funct. Mater.* **2006**, *16*, 1469.
[9] Bockstaller, M. R.; Mickiewicz, R. A.; Thomas, E. L. *Adv. Mater.* **2005**, *17*, 1331.
[10] Park, M.; Harrison, C.; Chaikin, P. M.; Register, R. A.; Adamson, D. H. *Science* **1997**, *276*, 1401.
[11] Hamley, I. W. *Nanotechnology* **2003**, *14*, R39.
[12] Yang, S. M.; Jang, S. G.; Choi, D. G.; Kim, S.; Yu, H. K. *Small* **2006**, *2*, 458.
[13] Decher, G. *Science* **1997**, *277*, 1232.
[14] Jackman, R. J.; Wilbur, J. L.; Whitesides, G. M. *Science* **1995**, *269*, 664.
[15] Michel, B.; Bernard, A.; Bietsch, A.; Delamarche, E.; Geissler, M.; Juncker, D.; Kind, H.; Renault, J. P.; Rothuizen, H.; Schmid, H.; Schmidt-Winkel, P.; Stutz, R.; Wolf, H. *Chimia* **2002**, *56*, 527
[16] Xia, Y. N.; Whitesides, G. M. *Annual Review of Materials Science* **1998**, *28*, 153.
[17] Loo, Y. L.; Willett, R. L.; Baldwin, K. W.; Rogers, J. A. *J. Am. Chem. Soc.* **2002**, *124*, 7654.
[18] Ginger, D. S.; Zhang, H.; Mirkin, C. A. *Angew. Chem. Int. ed.* **2004**, *43*, 30.
[19] Hong, S. H.; Mirkin, C. A. *Science* **2000**, *288*, 1808.
[20] Onclin, S.; Ravoo, B. J.; Reinhoudt, D. N. *Angew. Chem. Int. Ed.* **2005**, *44*, 6282.
[21] Pan, F.; Wang, P.; Lee, K.; Wu, A.; Turro, N. J.; Koberstein, J. T. *Langmuir* **2005**, *21*, 3605.
[22] Yang, S. Y.; Rubner, M. F. *J. Am. Chem. Soc.* **2002**, *124*, 2100.
[23] Moon, J. H.; Jang, S. G.; Lim, J. M.; Yang, S. M. *Adv. Mater.* **2005**, *17*, 2559.
[24] Yu, C. H.; Parikh, A. N.; Groves, J. T. *Adv. Mater.* **2005**, *17*, 1477.
[25] Park, J. W.; Thomas, E. L. *J. Am. Chem. Soc.* **2002**, *124*, 514.
[26] Harada, Y.; Girolami, G. S.; Nuzzo, R. G. *Langmuir* **2003**, *19*, 5104.
[27] Husemann, M.; Mecerreyes, D.; Hawker, C. J.; Hedrick, J. L.; Shah, R.; Abbott, N. L. *Angew. Chem. Int. Ed.* **1999**, *38*, 647.
[28] Hyun, J.; Chilkoti, A. *Macromolecules* **2001**, *34*, 5644.
[29] Zhou, D. J.; Bruckbauer, A.; Batchelor, M.; Kang, D. J.; Abell, C.; Klenerman, D. *Langmuir* **2004**, *20*, 9089.
[30] Schmelmer, U.; Jordan, R.; Geyer, W.; Eck, W.; Golzhauser, A.; Grunze, M.; Ulman, A. *Angew. Chem. Int. ed.* **2003**, *42*, 559
[31] Ahn, S. J.; Kaholek, M.; Lee, W. K.; LaMattina, B.; LaBean, T. H.; Zauscher, S. *Adv. Mater.* **2004**, *16*, 2141.
[32] Kaholek, M.; Lee, W. K.; LaMattina, B.; Caster, K. C.; Zauscher, S. *Nano Lett.* **2004**, *4*, 373.
[33] Maynor, B. W.; Filocamo, S. F.; Grinstaff, M. W.; Liu, J. *J. Am. Chem. Soc.* **2002**, *124*, 522.
[34] Hecht, S. *Angew. Chem. Int. Ed.* **2003**, *42*, 24.
[35] Okawa, Y.; Aono, M. *Nature* **2001**, *409*, 683.

[36] von Werne, T. A.; Germack, D. S.; Hagberg, E. C.; Sheares, V. V.; Hawker, C. J.; Carter, K. R. *J. Am. Chem. Soc.* **2003**, *125*, 3831.
[37] Boyen, H. G.; Kastle, G.; Zurn, K.; Herzog, T.; Weigl, F.; Ziemann, P.; Mayer, O.; Jerome, C.; Moller, M.; Spatz, J. P.; Garnier, M. G.; Oelhafen, P. *Adv. Funct. Mater.* **2003**, *13*, 359.
[38] Spatz, J. P.; Chan, V. Z. H.; Mossmer, S.; Kamm, F. M.; Plettl, A.; Ziemann, P.; Moller, M. *Adv. Mater.* **2002**, *14*, 1827.
[39] Sundrani, D.; Darling, S. B.; Sibener, S. J. *Nano Lett.* **2004**, *4*, 273.
[40] Cheng, J. Y.; Zhang, F.; Chuang, V. P.; Mayes, A. M.; Ross, C. A. *Nano Lett.* **2006**, *6*, 2099.
[41] Stoykovich, M. P.; Muller, M.; Kim, S. O.; Solak, H. H.; Edwards, E. W.; de Pablo, J. J.; Nealey, P. F. *Science* **2005**, *308*, 1442.
[42] Cheng, J. Y.; Zhang, F.; Smith, H. I.; Vancso, G. J.; Ross, C. A. *Adv. Mater.* **2006**, *18*, 597.
[43] Li, H. W.; Huck, W. T. S. *Nano Lett.* **2004**, *4*, 1633.
[44] Rockford, L.; Liu, Y.; Mansky, P.; Russell, T. P.; Yoon, M.; Mochrie, S. G. J. *Phys. Rev. Lett.* **1999**, *82*, 2602.
[45] Yang, X. M.; Peters, R. D.; Nealey, P. F.; Solak, H. H.; Cerrina, F. *Macromolecules* **2000**, *33*, 9575.
[46] Stoykovich, M. P.; Cao, H. B.; Yoshimoto, K.; Ocola, L. E.; Nealey, P. F. *Adv. Mater.* **2003**, *15*, 1180.
[47] Kim, S. O.; Kim, B. H.; Kim, K.; Koo, C. M.; Stoykovich, M. P.; Nealey, P. F.; Solak, H. H. *Macromolecules* **2006**, *39*, 5466.
[48] Edwards, E. W.; Montague, M. F.; Solak, H. H.; Hawker, C. J.; Nealey, P. F. *Adv. Mater.* **2004**, *16*, 1315.
[49] Xia, Y. N.; Yin, Y. D.; Lu, Y.; McLellan, J. *Adv. Funct. Mat.* **2003**, *13*, 907.
[50] Zhou, D.; Bruckbauer, A.; Ying, L. M.; Abell, C.; Klenerman, D. *Nano Lett.* **2003**, *3*, 1517.
[51] Allard, M.; Sargent, E. H.; Lewis, P. C.; Kumacheva, E. *Adv. Mater.* **2004**, *16*, 1360.
[52] Kumacheva, E.; Golding, R. K.; Allard, M.; Sargent, E. H. *Adv. Mater.* **2002**, *14*, 221.
[53] Fudouzi, H.; Kobayashi, M.; Shinya, N. *Adv. Mater.* **2002**, *14*, 1649.
[54] Cui, T. H.; Hua, F.; Lvov, Y. *Sens. Actuat. Phys.* **2004**, *114*, 501.
[55] Zhang, X. P.; Sun, B. Q.; Friend, R. H.; Guo, H. C.; Nau, D.; Giessen, H. *Nano Lett.* **2006**, *6*, 651.
[56] Ye, Y. H.; Badilescu, S.; Truong, V. V.; Rochon, P.; Natansohn, A. *Appl. Phys. Lett.* **2001**, *79*, 872.
[57] Schaak, R. E.; Cable, R. E.; Leonard, B. M.; Norris, B. C. *Langmuir* **2004**, *20*, 7293.
[58] Ozin, G. A.; Yang, S. M. *Adv. Funct. Mater.* **2001**, *11*, 95.
[59] Manandhar, P.; Huang, L.; Grubich, J. R.; Hutchinson, J. W.; Chase, P. B.; Hong, S. H. *Langmuir* **2005**, *21*, 3213.
[60] Velikov, K. P.; Christova, C. G.; Dullens, R. P. A.; van Blaaderen, A. *Science* **2002**, *296*, 106.
[61] Dziomkina, N. V.; Hempenius, M. A.; Vancso, G. J. *Adv. Mater.* **2005**, *17*, 237.
[62] Dziomkina, N. V.; Vancso, G. J. *Soft Matter* **2005**, *1*, 265.
[63] Lee, W. M.; Pruzinsky, S. A.; Braun, P. V. *Adv. Mater.* **2002**, *14*, 271.
[64] Vossen, D. L. J.; Fific, D.; Penninkhof, J.; van Dillen, T.; Polman, A.; van Blaaderen, A. *Nano Lett.* **2005**, *5*, 1175.

[65] van Blaaderen, A. *Science* **2003**, *301*, 470.
[66] Hoogenboom, J. P.; Vossen, D. L. J.; Faivre-Moskalenko, C.; Dogterom, M.; van Blaaderen, A. *Appl. Phys. Lett.* **2002**, *80*, 4828.
[67] Garcia-Santamaria, F.; Miyazaki, H. T.; Urquia, A.; Ibisate, M.; Belmonte, M.; Shinya, N.; Meseguer, F.; Lopez, C. *Adv. Mater.* **2002**, *14*, 1144.
[68] Lyles, B. F.; Terrot, M. S.; Hammond, P. T.; Gast, A. P. *Langmuir* **2004**, *20*, 3028.
[69] Gu, Z. Z.; Fujishima, A.; Sato, O. *Angew. Chem. Int. Ed* **2002**, *41*, 2068.
[70] Jonas, U.; del Campo, A.; Kruger, C.; Glasser, G.; Boos, D. *Proceed. Nat. Acad. Sci.USA* **2002**, *99*, 5034.
[71] Aizenberg, J. *Adv. Mater.* **2004**, *16*, 1295.
[72] Kaltenpoth, G.; Himmelhaus, M.; Slansky, L.; Caruso, F.; Grunze, M. *Adv. Mater.* **2003**, *15*, 1113.
[73] Masuda, Y.; Itoh, T.; Koumoto, K. *Langmuir* **2005**, *21*, 4478.
[74] Fustin, C. A.; Glasser, G.; Spiess, H. W.; Jonas, U. *Adv. Mater.* **2003**, *15*, 1025.
[75] Fustin, C. A.; Glasser, G.; Spiess, H. W.; Jonas, U. *Langmuir* **2004**, *20*, 9114
[76] Zheng, H. P.; Rubner, M. F.; Hammond, P. T. *Langmuir* **2002**, *18*, 4505.
[77] Jacobs, H. O.; Campbell, S. A.; Steward, M. G. *Adv. Mater.* **2002**, *14*, 1553.
[78] Suzuki, M.; Yasukawa, T.; Mase, Y.; Oyamatsu, D.; Shiku, H.; Matsue, T. *Langmuir* **2004**, *20*, 11005.
[79] Feng, J.; Wang, B.; Gao, C. Y.; Shen, J. C. *Adv. Mater.* **2004**, *16*, 1940.
[80] Ng, H. T.; Fang, A. P.; Huang, L. Q.; Li, S. F. Y. *Langmuir* **2002**, *18*, 6324.
[81] Lee, I.; Zheng, H. P.; Rubner, M. F.; Hammond, P. T. *Adv. Mater.* **2002**, *14*, 572.
[82] Cherniavskaya, O.; Adzic, A.; Knutson, C.; Gross, B. J.; Zang, L.; Liu, R.; Adams, D. M. *Langmuir* **2002**, *18*, 7029.
[83] Liu, S. T.; Maoz, R.; Sagiv, J. *Nano Lett.* **2004**, *4*, 845.
[84] Liu, S. T.; Maoz, R.; Schmid, G.; Sagiv, J. *Nano Lett.* **2002**, *2*, 1055.
[85] Tzeng, S. D.; Lin, K. J.; Hu, J. C.; Chen, L. J.; Gwo, S. *Adv. Mater.* **2006**, *18*, 1147.
[86] Kraus, T.; Malaquin, L.; Delamarche, E.; Schmid, H.; Spencer, N. D.; Wolf, H. *Adv. Mater.* **2005**, *17*, 2438.
[87] Arsenault, A.; Fournier-Bidoz, S.; Hatton, B.; Miguez, H.; Tetreault, N.; Vekris, E.; Wong, S.; Yang, S. M.; Kitaev, V.; Ozin, G. A. *J. Mater. Chem.* **2004**, *14*, 1778.
[88] Yao, J. M.; Yan, X.; Lu, G.; Zhang, K.; Chen, X.; Jiang, L.; Yang, B. *Adv. Mater.* **2004**, *16*, 81.
[89] Yan, X.; Yao, J. M.; Lu, G.; Li, X.; Zhang, J. H.; Han, K.; Yang, B. *J. Am. Chem. Soc.* **2005**, *127*, 7688.
[90] Choi, D. G.; Jang, S. G.; Yu, H. K.; Yang, S. M. *Chem. Mater.* **2004**, *16*, 3410.
[91] Choi, J.; Zhao, Y. H.; Zhang, D. Y.; Chien, S.; Lo, Y. H. *Nano Lett.* **2003**, *3*, 995.
[92] Yan, Q. F.; Chen, A.; Chua, S. J.; Zhao, X. S. *Adv. Mater.* **2005**, *17*, 2849.
[93] Cayre, O. J.; Paunov, V. N. *J. Mater. Chem.* **2004**, *14*, 3300.
[94] Hammond, P. T. *Adv. Mater.* **2004**, *16*, 1271.
[95] Clark, S. L.; Hammond, P. T. *Adv. Mater.* **1998**, *10*, 1515.
[96] Jeon, N. L.; Choi, I. S.; Whitesides, G. M.; Kim, N. Y.; Laibinis, P. E.; Harada, Y.; Finnie, K. R.; Girolami, G. S.; Nuzzo, R. G. *Appl. Phys. Lett.* **1999**, *75*, 4201.
[97] Liang, Z. Q.; Wang, Q. *Langmuir* **2004**, *20*, 9600.
[98] Lee, S. W.; Sanedrin, R. G.; Oh, B. K.; Mirkin, C. A. *Adv. Mater.* **2005**, *17*, 2749.
[99] Nyamjav, D.; Ivanisevic, A. *Chem. Mater.* **2004**, *16*, 5216.

[100] Pallandre, A.; Moussa, A.; Nysten, B.; Jonas, A. M. *Adv. Mater.* **2006**, *18*, 481.
[101] Hatzor, A.; Weiss, P. S. *Science* **2001**, *291*, 1019.
[102] Park, J.; Hammond, P. T. *Adv. Mater.* **2004**, *16*, 520.
[103] Mallwitz, F.; Laschewsky, A. *Adv. Mater.* **2005**, *17*, 1296.
[104] Birner, A.; Wehrspohn, R. B.; Gosele, U. M.; Busch, K. *Adv. Mater.* **2001**, *13*, 377.
[105] Lopez, C. *Adv. Mater.* **2003**, *15*, 1679.
[106] Norris, D. J.; Arlinghaus, E. G.; Meng, L. L.; Heiny, R.; Scriven, L. E. *Adv. Mater.* **2004**, *16*, 1393.
[107] Thylen, L.; Qiu, M.; Anand, S. *ChemPhysChem* **2004**, *5*, 1268.
[108] Yacaman, M. J.; Ascencio, J. A.; Liu, H. B.; Gardea-Torresdey, J. *J. Vac. Sci. Technol. B* **2001**, *19*, 1091.
[109] Tetreault, N.; Mihi, A.; Miguez, H.; Rodriguez, I.; Ozin, G. A.; Meseguer, F.; Kitaev, V. *Adv. Mater.* **2004**, *16*, 346.
[110] Jin, C. J.; Li, Z. Y.; McLachlan, M. A.; McComb, D. W.; De La Rue, R. M.; Johnson, N. P. *J. Appl. Phys.* **2006**, *99*.
[111] Jin, C. J.; McLachlan, M. A.; McComb, D. W.; De La Rue, R. M.; Johnson, N. P. *Nano Lett.* **2005**, *5*, 2646.
[112] Miguez, H.; Yang, S. M.; Ozin, G. A. *Langmuir* **2003**, *19*, 3479.
[113] Yang, S. M.; Miguez, H.; Ozin, G. A. *Adv. Funct. Mater.* **2002**, *12*, 425.
[114] Ye, J. H.; Zentel, R.; Arpiainen, S.; Ahopelto, J.; Jonsson, F.; Romanov, S. G.; Sotomayor-Torres, C. M. S. *Langmuir* **2006**, *22*, 7378.
[115] Ferrand, P.; Egen, M.; Zentel, R.; Seekamp, J.; Romanov, S. G.; Sotomayor-Torres, C. M. S. *Appl. Phys. Lett.* **2003**, *83*, 5289.
[116] Ferrand, P.; Minty, M. J.; Egen, M.; Ahopelto, J.; Zentel, R.; Romanov, S. G.; Sotomayor-Torres, C. M. S. *Nanotechnology* **2003**, *14*, 323.
[117] Miguez, H.; Yang, S. M.; Tetreault, N.; Ozin, G. A. *Adv. Mater.* **2002**, *14*, 1805-.
[118] Ferrand, P.; Egen, M.; Griesebock, B.; Ahopelto, J.; Muller, M.; Zentel, R.; Romanov, S. G.; Sotomayor-Torres, C. M. *Appl. Phys. Lett.* **2002**, *81*, 2689.
[119] Matsuo, S.; Fujine, T.; Fukuda, K.; Juodkazis, S.; Misawa, H. *Appl. Phys. Lett.* **2003**, *82*, 4283.
[120] Brozell, A. M.; Muha, M. A.; Parikh, A. N. *Langmuir* **2005**, *21*, 11588.
[121] Yan, Q. F.; Zhao, X. S.; Teng, J. H.; Chua, S. J. *Langmuir* **2006**, *22*, 7001.
[122] Ferrand, P.; Seekamp, J.; Egen, M.; Zentel, R.; Romanov, S. G.; Torres, C. M. S. *Microelectron. Eng.* **2004**, *73-74*, 362.
[123] Juarez, B. H.; Golmayo, D.; Postigo, P. A.; Lopez, C. *Adv. Mater.* **2004**, *16*, 1732.
[124] Jonsson, F.; Torres, C. M. S.; Seekamp, J.; Schniedergers, M.; Tiedemann, A.; Ye, J. H.; Zentel, R. *Microelectron. Eng.* **2005**, *78-79*, 429.
[125] Palacios-Lidon, E.; Galisteo-Lopez, J. F.; Juarez, B. H.; Lopez, C. *Adv. Mater.* **2004**, *16*, 341.
[126] Wang, L. K.; Yan, Q. F.; Zhao, X. S. *Langmuir* **2006**, *22*, 3481.
[127] Yan, Q. F.; Zhou, Z. C.; Zhao, X. S.; Chua, S. J. *Adv. Mater.* **2005**, *17*, 917.
[128] Vekris, E.; Kitaev, V.; von Freymann, G.; Perovic, D. D.; Aitchison, J. S.; Ozin, G. A. *Adv. Mater.* **2005**, *17*, 1269.
[129] Yan, Q. F.; Zhou, Z. C.; Zhao, X. S. *Chem. Mater.* **2005**, *17*, 3069.
[130] Jun, Y. H.; Leatherdale, C. A.; Norris, D. J. *Adv. Mater.* **2005**, *17*, 1908.
[131] Taton, T. A.; Norris, D. J. *Nature* **2002**, *416*, 685.
[132] Fudouzi, H.; Xia, Y. N. *Langmuir* **2003**, *19*, 9653.

[133] Fudouzi, H.; Xia, Y. N. *Adv. Mater.* **2003**, *15*, 892.
[134] Shipway, A. N.; Katz, E.; Willner, I. *ChemPhysChem* **2000**, *1*, 18.
[135] Zhu, H.; Snyder, M. *Curr. Opin. Chem. Biol.* **2003**, *7*, 55.
[136] Maes, H. E.; Claeys, C.; Mertens, R.; Campitelli, A.; Van Hoof, C.; De Boeck, J. *Adv. Eng. Mater.* **2001**, *3*, 781
[137] Klefenz, H. *Eng. Life Sci.* **2004**, *4*, 211.
[138] De Gans, B. J.; Duineveld, P. C.; Schubert, U. S. *Adv. Mater.* **2004**, *16*, 203.
[139] Falconnet, D.; Koenig, A.; Assi, T.; Textor, M. *Adv. Funct. Mater.* **2004**, *14*, 749.
[140] Agheli, H.; Malmstrom, J.; Larsson, E. M.; Textor, M.; Sutherland, D. S. *Nano Lett.* **2006**, *6*, 1165.
[141] Kung, L. A.; Kam, L.; Hovis, J. S.; Boxer, S. G. *Langmuir* **2000**, *16*, 6773.
[142] Khademhosseini, A.; Jon, S.; Suh, K. Y.; Tran, T. N. T.; Eng, G.; Yeh, J.; Seong, J.; Langer, R. *Adv. Mater.* **2003**, *15*, 1995.
[143] Garno, J. C.; Amro, N. A.; Wadu-Mesthrige, K.; Liu, G. Y. *Langmuir* **2002**, *18*, 8186.
[144] Bergman, A. A.; Buijs, J.; Herbig, J.; Mathes, D. T.; Demarest, J. J.; Wilson, C. D.; Reimann, C. T.; Baragiola, R. A.; Hu, R.; Oscarsson, S. O. *Langmuir* **1998**, *14*, 6785.
[145] Trau, D.; Jiang, J.; Sucher, N. J. *Langmuir* **2006**, *22*, 877.
[146] Nicolau, D. V.; Taguchi, T.; Taniguchi, H.; Yoshikawa, S. *Langmuir* **1998**, *14*, 1927.
[147] Cao, T. B.; Wei, F.; Jiao, X. M.; Chen, J. Y.; Liao, W.; Zhao, X.; Cao, W. X. *Langmuir* **2003**, *19*, 8127.
[148] Valsesia, A.; Colpo, P.; Meziani, T.; Lisboa, P.; Lejeune, M.; Rossi, F. *Langmuir* **2006**, *22*, 1763.
[149] Kumar, N.; Hahm, J. I. *Langmuir* **2005**, *21*, 6652.
[150] Shirahata, N.; Yonezawa, T.; Miura, Y.; Kobayashi, K.; Koumoto, K. *Langmuir* **2003**, *19*, 9107.
[151] Wadu-Mesthrige, K.; Xu, S.; Amro, N. A.; Liu, G. Y. *Langmuir* **1999**, *15*, 8580.
[152] Cai, Y. G.; Ocko, B. M. *Langmuir* **2005**, *21*, 9274.
[153] Sorribas, H.; Padeste, C.; Tiefenauer, L. *Biomater.* **2002**, *23*, 893.
[154] Veiseh, M.; Wickes, B. T.; Castner, D. G.; Zhang, M. Q. *Biomater.* **2004**, *25*, 3315.
[155] Veiseh, M.; Zareie, M. H.; Zhang, M. Q. *Langmuir* **2002**, *18*, 6671.
[156] Yap, F. L.; Zhang, Y. *Langmuir* **2005**, *21*, 5233.
[157] Lundqvist, M.; Sethson, I.; Jonsson, B. H. *Langmuir* **2004**, *20*, 10639.
[158] Vertegel, A. A.; Siegel, R. W.; Dordick, J. S. *Langmuir* **2004**, *20*, 6800.
[159] Valsesia, A.; Colpo, P.; Meziani, T.; Bretagnol, F.; Lejeune, M.; Rossi, F.; Bouma, A.; Garcia-Parajo, M. *Adv. Funct. Mater.* **2006**, *16*, 1242.
[160] Howell, S. W.; Inerowicz, H. D.; Regnier, F. E.; Reifenberger, R. *Langmuir* **2003**, *19*, 436.
[161] Morhard, F.; Pipper, J.; Dahint, R.; Grunze, M. *Sens. Actuat. B Chem.* **2000**, *70*, 232.
[162] Haupt, K.; Mosbach, K. *Trends Biotechnol.* **1998**, *16*, 468.
[163] Clemmens, J.; Hess, H.; Lipscomb, R.; Hanein, Y.; Bohringer, K. F.; Matzke, C. M.; Bachand, G. D.; Bunker, B. C.; Vogel, V. *Langmuir* **2003**, *19*, 10967.
[164] Ivanova, E. P.; Wright, J. P.; Pham, D.; Filipponi, L.; Viezzoli, A.; Nicolau, D. V. *Langmuir* **2002**, *18*, 9539.

[165] Bruckbauer, A.; Zhou, D. J.; Kang, D. J.; Korchev, Y. E.; Abell, C.; Klenerman, D. *J. Am. Chem. Soc.* **2004**, *126*, 6508.
[166] Orth, R. N.; Clark, T. G.; Craighead, H. G. *Biomed. Dev.* **2003**, *5*, 29.
[167] Biebricher, A.; Paul, A.; Tinnefeld, P.; Golzhauser, A.; Sauer, M. *J. Biotech.* **2004**, *112*, 97.
[168] Falconnet, D.; Pasqui, D.; Park, S.; Eckert, R.; Schift, H.; Gobrecht, J.; Barbucci, R.; Textor, M. *Nano Lett.* **2004**, *4*, 1909.
[169] Hoff, J. D.; Cheng, L. J.; Meyhofer, E.; Guo, L. J.; Hunt, A. J. *Nano Lett.* **2004**, *4*, 853.
[170] Hoff, J. D.; Hunt, A. *Biophys. J.* **2003**, *84*, 292A.
[171] Michel, R.; Reviakine, I.; Sutherland, D.; Fokas, C.; Csucs, G.; Danuser, G.; Spencer, N. D.; Textor, M. *Langmuir* **2002**, *18*, 8580.
[172] Ludden, M. J. W.; Péter, M.; Reinhoudt, D. N.; Huskens, J. *Small* **2006**, *2*, 1192.
[173] Jung, J. M.; Kwon, K. Y.; Ha, T. H.; Chung, B. H.; Jung, H. T. *Small* **2006**, *2*, 1010.
[174] Hyun, J.; Ahn, S. J.; Lee, W. K.; Chilkoti, A.; Zauscher, S. *Nano Lett.* **2002**, *2*, 1203.
[175] Doh, J.; Irvine, D. J. *J. Am. Chem. Soc.* **2004**, *126*, 9170.
[176] Holden, M. A.; Cremer, P. S. *J. Am. Chem. Soc.* **2003**, *125*, 8074.
[177] Valiokas, R.; Klenkar, G.; Tinazli, A.; Tampe, R.; Liedberg, B.; Piehler, J. *ChemBioChem* **2006**, *7*, 1325.
[178] Gamsjaeger, R.; Wimmer, B.; Kahr, H.; Tinazli, A.; Picuric, S.; Lata, S.; Tampe, R.; Maulet, Y.; Gruber, H. J.; Hinterdorfer, P.; Romanin, C. *Langmuir* **2004**, *20*, 5885.
[179] Kato, K.; Sato, H.; Iwata, H. *Langmuir* **2005**, *21*, 7071.
[180] Yu, T. Y.; Wang, Q.; Johnson, D. S.; Wang, M. D.; Ober, C. K. *Adv. Funct. Mater.* **2005**, *15*, 1303.
[181] Montemagno, C.; Bachand, G. *Nanotechnology* **1999**, *10*, 225-231.
[182] Bachand, G. D.; Soong, R. K.; Neves, H. P.; Olkhovets, A.; Craighead, H. G.; Montemagno, C. D. *Nano Lett.* **2001**, *1*, 42.
[183] Soong, R. K.; Bachand, G. D.; Neves, H. P.; Olkhovets, A. G.; Craighead, H. G.; Montemagno, C. D. *Science* **2000**, *290*, 1555.

Chapter 3

Patterned Self-Assembled Monolayers on Silicon Oxide Prepared by Nanoimprint Lithography and their Applications in Nanofabrication*

3.1 Introduction

Creating patterns of self-assembled monolayers (SAMs) using top-down and bottom-up approaches has received a rising interest. Such methods allow to chemically pattern a substrate, opening new possibilities for etch resists[1,2] or to control the position and attachment of molecules and particles with different functionalities on a substrate. Different applications have been demonstrated for patterned functionalized SAMs. For instance, the use of functionalized molecules has made it possible to fabricate sensors[3] and molecular electronic devices.[4,5] Working with proteins, biological arrays can be prepared[6] and, employing (non-functionalized) nanoparticles, photonic crystals can be fabricated.[7-9] Controlling the functionality of the chemical pattern allows to build-up complex systems.[10]

* This Chapter has been published in part in: P. Maury, M. Péter, V. Mahalingam, D. N. Reinhoudt, J. Huskens, *Adv. Funct. Mater.* **2005,** *15*, 451.

The endgroup functionality of a patterned SAM can, for example, be used to direct the assembly of functionalized nanoparticles. Positioning of functionalized particles can be used in chemistry to study specific interactions between SAM and nanoparticle interfaces on patterned substrates, in biology for sensors, and in physics for photonic crystals as well as for data storage. Specific attachment of functionalized particles has already been studied, but typically on micrometer scale patterns employing micrometer-sized particles.[11,12] Also the deposition of non-functionalized particles has been studied, again using micrometer-scale patterns.[13]

Several methods exist to pattern SAMs, the most known being microcontact printing[14] and dip-pen nanolithography,[15] which employ the transfer of an ink to the substrate, while classical top-down techniques, such as electron-beam lithography (EBL) and photolithography, have also been used either by using the polymer template[16] or by local modification of the end-group functionality of the SAM upon irradiation.[17] These top-down methods have been mainly used for silanes on silicon oxide because silanes are difficult to be patterned by microcontact printing. This difficulty is due to the tendency of silanes to polymerize in the presence of water from the environment. Combination of electron-beam lithography and gas-phase silanation gives good results but EBL is time consuming and expensive. Therefore another soft lithography technique was chosen to pattern silane-based SAMs, namely nanoimprint lithography (NIL).[18]

In NIL, a hard stamp (e.g. a patterned Si wafer) is pressed against a substrate covered with a thin layer of polymer. First, sample and stamp are heated above the glass transition temperature (T_g) of the polymer and then pressure is applied. After cooling down the system below the glass temperature of the polymer, the pressure is released and the stamp is removed. Features of the stamp are thus transferred into the polymer.

A thin residual layer of polymer remains, which can be removed in an etching step. This method allows patterning in 3D with feature sizes down to 6 nm.[19] Using this technique, designs of rather arbitrary shape and aspect ratios up to 5 can be molded into the polymer by choosing adequate experimental conditions such as temperature, pressure, and imprint time. The resolution of NIL is limited by the stamp resolution and by the polymer properties when imprinting features below 10 nm. This technique is characterized by its high resolution, low cost, and high throughput.[20] It has been widely used in physics for electronic and photonic applications,[21,22] in biology,[23] and, to a lesser degree, in chemistry.[24]

This chapter presents the use of NIL and self-assembly to produce patterned SAMs of silanes with different end-group functionalities on SiO_2. The patterned SAMs were characterized with various methods. Patterned SAMs have been used to create arrays of functionalized nanoparticles, directed by the SAM endgroup functionality. Results using micrometer and sub-micrometer-sized patterns and functionalized particles (polystyrene and silica) with dimensions down to 50 nm are shown.

3.2 Results and discussion

3.2.1 Process

The polymer pattern, produced by NIL followed by residual layer removal, was used as a mask to evaporate a silane from the gas phase onto the uncovered regions. The polymer was removed and in some cases a second gas phase functionalization with a different silane was performed. The SAM patterns were transformed into patterns of functionalized particles by means of the interaction between the functional groups of the SAM and those of the particles Metal evaporation on patterned SAMs and subsequent lift-off have also been performed to show the possibility of further applications in molecular electronics. These processes are summarized in Scheme 1.

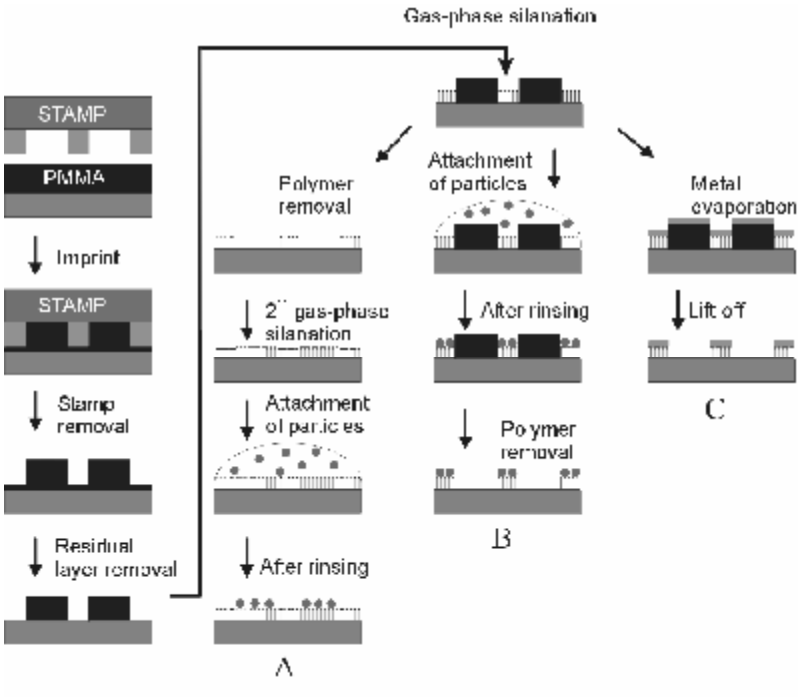

Scheme 1. *Schematic representations of the NIL process and of three applications after SAM patterning. A) Evaporation of a second type of silane after mask removal and attachment of functionalized particles. B) Attachment of functionalized particles using the polymer template, followed by polymer removal. C) Metal evaporation followed by metal lift-off.*

3.2.2 Nanoimprint lithography

Imprinted structures obtained after the NIL process are complementary to the shape of the features of the stamp used. Several stamps with features down to 50 nm were fabricated by e-beam lithography and RIE. Another type of stamp was produced using shadow mask lithography by means of a nanostencil. Some of the stamp designs are shown in Figure 1a-e, including dots, lines, protruding squares, lines, and grids.

For Figures 1a-e the stamp height was 140 nm. The defects observed in some cases were produced during the etching process. Fig 1f shows a stamp produced using a nanostencil with 300 nm high features.

SEM images of imprints performed at a temperature of 180 °C and a pressure of 40 bar are shown in Figure 2. Figures 2d-f show imprints after residual layer removal using O_2 plasma. Fig 2f shows imprints made using a stamp fabricated by shadow mask lithography using a nanostencil. The imprints have designs complementary to the ones of the stamps, with positive (protrusions) as well as negative (cavities) patterns. Negative patterns are usually more difficult to reproduce because more polymer flow is involved in the replication process. Figure 2c and d show negative patterns reproduced with fidelity.

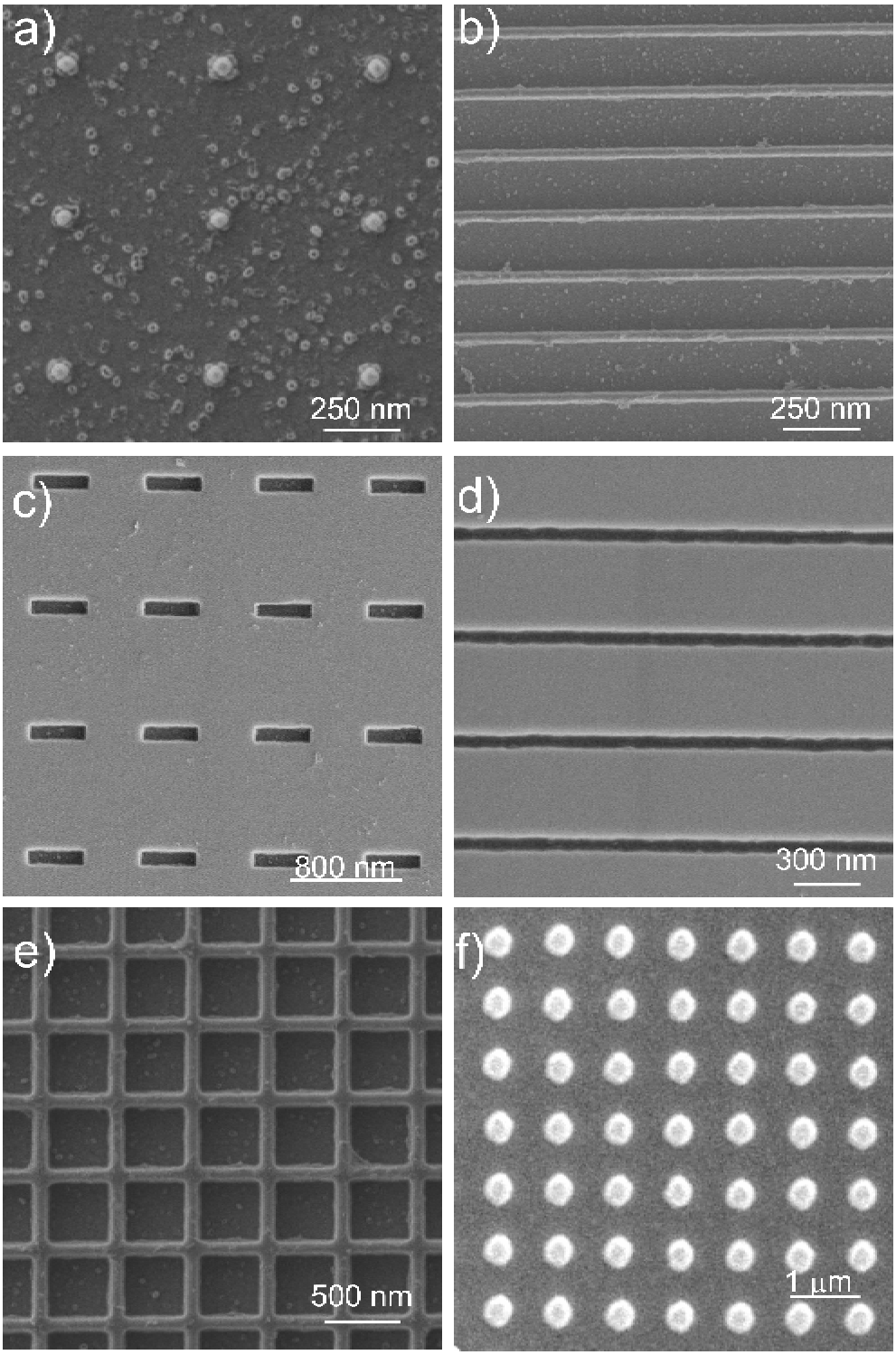

Figure 1. *SEM images of the various designs included in the NIL stamp. The stamp shown from a) to e) were produced by e-beam lithography and RIE while the one shown in f) was produced by shadow mask lithography.*

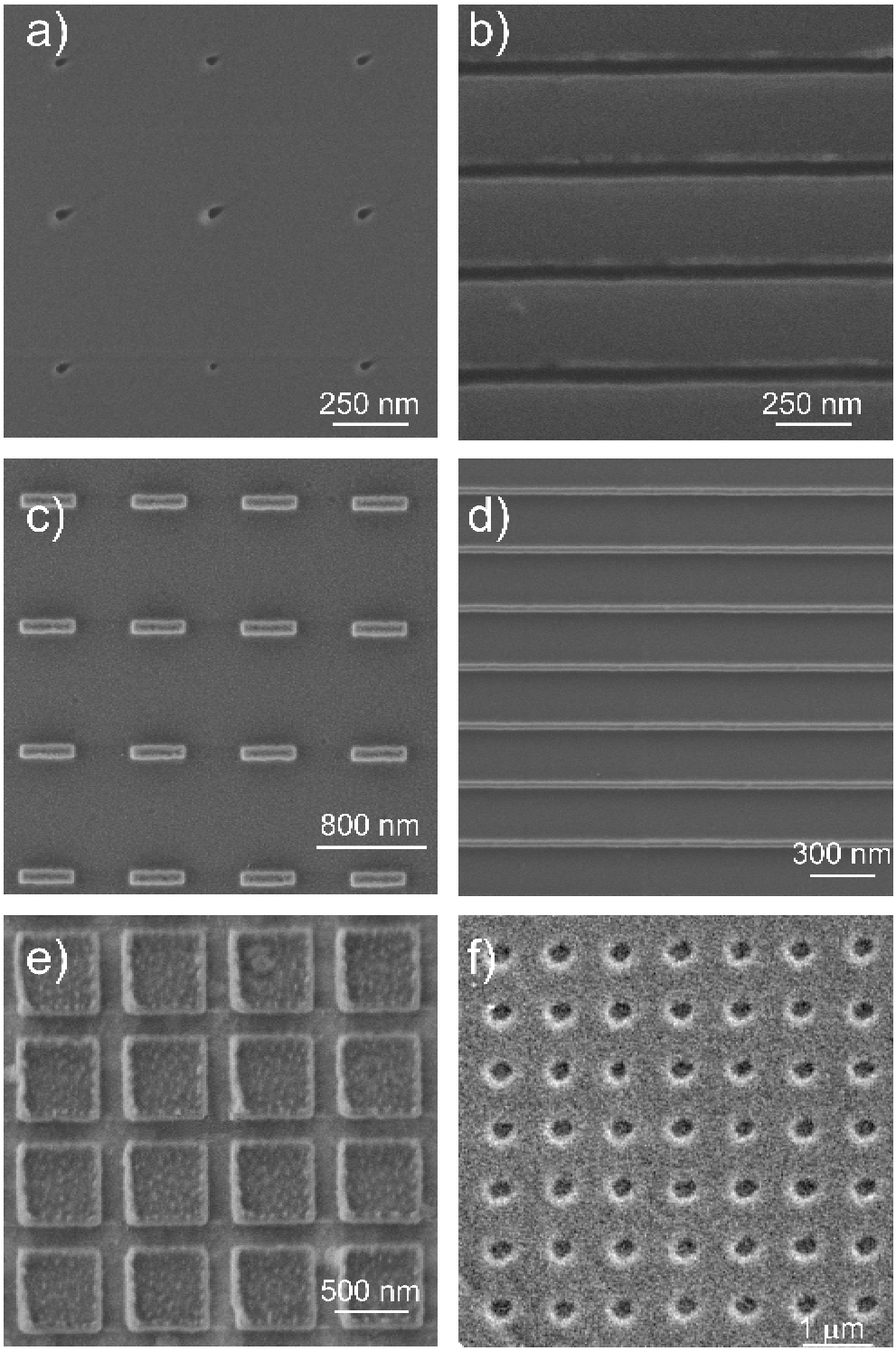

Figure 2. *SEM images of imprints into PMMA made using the stamps shown in Figure 1. The inprints were performed with a heating temperature of 180 °C and a pressure of 40 bar.*

3.2.3 Monolayer patterning using NIL

Gas-phase deposition of silanes was chosen to form the monolayers to avoid damaging the polymer templates e.g. by swelling in a solvent. For making unpatterned reference samples, SiO_2 substrates were prepared by cleaning them in piranha, thoroughly rinsing with Millipore water and drying in a N_2 flow. After cleaning, the substrates and a drop of silane were placed in a dessiccator in which and vacuum was depressurized. After several hours, the dessiccator was vented and the substrates were cleaned, using ultrasonication in acetone during 1 min and subsequently in ethanol during 1 min, and finally dried in a N_2 flow. Samples were characterized using contact angle goniometry, ellipsometry, XPS and AFM. Ellipsometry data showed that 2 h was enough to form a monolayer. The AFM pictures, Figure 3, show that the SAMs are smooth, with a roughness of 0.5 nm for amino- and methyl-terminated monolayers. A scratch made by the AFM tip allowed measuring the height of the monolayer, which was found to be 1.1 nm in agreement with the known height of the SAM.

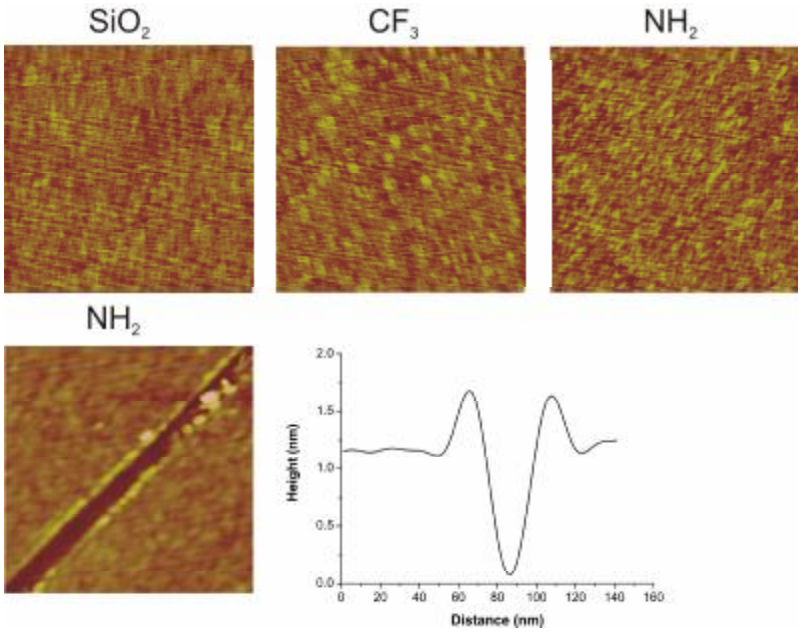

Figure 3. *Tapping mode height AFM images of a silicon oxide substrate and of methyl- and amino-terminated monolayers formed from the gas phase. A scratch was made by an AFM tip to measure the height of the amino monolayer.*

For the preparation of NIL-patterned SAMs, a 400 nm thick layer of PMMA (MW 350 kD) was deposited on silicon oxide substrates by spin coating (see Scheme 1, left column). NIL was performed at a pressure of 40 bar and a temperature of 180 ºC. The residual layer was removed either by O_2 plasma etching or by dipping the samples in acetone for 60 s. Figure 4 shows AFM images of a NIL-patterned substrate before and after residual layer removal by dipping in acetone for 60 s. The height profile shows a decrease of the FWHM of about 800 to 600 nm, consistent with the isotropic polymer dissolution process. The figure shows, however, that the imprinted lines after residual layer removal are still rectilinear and that the linewidths of the exposed areas after residual layer removal are comparable to the spacing between the tops of the polymer patterns before residual layer removal,[25] which can also be obtained by anisotropic etching.

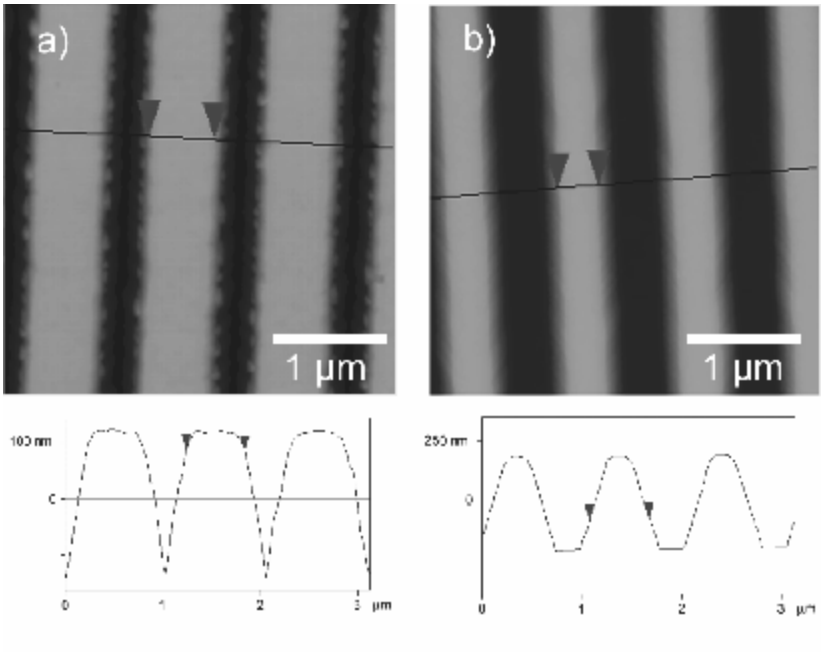

Figure 4. *Contact mode height AFM images of an imprint before (a) and after residual layer removal (b) by dipping the imprint in acetone for 60 s. The marks on the cross sections of the height images indicate widths of 800 and 600 nm respectively.*

The residual layer was removed in acetone because dry etching, which is the usual method to remove the residual layer, can cause damage to the substrate.[26] In an O_2 plasma process, even for an exposure of only few seconds, bombarding with ions can slightly modify the height of the exposed silicon as well as increase the hydrophilic nature of the substrate.[27] For example, structures with a typical height of 1.5 nm were found after O_2 plasma etching and some contrast in the AFM friction images could be seen. Therefore, AFM studies of SAM formation on the exposed parts of the imprinted substrates would be difficult to analyze when using plasma etching.

AFM images of a NIL-patterned sample after residual layer removal in acetone, followed by complete polymer removal showed differences neither in height nor in friction. An XPS spectrum of the same sample showed a clean silicon substrate with low carbon content, identical to a blank unprocessed silicon wafer cleaned in piranha, see Figure 5. Therefore, this proves that the polymer can be completely removed and that the method used here for removal of the residual layer did not lead to surface changes of the substrate.

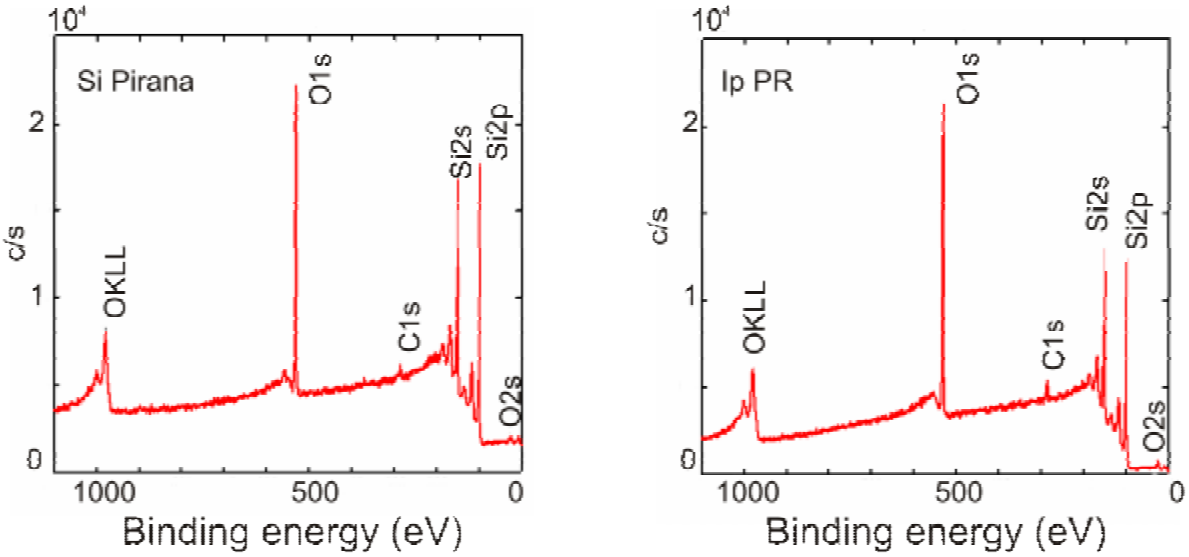

Figure 5. *XPS spectra of a substrate after cleaning with piranha (left) and after imprint and polymer removal (right).*

Imprints were performed on PMMA films deposited on silicon substrates treated with piranha in order to produce an oxidized surface necessary for the covalent attachment of the silanes. Different kinds of silanes, with CF_3-, NH_2-, Br-, and CH_3-terminal groups respectively, were deposited to modify the outer surface of the NIL-patterned substrates. The polymer left after imprinting and removal of the residual layer acts as a mask for gas-phase evaporation of the silane adsorbates. Finally, the polymer was removed in acetone using ultrasonication.

Figure 6 shows AFM images of an array of fluoroalkyl SAM lines of 5 µm width at a 15 µm period (Figure 6a and b) and aminoalkyl SAM lines of 400 nm width at a 1 µm period (Figure 6c and d). The SAMs have formed at the complementary areas of the NIL patterns. The quality of the patterned SAMs was found to be the same as on non-patterned SAM blanks.

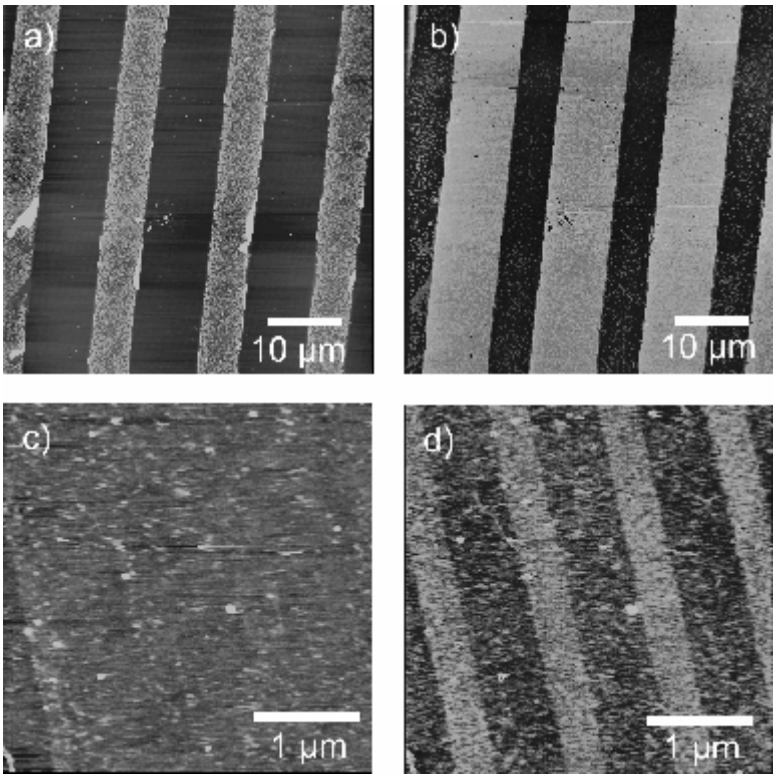

Figure 6. *Contact mode height (a, c) and friction (b, d) AFM images of 5 mm fluoroalkyl SAM lines at 15 mm period (a, b) and of 400 nm aminoalkyl SAM lines at 1 mm period (c,d) on NIL- patterned substrates followed by SAM formation and polymer removal. In the friction images, brighter areas indicate higher friction.*

The measured height of the patterned layer, when investigating large patterns (5 µm lines), was found to correspond to the height of a monolayer. In the case of small patterns, such as Figure 6c, the height was hard to measure accurately, probably due to contamination of the sample.

In the case of the NH_2-terminated monolayer, a higher friction force was observed relative to the substrate (Figure 6d), in agreement with the hydrophilic nature of this silane adsorbate. In contrast, for the hydrophobic monolayers such as CF_3-terminated SAMs (Figure 6b), and CH_3- and Br-terminated monolayers (not shown), lower friction forces were observed relative to the substrate (Table 1).

Table 1*. Advancing and receding water contact angles on unpatterned SAMs, monolayer thickness (measured by contact mode AFM) and relative friction forces on patterned SAMs. Patterned samples were prepared by forming a SAM on a NIL patterned substrate, followed by polymer removal.*

Adsorbates	q_{adv}/q_{rec}	**Height (nm)**	**Friction force**
N-[3-(trimethoxysilyl)propyl]-ethylenediamine	65/20	0.8	High
dodecyltrichlorosilane	109/89	0.7	Low
bromoundecyltrichlorosilane	101/83	0.7	Low
1H,1H,2H,2H-perfluorodecyltrichlorosilane	117/76	3.4	Low

Figure 7 shows AFM height (left) and friction (right) images of an array of fluoroalkyl SAM lines of about 150 nm width at a period of 500 nm (top) as well as an array of dots of about 125 nm diameter at a period of 500 nm (bottom). It shows that this process still works for creating silane SAM patterns with dimensions close to 100 nm. The observed edge roughness of several 10s of nm can be attributed not only to the process (mainly to the quality of the stamp, but possibly also to non-optimized imprint parameters and the isotropic residual layer removal), but also to the difficulty of imaging such samples using AFM.

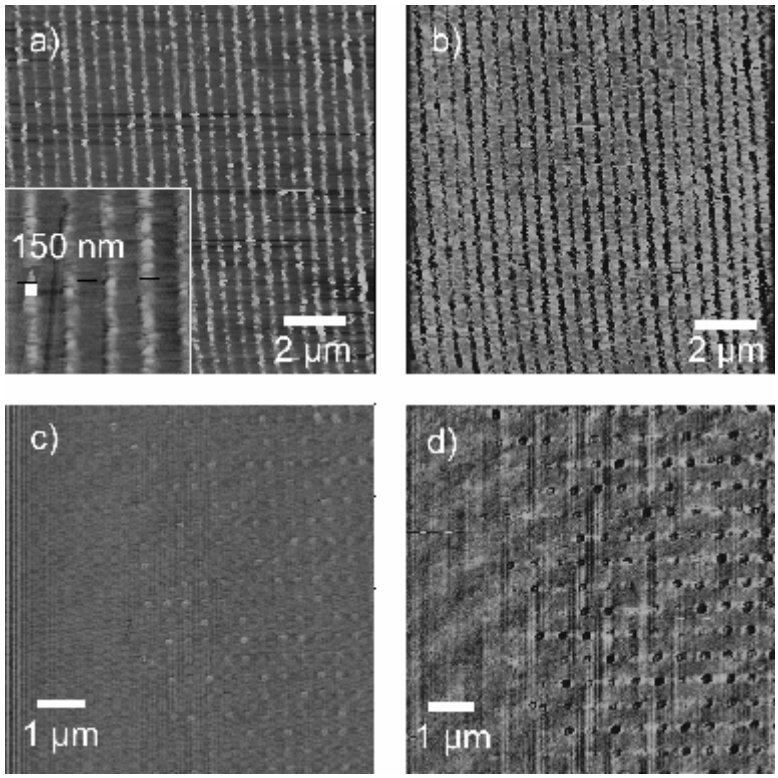

Figure 7. *Contact mode height (a, c) and friction (b, d) AFM images of fluoroalkyl SAM lines (a, b) and dots (c, d). The lines are 150 nm width at a period of 500 nm while dots are 125 nm in diameter with a period of 500 nm. Brighter areas in the friction images indicate higher friction.*

XPS imaging of fluoroalkyl SAMs patterned by NIL (Figure 8) showed the presence of fluorine only in the areas imprinted by NIL and thus free for SAM formation. Partial spectra of F_{1s} and C_{1s} in and outside the squares prove the selectivity of the SAM formation process because they show the presence of F and C-F peaks respectively in the squares while they are absent outside them. Thus, these results confirm that SAM formation occurred exclusively in the NIL-patterned areas.

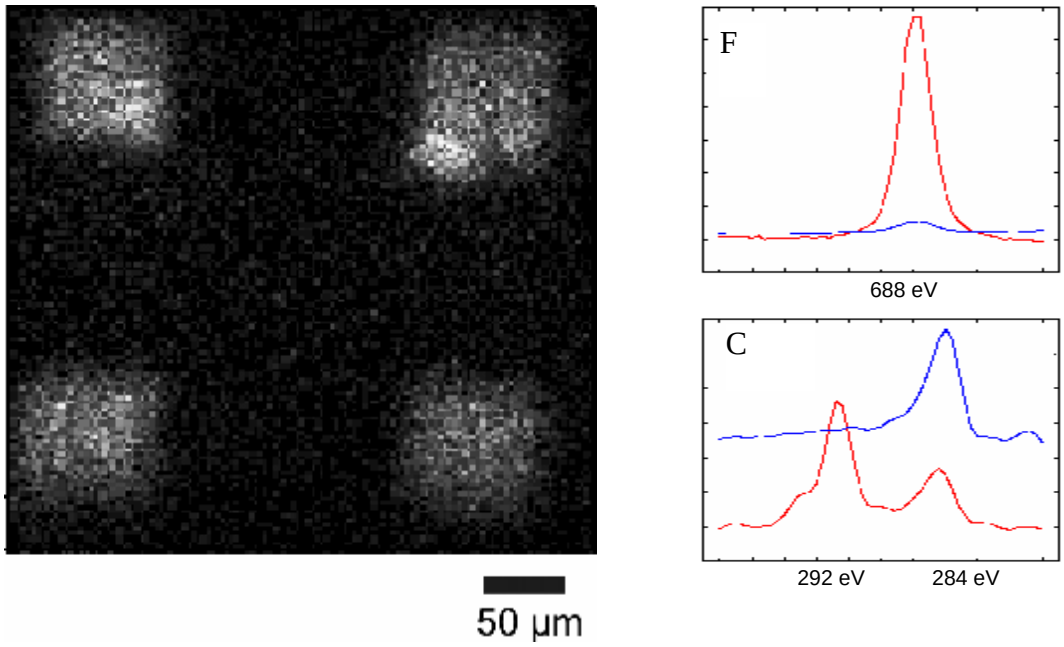

Figure 8. *XPS F mapping of 100 mm fluorinated SAM squares and partial spectra made inside (red) and outside (blue) a square. The sample was prepared by imprinting an array of squares followed by residual layer removal. A fluoroalkylsilane was evaporated on the sample and the polymer was removed in acetone by ultrasonication.*

NIL-patterned SAMs after polymer removal were subjected to evaporation of a second silane adsorbate (Scheme 1, path A). As a result, the substrate was chemically patterned with two different kinds of SAMs. Figure 9 shows height (a) and friction (b) AFM images of a sample patterned with an alkyl SAM. Shown in the same figure are the height (c) and friction (d) AFM images of the same sample after subsequent formation of an aminoalkyl SAM in the remaining free areas. For the first silanation, a higher friction force was observed on the substrate than on the alkyl SAM. After the second silanation, the friction was higher on the aminoalkyl SAM than on the alkyl SAM, in agreement with the hydrophilic nature of the respective SAMs, see Table 1.

Evaporation of the aminoalkyl silane on the 150 nm fluoroalkyl SAM lines and 125 nm dots (see Figure 7) led to similar results. Assuming that gas-phase adsorption of silanes is not limited by the size of the imprinted features, the resolution of SAM patterning using NIL is thus only limited by the resolution of NIL itself.

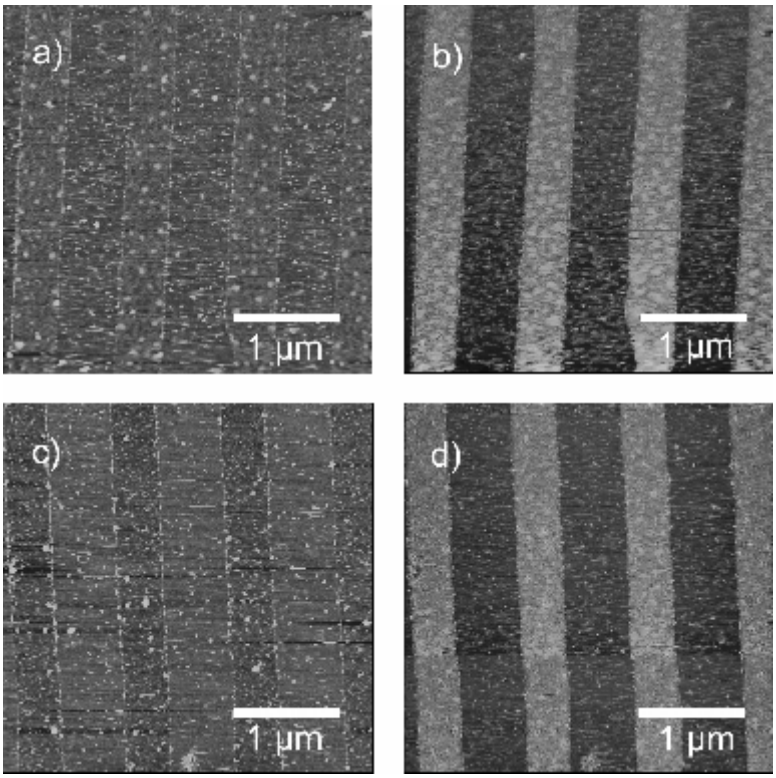

Figure 9. *Contact mode height (a, c) and friction (b, d) AFM images of a substrate patterned with 600 nm alkyl SAM lines at 1 mm period, made using NIL (a, b); and after subsequent evaporation of an aminoalkylsilane (c, d).*

3.2.4 Deposition of nanoparticles on NIL-patterned SAMs

Carboxylate-functionalized nanoparticles were chosen for electrostatic attachment on the aminoalkyl SAMs after protonation. Protonation of the aminoalkyl monolayer was performed by rinsing the sample with a MES buffer (pH = 5.6). Two kinds of functionalized particles were attached by drop casting: i) 50 nm silica particles functionalized with carboxylic acid groups,[28] and ii) 350 nm polystyrene (PS) beads functionalized with carboxylic acid groups. Particles were adsorbed on NIL-patterned aminoalkyl SAMs without removal of the polymer. The polymer behaves as a physical barrier to prevent the deposition of particles on the protected areas (see Scheme 1, path B). Figure 10 shows SEM images of 350 nm carboxylate-functionalized PS beads attached on an aminoalkyl SAM formed on a NIL-patterned substrate. The PS beads attached preferentially to the aminoalkyl SAM. In Figure 10a, the ordered PS beads indicate that wetting of the pattern by the suspension is not a problem, as the particles show the characteristic zigzag arrangements caused by a line width between d and $2d$ (where d is the diameter of the particles).[13] In Figure 10b, the ordered and packed beads seem to center at the SAM line. This is probably due to the drying process under N_2 flow.

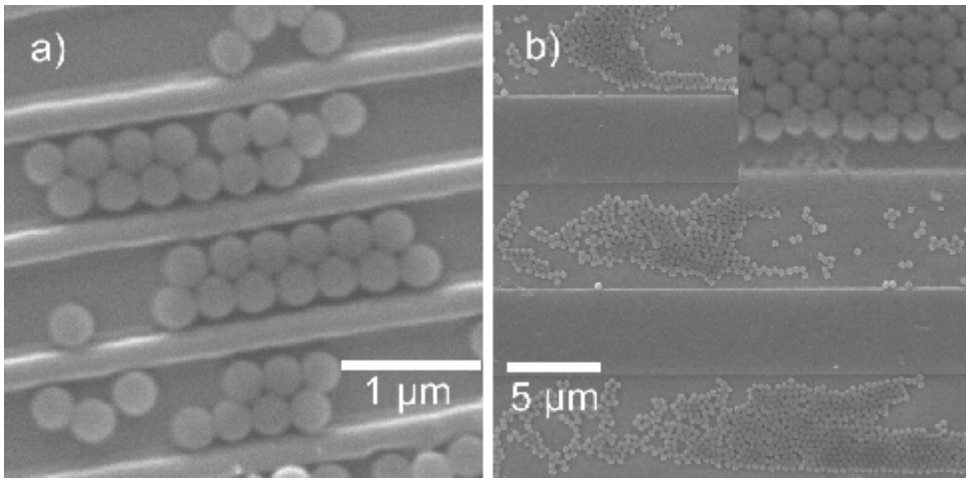

Figure 10. *SEM images of 350 nm carboxylate-functionalized PS beads adsorbed to the 700 nm and 5 mm aminoalkyl SAM lines prepared by NIL followed by silane adsorption. The inset is a close-up showing close-packed PS beads.*

Figure 11 shows SEM images of silica particles attached on the aminoalkyl SAM areas of a NIL-patterned sample, after subsequent removal of the polymer. This was not attempted for PS beads, since PS beads may dissolve in acetone while removing the mask. When silica particles were used, the polymer template could be removed in acetone because silica particles do not dissolve in acetone. Comparison with SEM pictures made before polymer removal (not shown) showed no damage of the particle pattern. Dense packing of the particles was observed for all patterns independently of the linewidth. Places initially covered by the polymer were found to be free of particles. However, the edges of the patterns are not well defined due to drying phenomena as described above.

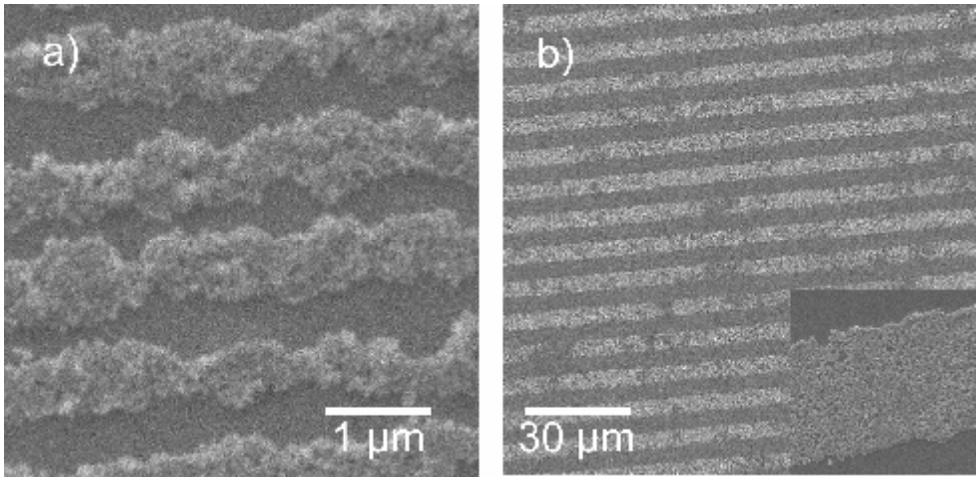

Figure 11. *SEM image of 50 nm carboxylate-functionalized silica particles adsorbed to 700 nm (a) and 5 mm (b) aminoalkyl SAM line; the polymer template was removed afterwards. The inset shows a close-up of close-packed silica particles.*

The advantage of the current process is that the chemical SAM pattern allows for attachment of particles, and possibly also molecules and proteins, onto the SAM areas while the polymer template masks the remainder of the surface. This method can be compared to Template-Assisted Self-Assembly (TASA)[29,30] that uses a template to assemble monodispersed colloids into organized structures by capillary forces. The difference is that in the method presented here, the particles are electrostatically attached to the monolayer and thus the template can be removed after attachment of the particles. Another advantage is that a second monolayer can be formed on the substrate and attachment of e.g. another kind of particle can be performed.

Alternatively, particle adsorption was performed on substrates patterned with two adsorbates (Scheme 1, path A). As described above, an alkyl SAM was formed on a NIL-patterned substrate followed by polymer removal. Increasing the immersion time in acetone, while removing the residual layer, allowed to reduce the width of the polymer lines obtained after NIL.

After complete removal of the polymer, a second adsorbate, an aminoalkyl SAM, was attached to the areas previously protected by polymer. Finally, carboxylate-functionalized particles were electrostatically attached to the sample (See Scheme 1, path A). Figure 8 shows a SEM image of carboxylate-functionalized silica particles attached to the aminoalkyl SAM areas, which are in this case only 200 nm wide. The parts corresponding to the alkyl SAM appear clean of particles. Carboxylate-functionalized silica particles were densely packed and matched closely the dimension of the aminoalkyl SAM areas, as it can be noted that the edges of the lines are relatively well defined. A height of 50 nm was measured by AFM which corresponds to a monolayer of particles. Close-packed particles can be observed in the inset of Figure 12. Additionally, 350 nm PS carboxylate-functionalized beads were used and selective attachment on the aminoalkyl SAM was observed as well (images not shown). CF_3- and CH_3- terminated monolayers showed the same properties with respect to attachment of particles. Namely, particle attachment on CF_3/NH_3^+-terminated SAMs was found to be as selective as on CH_3/NH_3^+-terminated SAMs patterns. The selectivity of particle attachment did not change with pattern sizes. High selectivity was obtained for both silica particles and PS beads, as no particles can be seen on the alkyl SAM parts. The main advantages of the chemical patterning over the usual template patterning of arrays of particles are that the liquid can wet very well the pattern as there are no physical barriers to prevent it and there is no risk of introducing disorder in the array of particles while removing the template.

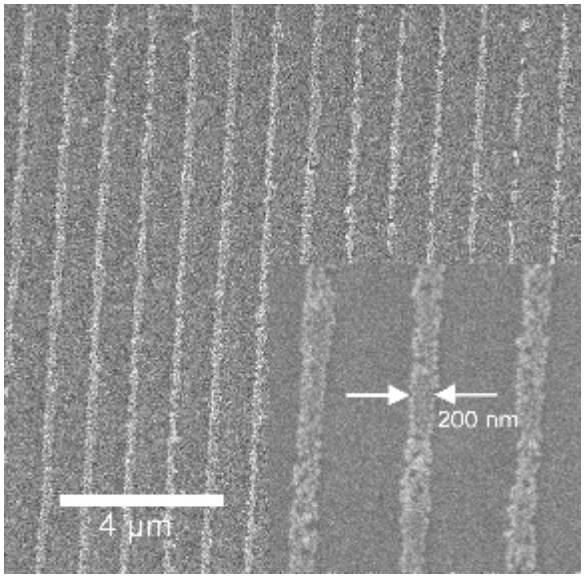

Figure 12. *SEM image of 50 nm carboxylate-functionalized silica particles adsorbed to a NIL-patterned aminoalkyl SAM (300 nm wide lines), the complementary pattern (700 nm wide lines) corresponding to an alkyl SAM region. The inset shows a close-up of a close-packed area.*

3.2.5 Towards molecular devices

NIL-patterned substrates are three-dimensional in contrast to the quasi two-dimensional nature of a patterned SAM. One of the advantages of using NIL to pattern SAMs is that the remaining patterned polymer can be used for additional microelectronic processes such as metal lift-off. In order to demonstrate the feasibility of this process (Scheme 1, path C), an aminoalkyl monolayer was formed on an imprint and a 10 nm-thick layer of gold was evaporated on top. The polymer was removed in acetone by ultrasonication. Figure 13a shows an AFM image of gold lines obtained with this process. The metal sticks well on the top of the monolayer after lift-off, which can be used later as a top-electrode. A line thickness of 12 nm was extracted from the height profile of the AFM image that corresponds to the thickness of the evaporated gold.

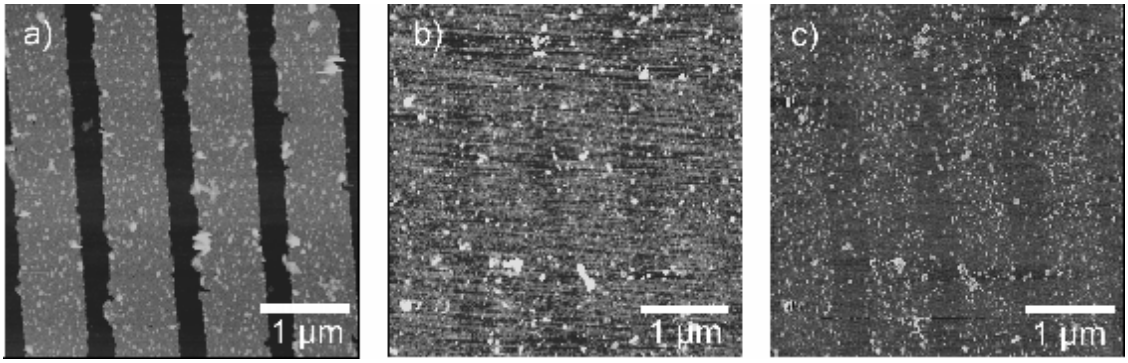

Figure 13. *Contact mode height (a, b) and friction (c) AFM images of 800 nm lines prepared by NIL and evaporation of an aminoalkyl silane in the vacant areas, followed by evaporation of a 10 nm-thick film of Au and the subsequent removal of the polymer in acetone and ultrasound before (a) and after (b, c) wet etching of the gold layer.*

Thereafter, the gold layer was etched using a wet-etching solution. Figures 13b and c show the same sample as in Figure 13a, after 6 min in a solution of $Na_2S_2O_3$ (0.1 M), KOH (1.0 M), $K_3Fe(CN)_6$ (10 mM), and $K_4Fe(CN)_6$ (10 mM). The 800 nm width of the aminoalkyl SAM is retrieved, in height (Figure 13b) as well as in friction (c). This suggests that the monolayer remains after gold evaporation and lift-off. This experiment shows that an aminoalkyl SAM can be an alternative to the commonly used titanium adhesion layer to deposit gold on silicon oxide. This can be employed in the fabrication of hybrid electronic devices such as organic field-effect transistors (OFETs) because the use of a titanium adhesion layer generally diminishes the injected current from the metal contacts to the organic semiconductor layer at the substrate interface where charge transport takes place.[31]

Additionally, a simplified fabrication procedure can be achieved considering that a silane monolayer is generally grown on the substrate in the region between the contacts to make the organic semiconductor compatible with the inorganic substrate.[32] The experiment also shows that molecular electronic devices can be made by multiprocessing i.e. combining self-assembly and NIL when using SAM containing functional groups.

3.3 Conclusions

In conclusion NIL was shown to be a soft lithography method that can be used for chemical patterning of silicon oxide substrates with a single monolayer as well as binary monolayers. A large range of monolayers with different end-groups can be used. This method allows to pattern with a high resolution on large areas. Patterns close to 100 nm have been demonstrated here, which would be very difficult and/or very expensive to produce otherwise.

Initial results in the use of such patterns in nanoparticle deposition have been shown. Both substrates with the polymer patterns still maintained and substrates with binary SAMs have been employed. Whereas the polymer patterns of the former can function as physical barriers resisting adsorption while the SAM directs the adsorption to the complementary areas, it is clear that drop casting causes imperfect particle patterns, although this could potentially be solved using other deposition strategies, see Chapter 4. Nevertheless, the advantage of using a functional SAM to direct the particle deposition is clearly shown by the fact that the polymer can be removed afterwards while retaining the particle assemblies. In contrast, the binary SAM samples have the advantage of eliminating such wetting problems. The potential of using SAMs is shown here even more powerful, as the deposition selectivity can be close to perfect.

Thus, this rather simple stepwise process allows the fabrication of sub-micrometer chemical patterns, which can be either followed by metal lift-off, or can be used for selective attachment of sub-micrometer functionalized particles onto them by drop casting. The accurate control of the position of particles at sub-micrometer range can potentially be applied to chemical studies of specific interactions between SAM and nanoparticle interfaces, to photonic crystals, and to memory devices.

3.4 Experimental Section

Compounds

1H,1H,2H,2H-perfluorodecyltrichlorosilane, dodecyltriethoxysilane (from ABCR), N-[3-(trimethoxysilyl)propyl]-ethylenediamine (Aldrich), dodecyltrichlorosilane (Acros), bromoundecyltrichlorosilane (Gelest) and PMMA (MW 350 kD, Aldrich) were used. Carboxylate-functionalized PS beads in aqueous suspension (350 nm diameter) were obtained from Polyscience Inc. The fabrication of 50 nm carboxylate-functionalized silica particles by Dr. Venkataraman Mahalingam has been described elsewhere.[28]

Analysis

The quality and reproducibility of the gas-phase evaporation were investigated by water contact-angle goniometry, ellipsometry, AFM, and XPS. Water contact angle measurements and ellipsometry were performed on a large number of samples, before and after ultrasound of 20 min. Contact angles were determined using a Krüss Contact Angle Measurement System G 10, and the data processed with the program Drop Shape Analysis 1.51. In the case of unpatterned films, the monolayer thickness was measured by opening a trench on the monolayer by means of the AFM tip.

Quantitative surface elemental analysis and spatial localization were performed. XPS was performed on patterned SAM using a PHI Quantera Scanning ESCA Microprobe. Samples were investigated using an atomic force microscop AFM Nanoscope III (Veeco, Digital Instruments, USA) in contact mode equipped with a Si_3N_4 tip with a J scanner at a scan rate of 1.5 Hz. SEM investigation was performed with a JEOL 5610. In the case of PS beads attachment, the sample were covered with 5 nm of Au to facilitate SEM observation.

NIL

The stamps were made by photolithography followed by reactive ion etching (RIE, Elektrotech Twin system PF 340) or by e-beam lithography followed by titanium evaporation and lift-off. They consisted of gratings composed of 400 nm wide lines at 1 μm period, 5 μm lines at 10 μm period, 5 μm lines at 15 μm period with a height of 300 nm. A second type of stamps contained 150 nm wide lines at a period of 500 nm and 125 nm dots at a period of 500 nm with a height of 85 nm. A 1H,1H,2H,2H-perfluorodecyltrichlorosilane was used as an anti-adherent layer to facilitate the stamp-imprint separation. Silicon substrates were oxidized first by immersion in piranha solution (concentrated H_2SO_4 and 33% aqueous H_2O_2 in a 3:1 ratio. **Warning**! piranha should be handled with caution; it is known to detonate unexpectedly) for 15 min (SiOx thickness 1.5 nm) and then covered with a 400 nm thick layer of PMMA by spin coating. Stamp and substrate were put in contact and a pressure of 40 bar was applied at a temperature of 180 ºC using a hydraulic press (Specac). The residual layer was removed by dipping the samples in acetone during 60 s or by O_2 plasma during 20 s using a RIE system.

The imprints consisted then in 10 μm polymer lines at 15 μm period, 5 μm polymer lines at 10 μm and 600 nm polymer lines at 1 μm period. When necessary, the polymer template was removed in acetone and ultrasound during 2 h. The imprint cycle time was 20 min and the imprinted area was 2×2 cm^2. The stamps were changed approximately every 50 imprints.

SAM formation

The gas-phase evaporation of silanes was performed in a desiccator under vacuum. The samples were left several hours or overnight and then carefully rinsed with ethanol and Millipore water.

Nanofabrication

Samples were rinsed with 4-morphilineethanesulfonic acid monohydrate (MES, pH = 5.6) buffer. Particle attachment was performed using a suspension of either 50 nm carboxylate-functionalized silica particles or 350 nm carboxylate-functionalized PS beads. Attachment was performed by casting a drop of the suspension on the substrate and leaving it to dry for 1 h. Samples were placed in a standing position in the suspension to avoid non-specific interactions induced by gravity. Samples were then copiously rinsed with high purity water and carefully dried in a N_2 flow.

A 10 nm layer of gold was evaporated using a metal evaporator BAK 600 in a vacuum of 1×10^{-6} mbar. The metal lift-off was made in acetone and ultrasound. For the wet etching of gold, the sample was immersed during 6 min in gold wet-etching solution ($Na_2S_2O_3$ (0.1 M), KOH (1.0 M), $K_3Fe(CN)_6$ (10mM), and $K_4Fe(CN)_6$ (10 mM), etching rate: ~3 nm/ min).

3.5 References

[1] B. Michel, A. Bernard, A. Bietsch, E. Delamarche, M. Geissler, D. Juncker, H. Kind, H.; J. P. Renault, H. Rothuizen, H. Schmidt, P. Schmidt-Winkel, R. Stutz, H. Wolf, *IBM J. Res. Dev.* **2001**, *45*, 697.
[2] N. Abbot, A. Kumar, G. M. Whitesides, *Chem. Mater.* **1994**, *6*, 596.
[3] N. J. van der Veen, S. Flink, M. A. Deij, R. J. M. Egberink, F. C. J. M. van Veggel, D. N. Reinhoudt, *J. Am. Chem. Soc.* **2000**, *122*, 6112.
[4] C. Zhou, M. R. Deshpande, M. A. Reed, *Appl. Phys. Lett.* **1997**, *71*, 611.
[5] Y. Chen, D. A. Ohlberg, X. Li, D. R. Stewart, J. O. Jeppesen, K. A. Nielsen, J. F. Stoddart, D. L. Olynick, E. Anderson, *Appl. Phys. Lett.* **2003**, *82*, 1610.
[6] H. Zhu, M. Snyder, *Curr. Opin. Chem. Biol.* **2003**, *7*, 55.
[7] G. Kaltenpoth, M. Himmelhaus, L. Slansky, F. Caruso, M. Grunze, *Adv. Mater.* **2003**, *15*, 1113.
[8] I. Lee, H. Zheng, M. F. Rubner, P. T. Hammond, *Adv. Mater.* **2002**, *14*, 572.
[9] V. Santhanam, R. P. Andres, *Nano Lett.* **2003**, *4*, 41.
[10] T. Auletta, B. Dordi, A. Mulder, A. Sartori, S. Onclin, C. M. Bruinink, M. Péter, C. A. Nijhuis, H. Beijleveld, H. Schönherr, G. J. Vancso, A. Casnati, R. Ungaro, B. J. Ravoo, J. Huskens, D. N. Reinhoudt, *Angew. Chem. Int. Ed.* **2004**, *43*, 369.
[11] C. Fustin, G. Glasser, H. W. Spiess, U. Jonas, *Adv. Mater*. **2003**, *15*, 1025.
[12] Y. Masuda, M. Itoh, T. Yonezawa, K. Koumoto, *Langmuir* **2002**, *18*, 4155.
[13] Y. Xia, Y. Yin, Y. Lu, J. McLellan, *Adv. Funct. Mater.* **2003**, *13*, 907.
[14] Y. Xia, G. M. Whitesides, *Angew. Chem. Int. Ed.* **1998**, *37*, 550.
[15] R. D. Piner, J. Zhu, F. Xu, S. Hong, C. A. Mirkin, *Science* **1999**, *283*, 661.
[16] A. Pallandre, K. Glinel, A. M. Jonas, B. Nystem, *Nano Lett.* **2004**, *4*, 365.
[17] A. Golzhauser, W. Eck, W. Geyer, V. Stadler, T. Weimann, P. Hinze, M. Grunze, *Adv. Mater.* **2001**, *13*, 806.
[18] S. Y. Chou, P. R. Krauss, P. J. Renstrom, *Science* **1996**, *272*, 85.
[19] S. Y. Chou, P. R. Kraus, *Microelectron. Eng.* **1997**, *35*, 237.
[20] C. M. Sotomayor Torres, *Alternative Lithography*, Kluwer Academic Publ. **2004**.
[21] W. Wu, J. Gu, H. Ge, C. Keimel, S. Y. Chou, *Appl. Phys. Lett.* **2003**, *83*, 2268.
[22] Z. Yu, P. Deshpande, W. Wu, J. Wang, S. Y. Chou, *Appl. Phys. Lett.* **2000**, *77*, 927.
[23] G. D. Bachand, R. K. Soong, H. P. Neves, A. Olkhovets, H. G. Craighead, C. D. Montemagno, *Nano Lett.* **2001**, *1*, 42.
[24] M. D. Austin, S. Y. Chou, *Nano Lett.* **2003**, *3*, 1687.
[25] When the immersion time in acetone was extended, the lateral dissolution of PMMA produced a reduction of the width of the polymer lines (e.g. from 600 nm to 200 nm in 90 s).
[26] C. H. Chen, J. P. Ibbetson, E. L. Hu, U. K. Mishra, *Appl. Phys. Lett.* **1997**, *71*, 494.
[27] A. Szekeres, S. Alexandrova, K. Kirov, *Phys. Stat. Sol.* **1980**, *62*, 727.
[28] V. Mahalingam, S. Onclin, M. Péter, B. J. Ravoo, J. Huskens, D. N. Reinhoudt, *Langmuir* **2004**, *20*, 11756.
[29] Z.-Z. Gu, A. Fujishima, O. Sato, *Chem. Mater.* **2002**, *14*, 760.
[30] Y. Yin, Y. Xia, *J. Am. Chem. Soc.* **2001**, *123*, 771.
[31] R. A. Street, A. Salleo, *Appl. Phys. Lett.* **2002**, *81*, 2887.
[32] Charge injection through metal-organic semiconductor junctions is determined by the energy difference between the work function of the metal and the relevant molecular orbital of the semiconductor (HOMO or LUMO) both measured relative to

the vacuum level. Most of the stable organic semiconductors reported in the literature are p-type and the HOMO level (e.g. pentacene, activation energy + energy gap = 5.1 eV) for most of them aligns well with the Fermi level of gold (work function = 5.1 eV) leading to the formation of ohmic contacts for hole injection. In contrast, Ti leads to the formation of an energy barrier and the electrodes block injection of holes. T. Li, J. W. Balk, P. P. Ruden; I. H. Campbell, D. L. Smith, *J. Appl. Phys.* **2002**, *91*, 4312.

Chapter 4

Directed Assembly of Nanoparticles onto Polymer Imprinted or Chemically Patterned Templates Fabricated by Nanoimprint Lithography*

4.1 Introduction

Several techniques have been employed to direct the deposition of nanoparticles[1,2,3] in order to produce nanoparticle patterns that fulfill the requirements of order and generic design. One method makes use of topographical templates, made of silicon[4] or a polymer,[5] to confine non-functionalized particles within the pattern. Pattern confinement has been used for instance to obtain special nanoparticle arrangements,[6,7,8] to control lattice and superlattice symmetry,[9,10,11] and to pattern multilayers of particles on both large[12] and small scales.[5] Another method employs self-assembled monolayer (SAM) templates to fabricate chemically patterned substrates. SAMs introduce differences in wettability[13,14] or electrostatic charge[15,16] to direct the particles to the intended areas.

---

* This Chapter has been published in part in: P. Maury, M. Escalante, M. Péter, D. N. Reinhoudt, J. Huskens, *Adv. Mater.* **2005,** *17,* 2718.

For this purpose, microcontact printing (μCP)[16] and scanning probe lithography (SPL)[17] have been used to chemically modify substrates on both large and small scales. Hammond[18,19] has shown an alternative way which consists of a combination of chemical and topographical patterns by printing polyelectrolyte multilayers to direct the positioning of particles. Patterns obtained in any such way can potentially be used for photonic band gap devices,[20,21,22] ionic and biological sensors on surfaces,[23] molecular recognition,[24,25] single electron transistors,[26] and high-density data storage systems.[27]

Nanoparticles have been attached to substrates using immersion in a suspension[15,18] or procedures based on capillary forces exerted on the nanoparticles.[4,16] Among the latter procedures, the so-called meniscus method[2] is popular because of its ease of application and the close packing of the resulting nanoparticles arrays. Close packing of the particles is obtained because of interparticle capillary forces at the drying front of the meniscus and the substrate. To apply this principle to the whole substrate, the meniscus is moved mechanically by using a withdrawing motor[2] or by evaporation of the solvent.[11] Additionally, the number of layers of particles is controlled in part by the meniscus translation rate.

In Chapter 3 an alternative procedure for preparing patterned nanoparticle arrays is demonstrated by combining nanoimprint lithography (NIL),[28] which allows control of the lateral dimensions down to 6 nm,[29] with self-assembly of silanes on silicon oxide in the μm- and sub-μm range to direct the nanoparticle assembly. Although drop-casting of the functionalized nanoparticle suspension on the substrate resulted in high selectivity, the coverage was not homogeneous on the whole surface and only short range order was observed due to a lack of control over the solvent evaporation process.

In this Chapter a multistep process is reported based on the previous nanoimprint procedure in combination with chemically directed nanoparticle assembly by vertical deposition, thus employing the moving meniscus principle to allow versatile patterning of nanoparticles on different types of substrates. In this manner, hexagonal close packing was found on μm-size features, and typical confined particle geometries were observed on sub-μm features. The templates of confined NPs were used as shadow masks for further processes such as metal lift-off and Si etching. These techniques are known as Nanosphere Lithography.

4.2 Results and discussion

4.2.1 Nanoparticle patterning

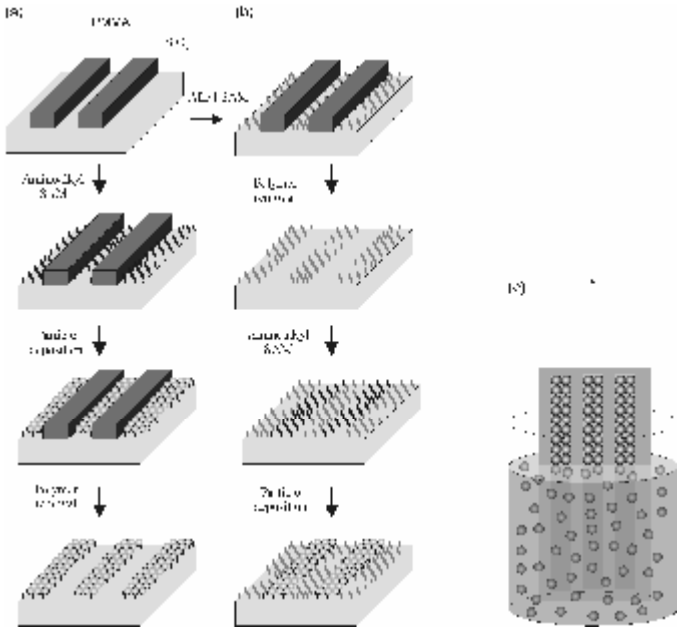

Scheme 1. *Schematic representation of the processes to fabricate patterns of nanoparticles using chemical templates in combination with (a) or without physical barriers (b). The polymer templates were prepared by nanoimprint lithography, SAMs were formed by gas-phase deposition, and nanoparticles were attached using a vertical deposition set-up (c), in which the samples were withdrawn vertically from the nanoparticle suspensions at a constant speed.*

Scheme 1 depicts the multistep nanofabrication process used to produce the two kinds of patterned nanoparticle substrates. NIL was performed on PMMA films spin-coated on silicon oxide substrates. The feature width (W for linewidth and D for hole diameter) varied from 5 μm down to 60 nm in arrays with different periodicities. After removing the residual PMMA layer in O_2 plasma, silane SAMs were deposited from the gas phase onto the unprotected areas of the substrates. Two types of silanes, i.e. an aminoalkylsilane and an alkylsilane, were used. Deposition of the aminoalkyl SAM resulted in substrates which were both topographically and chemically patterned. Alternatively, the substrate was initially functionalized with an alkyl SAM, followed by removal of the PMMA by sonication in acetone, and formation of an aminoalkyl SAM from the gas phase onto the areas previously covered by PMMA. This led to topographically flat, solely chemically functionalized templates.

Figure 1. *Picture of the home made vertical deposition set-up. The withdrawing*

device is shown on the left where the substrate is slowly withdrawn by the step motor on top. The motor speed is reduced by means of a gearbox. The electronic motor controller, power supply and function generator (whose frequency defines the withdrawal speed) are shown on the right.

At this stage both types of substrates were rinsed with a MES buffer (pH = 5.6) in order to protonate the terminal amino groups of the aminoalkyl SAMs to allow selective attachment of carboxylate-functionalized nanoparticles. The topographical and chemical templates thus consisted of positively charged areas (protonated aminoalkyl SAMs) and neutral areas (PMMA or alkyl SAM). Carboxylate-functionalized nanoparticles were attached using a vertical deposition setup, see Figure 1. Substrates with line patterns were withdrawn with the lines parallel to the withdrawal direction as indicated in Scheme 1c. Carboxylate-functionalized nanoparticles of different diameter (d) and type were used, namely 350 nm polystyrene (PS) beads and 55 nm silica (SiO_2) nanoparticles.

When using SiO_2 nanoparticles, the PMMA template can be removed by sonication in acetone, which is not the case for PS beads which also dissolve in this solvent. Scanning electron microscopy (SEM) was used to characterize the substrates.

Figure 2 shows PS beads adsorbed to imprinted PMMA substrates of various designs, functionalized with aminoalkyl SAMs. Except for Figure 2d, no particles can be seen on the PMMA areas. No attachment occurred when the exposed areas of the substrate were covered with an alkyl SAM (not shown), while on the aminoalkyl SAM regions, PS beads attached in an ordered fashion. Figures 2a, b, and c show images for linewidths of 5 μm, 700 nm, and 500 nm, respectively. On the micrometer lines, particles arranged with hexagonal close-packing (see inset of Figure 2a). When the linewidth was comparable to the diameter of the beads, the effect of the pattern confinement became apparent, leading to zigzag patterns on the 700 nm lines (Figure 2b) and single particle lines on the 500 nm lines (Figure 2c). Figure 2d shows a superlattice of 350 nm PS beads obtained by lowering the withdrawal speed on a substrate patterned with 700 nm wide aminoalkyl lines. The first layer of nanoparticles adsorbed as a single line to the center of the 700 nm wide imprinted lines, and the second layer arranged on the voids left by the first layer and the polymer lines. Micrometer 2D patterns were studied as well, with hole (Figure 2e) and pillar patterns (Figure 2f).

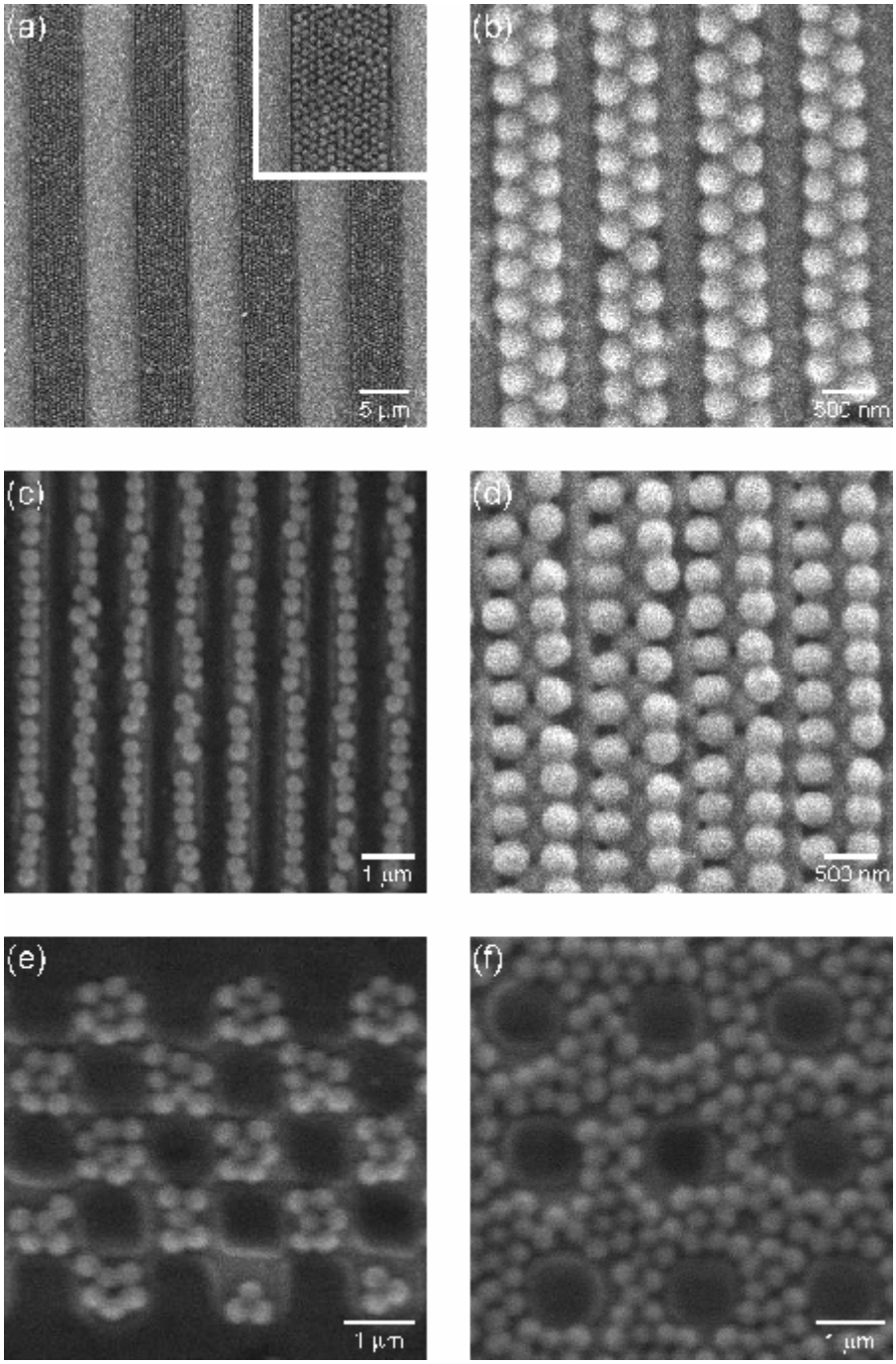

Figure 2. *SEM images of 350 nm carboxylate-functionalized PS particles selectively attached to aminoalkyl SAMs deposited on various NIL-imprinted substrates.*

Sub-300 nm features were investigated taking advantage of the ease to produce patterns on the sub-500 nm scale by NIL. Smaller diameter particles were then needed to fit in the PMMA templates. Silica nanoparticles were chosen to demonstrate the versatility of the procedure with the additional advantage that in this case the polymer template can be removed afterwards. Figures 3a and b show images of 55 nm silica particles confined in 100 nm and 60 nm wide imprinted lines leading to zigzag arrays and single particle lines, respectively. For Figures 3c and d, 180 nm and 100 nm imprinted holes were used, respectively. In all cases, the aminoalkyl SAM acts as an anchor when using a topographical template as the substrate, which allows easy removal of the polymer. Therefore, the SAM eliminates the need of harsh post-processing conditions such as melting the beads to anchor them onto the substrate[4] or using an etching solution to remove a silica pattern.[5]

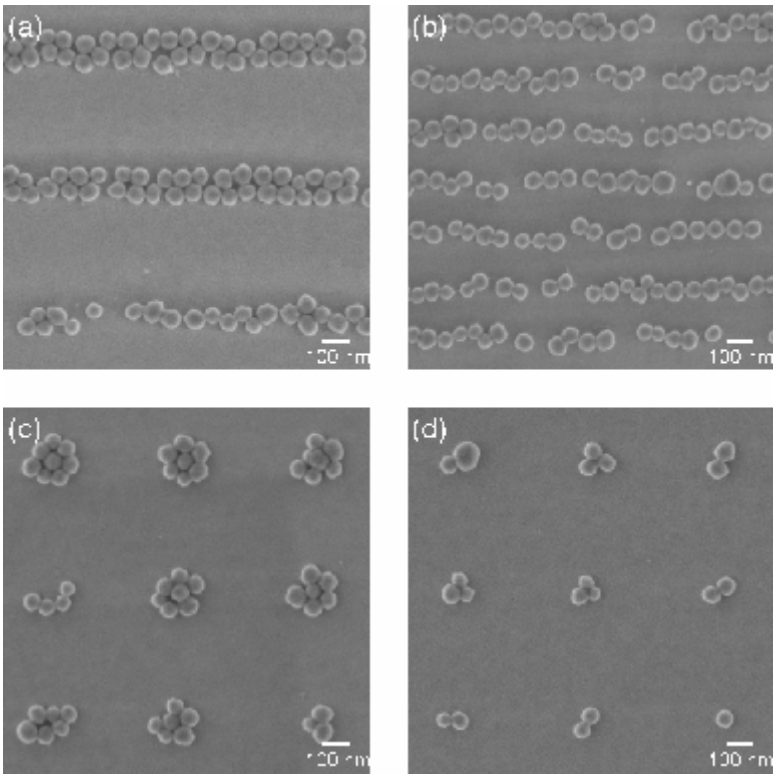

Figure 3. *SEM images of 55 nm carboxylate-functionalized SiO_2 nanoparticles assembled on PMMA-imprinted sub-300 nm patterns with aminoalkyl SAMs.*

Additionally, the chemically patterned flat substrates were used to direct the nanoparticle assembly. The vertical deposition process to attach the particles was the same as for topographical templates. Figure 4a shows PS beads attached to micrometer lines, and Figure 4b shows silica nanoparticles on 300 nm lines. Figures 4c and d depict PS beads and silica nanoparticles assembled on circular patterns. The particle arrangement closely followed the aminoalkyl patterns in all cases.

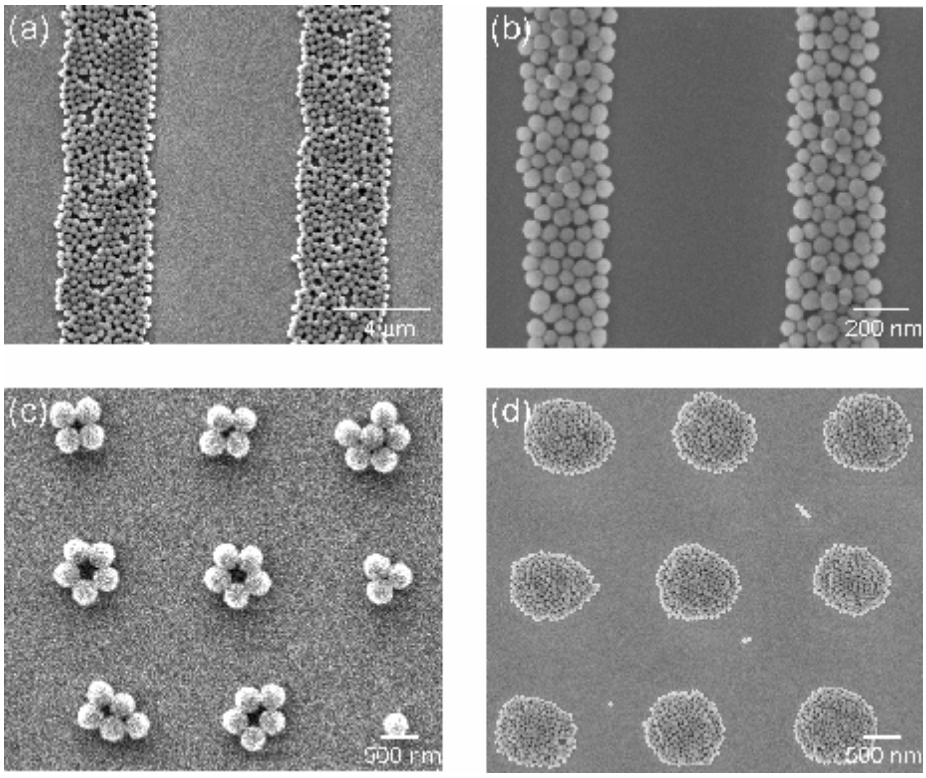

Figure 4. *SEM images of 350 nm PS (a, c) and of 55 nm SiO_2 nanoparticles (b, d) assembled on chemical patterns of various geometries and dimensions formed by aminoalkyl and alkyl SAMs.*

Compared to previous experiments with drop-casting,[29] vertical deposition significantly improved the particle packing and order on larger areas while high selectivity was maintained on topographically as well as on chemically patterned templates.

The particle confinement caused by the PMMA design was studied by decreasing the linewidth from micrometer to sub-100 nm scales. When the linewidth W was much larger than the particle size d, particles arranged with hexagonal symmetry.

On sub-micrometer patterns, the effect of particle confinement in the templates was observed. In accordance with Xia,[4] particles arranged in zigzag chains when $W < 2d$ (Figures 2b and 2a), and as single particle chains when $W < 1.5d$ (Figures 2c and 3b). An alternative type of confinement was achieved by chemical patterning only, owing to: i) specific electrostatic interactions between particles and surfaces and/or: ii) hydrophobic effects on the wetting of the suspension. The degree of order of the particles was comparable for micrometer (Figure 4a) and sub-micrometer lines (Figure 4b), even though the type of particle used was different. Particles arranged in a close-packed configuration but hexagonal order could only be seen in some parts.

The edges of the lines of particles were better defined in the case of arrays made from topographical templates than the ones made from chemical templates. Typical, e.g. zigzag, arrangements of nanoparticles due to confinement were found using topographical templates, which could not be observed for only chemically patterned substrates.

The withdrawal speed for the deposition of one layer of particles was the same for all kinds of patterns and substrates, i.e. 0.5 μm/s for PS beads and 1 μm/s for SiO_2 particles. By decreasing the speed (to 0.25 μm/s), bilayers of PS particles were obtained on topographical substrates (Figure 2d). The height of the PMMA template was in this case slightly smaller (300 nm) than the particle diameter (350 nm). The novel bilayer configuration is characterized by the arrangement of the second layer of nanoparticles in a square lattice where the parameters (r = 470 nm, period 1 μm) are controlled by the PMMA template. Additionally, particles were adsorbed on other 2D designs.

On PMMA templates, the 350 nm PS nanoparticles formed hexagons in 1 μm square holes (D/d = 3, Figure 2e), while similar structures and fractions thereof are formed by 55 nm SiO_2 nanoparticles in 200 nm holes (Figure 3c). Dimers and trimers of the latter nanoparticles were found in the 100 nm holes (D/d = 1.7) as shown in Figure 3d. In the case of polymer pillars (Figure 2f), close-packed PS particles covered the whole areas surrounding the pillars. In contrast, on chemically patterned 1 μm circular templates, clusters of PS beads were obtained containing from two to six beads, with a majority of pentagons, attached to the aminoalkyl dots, as shown in Figure 4c. Clusters were positioned on the centers of the amino SAM patterns as a result of inter-particle capillary forces.[15] When using 55 nm silica nanoparticles (Figure 4d), these assembled in a close-packed configuration matching the aminoalkyl SAM circles. We can conclude that particles generally tend to arrange as expected from the D/d ratio for both topographical and chemical confinement, for both micrometer down to far sub-micron features.

Similar experiments on chemically patterned substrates (prepared by photolithography) were carried out by Jonas et al.,[14] but they used unfunctionalized particles. They attributed their selectivity to differences in wettability of the chemical templates, which prevented particle attachment on the hydrophobic pattern areas. Resolutions of 4 μm for lines of particles and 50 μm for dots were reported. In contrast, the current study shows a resolution of 300 nm for lines and 1 μm for dots using chemical confinement of the functionalized particles by using a combination of techniques where NIL is employed as the patterning method.

4.2.2 Nanosphere lithography

The sedimentation and attachment of nanoparticles on a substrate take place in such a way that the packing factor is maximized. In the case of single layer attachment the nanospheres tend to arrange in a close packed hexagonal array that can be used as a template for lithography. This type of lithography can be additive if a material (in general metal) is deposited on the particles and the particles are removed as in lift-off. In contrast, the processes can be subtractive if the nanosphere template is used as a polymer mask for etching. These techniques are known as colloidal or nanosphere lithography (NSL).[30]The advantages of these techniques are that only simple and inexpensive equipment is needed and that they are capable of high resolution and large area coverage. Periodic patterns are obtained as a result of periodic nanosphere packing on a substrate. The disadvantage of the techniques, in their reported form, is that the designs are limited to the particle arrangement, in general a hexagonal pattern. Patterning nanoparticles would add an extra degree of freedom for the structure design and therefore allow for fabrication of a new range of designs based on nanosphere lithography.

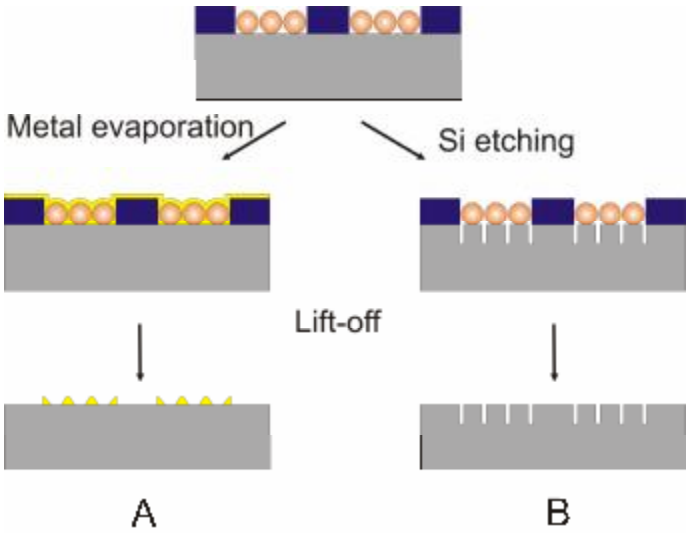

Scheme 2 . *Schematic representation of nanosphere lithography: (A) metal lift-off and (B) Si etching.*

Here, nanosphere lithography, both additive and subtractive, was performed on patterned colloids, see Scheme 2. Samples were prepared as mentioned above (Section 4.2.1), using PMMA templates produced by NIL, subsquently functionalized using an aminoalkyl SAM. Several patterns, such as 5 μm wide lines with 10 μm period, 700 nm lines with 1 μm period and 1 μm diameter dots with 1 μm period were imprinted. Thereafter, 350 nm carboxylate-functionalized nanoparticles were attached on the patterned substrates using vertical deposition. In the case of additive nanosphere lithography, 15 nm Au (with a 5 nm Cr adhesion layer) or 20 nm Cr were evaporated on the patterned substrates (Scheme 2, path A). For subtractive nanosphere lithography, etching was performed with SF_6/O_2 (25/2) that gives an etching rate of 50 nm/min. Lift-off of PMMA and PS beads was performed in acetone using ultrasonication for 2 h. Figure 5 shows SEM images of the results of the combination of additive colloidal lithography and NIL after Au lift-off (a, b) and after Cr lift-off (c-f).

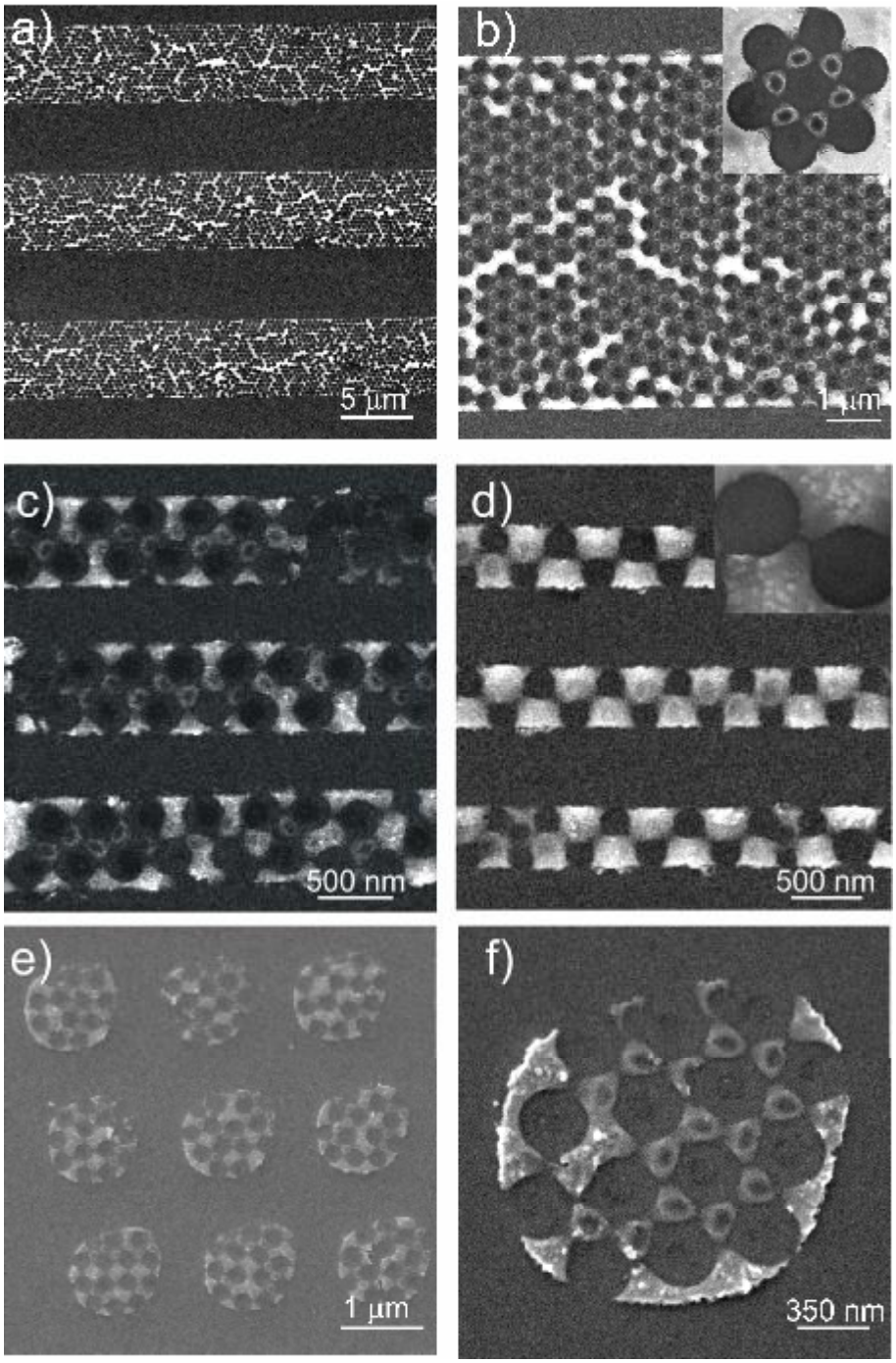

Figure 5. *SEM images of samples obtained after nanoparticle confinement in 5 mm lines, 700 nm lines and 1 mm dots, followed by Au (a, b) or Cr (c-f) evaporation and lift-off.*

The results were comparable to the ones obtained with nanosphere lithography on non patterned substrates.[31] Figures 5a and b show the region of the 5 µm lines at low and high magnification respectively.

The uncovered circular areas on Si correspond to the parts previously protected by the colloids and their size is approximately 310 nm. The metal features corresponding to the evaporation through the colloids interstices have oval shapes 125 nm long and 85 nm wide, see insert Figure 5b. The hexagonal Au patterns are restricted to the parts that were not protected by the PMMA layer. Figures 5 c-f show the results obtained with physically confined colloids in 1D within lines and in 2D inside dots with dimensions comparable to the size of the colloids. When colloids were confined as a zigzag chain, the metal features also had a zigzag configuration. On the other hand, when the colloids were not closely packed, metal diffusion occurred resulting in chessboard-like features, see Figure 5d. For the 1 μm diameter dots (circles), shown in Figures 5e and f, an average of 14 nanospheres were confined and the four inner nanospheres were arranged in an approximately hexagonal pattern. The metal structures in the center are similar to the ones observed in Figure 5b.

In the case of subtractive colloidal lithography, patterned nanoparticles within a PMMA template were used directly as a mask for reactive ion etching of Si with SF_6/O_2, see Scheme 2, path B. The etch selectivity of Si with respect to the polymer is high. Three etching times were used to obtain different aspect ratio nanostructures. Thereafter, the nanoparticles were removed in acetone using ultrasonication.

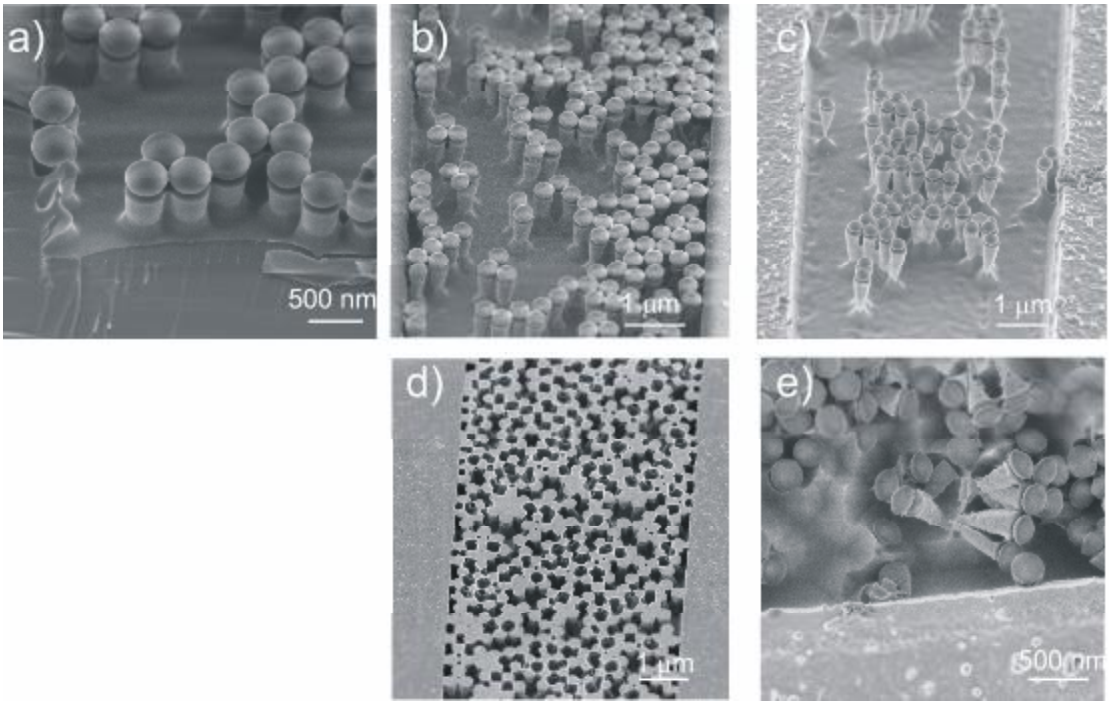

Figure 6. *SEM images of samples after nanoparticle confinement in 5 mm lines and etching during 6 min (a), 10 min (b, d) and 16 min (c, e). Figure d shows the results after nanoparticle removal. (a, b, c, d) are tilted view images while (e) is a top view image.*

Figures 6 a-c show loosely packed nanoparticles patterned in 5 µm lines after etching times of 6, 10 and 16 min. The resulting nanopillars were 300, 500 and 800 nm high. Shrinkage of the base of the nanopillars was noticed after etching times of 10 and 16 min. Figures 6d and e show close packed nanoparticles patterned in 5 µm lines after 10 and 16 min etching, while d shows the substrate after nanoparticles removal. Etching results depended on the degree of packing of the nanoparticles so that for close-packed nanoparticles an undercut was observed after etching for 10 min, and nanopillars collapsed after 16 min.

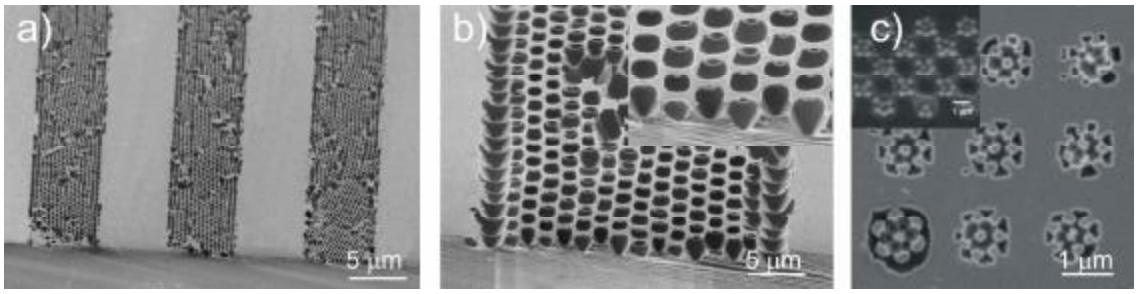

Figure 7. *SEM images of samples after nanoparticle confinement in 5 mm lines (a, b), and 1 mm dots (c), followed by etching during 10 min and nanoparticle removal. (a, b) are tilted view images while (c) is top view image.*

Figure 7 shows SEM images of a sample after subtractive nanoparticle patterning in 5 µm lines and 1 µm dots after etching during 10 min and nanoparticle removal in acetone. The Si surface resulting when nanoparticles were patterned in the 5 µm lines, resembles a porous membrane produced by the underetch. In the case of dot patterns the hexagonal arrangement of nanoparticles is transferred into the Si substrate.

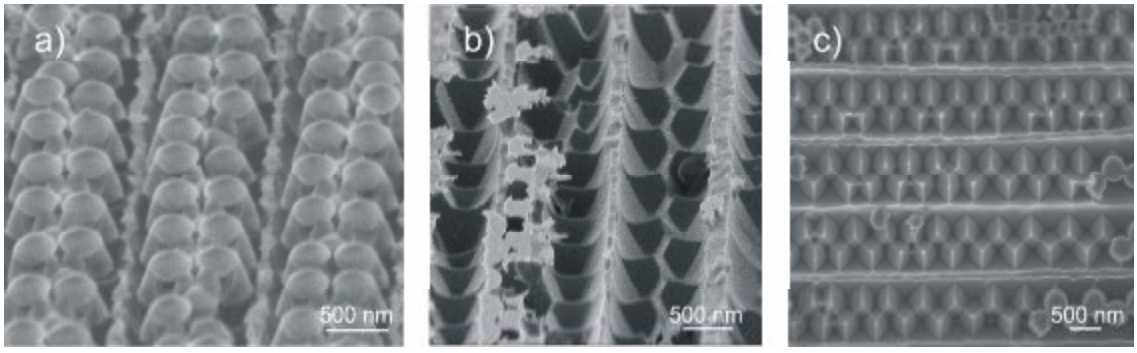

Figure 8. *SEM images of samples after nanoparticles confinement in 700 nm lines and 10 min etching (a) and subsequent nanoparticles removal (b, c). (a, b) are tilted view images while (c) is top view image.*

Figure 8 shows 700 nm lines after nanoparticles attachment, etching for 10 min and nanoparticle removal. When the membrane created by the under etch is removed, zigzag cavities appear.

4.3 Conclusions

A versatile method for the fabrication of nanoparticle patterns of ordered functionalized nanoparticles has been demonstrated by using a combination of three methods: NIL to control the lateral size, gas phase self-assembly of silanes for anchoring the functionalized nanoparticles, and the moving meniscus method to control their ordering. Two types of substrates were used: substrates patterned topographically and chemically, and flat substrates patterned chemically only. Designs of various shapes could be obtained, with different densities on both micrometer and nanometer scales. The maximum resolution achieved for lines of particles was 60 nm for topographical/chemical templates and 300 nm for chemically patterned substrates. We believe that chemically patterned substrates can be of great interest in the investigation of particle anchoring properties, by modifying the end-functional group of the nanoparticles and/or of the SAMs. Owing to nanosphere patterning, a number of new designs could be obtained by Nanosphere Lithography in contrast with the fixed hexagonal design obtained with non-patterned nanospheres.

4.4 Experimental Section

Compounds

N-[3-(trimethoxysilyl)propyl]-ethylenediamine (Aldrich), dodecyltrichlorosilane (Acros) and PMMA (MW 350 kD, Aldrich) were used as such. Carboxylate-functionalized PS beads in aqueous suspension (350 nm ± 10 nm diameter) were obtained from Polyscience Inc. Fabrication of 50 nm carboxylate-functionalized silica particles by Dr. Venkataramanan Mahalingam has been described elsewhere.[32]

Substrate preparation

The stamps for NIL were made by photolithography followed by reactive ion etching (RIE, Elektrotech Twin system PF 340) or by e-beam lithography followed by titanium evaporation and lift-off. They consisted of gratings composed of 400 nm wide lines at 1 μm period and 5 μm lines at 10 μm period, all with a height of 300 nm. A second type of stamps contained 150 nm wide lines at a period of 500 nm and 125 nm dots at a period of 500 nm, both with a height of 85 nm. 1H,1H,2H,2H-Perfluorodecyltrichlorosilane was used as an anti-adhesion layer to facilitate the stamp-imprint separation. Silicon substrates were oxidized first by immersion in piranha solution (concentrated H_2SO_4 and 33% aqueous H_2O_2 in a 3:1 ratio. **Warning**! piranha should be handled with caution; it is known to detonate unexpectedly) for 15 min (SiO_2 thickness 1.5 nm) and then covered with a 400 nm thick layer of PMMA by spin coating. Stamp and substrate were put in contact and a pressure of 40 bar was applied at a temperature of 180 ºC using a hydraulic press (Specac). The residual layer was removed by dipping the substrates in acetone during 60 s or by O_2 plasma during 20 s using a RIE system. The imprints consisted then of gratings formed by 5 μm polymer lines at 10 μm, and 600 nm polymer lines at 1 μm period. The imprint cycle time was 20 min and the imprinted area was 2×2 cm^2. The stamps were changed approximately every 50 imprints.

SAM formation

After imprint and residual layer removal, SAM formation was performed by gas-phase evaporation of silanes in a desiccator under vacuum.[20] The substrates were left several hours or overnight and then carefully rinsed with ethanol and Millipore water.

For chemically patterned substrates, the polymer template was removed for 2 h in acetone and ultrasound, followed by a subsequent SAM formation with the aminoalkylsilane. The aminoalkyl SAM yielded positively charged areas while the alkyl SAM constituted neutral areas. At the same time the surface energy (hydrophobicity) is discontinuous at the boundaries between the aminoalkyl (θ_a=75°) and alkyl SAM areas (θ_a= 110°).

Particle deposition and nanofabrication

Substrates were rinsed with 4-morphiline-ethanesulfonic acid monohydrate (MES, pH = 5.6) buffer. Particle attachment was performed using a suspension of either 55 nm carboxylate-functionalized silica nanoparticles or 350 nm carboxylate-functionalized PS beads (1 to 3 w%). The vertical deposition set-up consisted of a step motor (RS instruments, Code 191-8334) driven by a control card (RS instruments, GSM2 unipolar stepper motor driver). A gear box is attached to the motor to decrease the number of rpm (RS instruments 641:1). The withdrawal speed can be varied over a range of 0.1 μm/s up to several μm/s. The whole apparatus was placed in a closed box to protect the experiment from air drafts. The substrates were not rinsed afterwards. For the experiments described here, the concentration was kept constant and the withdrawal speed modified from 0.25 to 1 μm/s. The withdrawal speed was 0.5 μm/s for the PS and 1 μm/s for the SiO_2 nanoparticles. For a withdrawal speed of 0.25 μm/s, a bilayer of particles was deposited on the 700 nm lines, of which the top layer of particles follows a square lattice. When necessary, the PMMA template was removed in acetone and ultrasound during 1 min. A 15 nm layer of gold (with an adhesion layer of 5 nm chromium) and a layer of 20 nm chromium were evaporated using a metal evaporator BAK 600 in a vacuum of 1×10^{-6} mbar.

The metal lift-off was made in acetone and ultrasound. The dry etching was made using an Adixen AMS 100 speeder with SF_6/O_2 (25/2) with a etch rate of 50 nm/min.

Analysis

In the case of PS beads attachment, SEM investigation was performed with a JEOL 5610 apparatus. The substrates were covered with 5 nm of Au to facilitate SEM observation. SiO_2 particles were imaged using a LEO 1550 FEG SEM.

4.5 References

[1] R. Mayoral, J. Requena, J. S. Moya, C. Lopez, A. Cintas, A. Miguez, F. Meseguer, L.Vasquez, M. Holgado, M. Blanco, *Adv. Mater*. **1997**, *9*, 257.
[2] Z. Gu, A. Fujishima, O. Sato, *Chem. Mater*. **2002**, *14*, 760.
[3] E. Kumacheva, R. K. Golding, M. Allard, E. H. Sargent, *Adv. Mater.* **2002**, *14*, 221.
[4] Y. Xia, Y. Yin, Y. Lu, J. McLellan, *Adv. Funct. Mater*. **2003**, *13*, 907.
[5] D. Xia, A. Biswas, D. Li, S. R. J. Brueck, *Adv. Mater*. **2004,** *16*, 1427.
[6] Y. Yin, Y. Xia, *J. Am. Chem. Soc*. **2003,** *125*, 2048.
[7] U. Kamp, V. Kitaev, G. von Freymann, G. A. Ozin, S. A. Mabury, *Adv. Mater.* **2005**, *17*, 438.
[8] S. Fournier-Bidoz, V. Kitaev, D. Routkevitch, I. Manners, G. A. Ozin, *Adv. Mater*. **2004,** *16*, 2193.
[9] K. M. Chen, X. Jiang, L. C. Kimerling, P. T. Hammond, *Langmuir* **2000**, *16*, 7825.
[10] I. Lee, H. Zheng, M. F. Rubner, P. T. Hammond, *Adv. Mater.* **2002**, *14*, 572.
[11] Y.-H. Ye, S. Badilescu, V.-V. Truong, P. Rochon, A. Natasohn, *Appl. Phys. Lett.* **2001**, *79*, 872.
[12] Y. A. Vlasov, X. Bo, J. C. Sturm, D. J. Norris, *Nature* **2001**, *414*, 289.
[13] C.-A. Fustin, G. Glasser, H. W. Spiess, U. Jonas, *Adv. Mater.* **2003**, *15*, 1025.
[14] C.-A. Fustin, G. Glasser, H. W. Spiess, U. Jonas, *Langmuir* **2004**, *20*, 911.
[15] J. Aizenberg, P. V. Braun, P. Wiltzius, *Phys. Rev. Lett.* **2000,** *84*, 2997.
[16] D. Quin, Y. Xia, B. Xu, Y. C. Zhu, G. M. Whitesides, *Adv. Mater.* **1999**, *11*, 1433.
[17] X. Liu, L. Fu, S. Hong, V. P. Dravid, C.A. Mirkin, *Adv. Mater*.**2002**, *14*, 231.
[18] K. M. Chen, X. Jiang, L. C. Kimerling, P. T. Hammond, *Langmuir* **2000**, *16*, 7825.
[19] I. Lee, H. Zheng, M.F. Rubner, P.T. Hammond, *Adv. Mater.* **2002**, *14*, 572.
[20] N. Tetrealt, H. Miguez, G. A. Ozin, *Adv. Mater.* **2004**, *16*, 1471.
[21] G. A. Ozin, S. M. Yang, *Adv. Funct. Mater.* **2001**, *11*, 95.
[22] Y. A. Vlasov, X. Bo, J. C. Sturm, D. J. Norris, *Nature* **2001**, *414*, 289.

[23] S. Morokoshi, K. Ohhori, K. Mizukami, H. Kitano, *Langmuir* **2004**, *20*, 8897.
[24] J. Choi, Y. Zhao, D. Zhang, S. Chien, Y. H. Lo, *Nano Lett.* **2003**, *3*, 995.
[25] V. Paraschiv, S. Zapotoczny, M. R. de Jong, G. J. Vancso, J. Huskens, D. N. Reinhoudt, *Adv. Mater*. **2002**, *14*, 722.
[26] J. Liu, T. Lee, D. B. Janes, B. L. Walsh, M. R. Melloch, J. M. Woodall, R. Reifenberger, R. P. Andres, *Appl. Phys. Lett*. **2000**, *77*, 373.
[27] F. J. Castaño, Y. Hao, M. Hwang, C. A. Ross, B. Vögeli, H. I. Smith, S. Haratani, *Appl. Phys. Lett.* **2001**, *79*, 1504.
[28] P. Maury, M. Péter, V. Mahalingam, D. N. Reinhoudt, J. Huskens, *Adv. Funct. Mater.* **2005,** *15*, 451.
[29] S. Y. Chou, P. R. Krauss, P. J. Renstrom, *Science* **1996**, *272*, 85.
[30] J. C. Hulteen, R. P. van Duyne, *J. Vac. Sci. Technol. A* **1995**, *13(3)*, 1553.
[31] C. W. Kuo, J. Y. Shiu, Y. H. Cho, P. Chen, *Adv. Mater.* **2003**, *15*, 1065.
[32] V. Mahalingam, S. Onclin, M. Péter, B. J. Ravoo, J. Huskens, D. N. Reinhoudt, *Langmuir* **2004**, *20*, 11756.

Chapter 5

Patterning the Molecular Printboard: Patterning Cyclodextrin Monolayers on Silicon Oxide using Nanoimprint Lithography*

5.1 Introduction

Several applications in Nanotechnology (molecular electronics, sensors, photonic crystals) need new lithographic tools for accurate control of the positioning of molecules. This goal can be achieved by combining top-down techniques, that allow control over the lateral dimensions, and bottom-up techniques, that permit direct positioning of molecules.

As shown in Chapter 3, NIL is an adequate top-down tool in combination with bottom-up techniques in order to create SAM patterns with nanometer resolution. The bottom-up assembly allows choosing the type of anchoring according to the intended application.

---

* This Chapter has been in part published in: P.A. Maury, O. Crespo-Biel, M. Péter, D. N. Reinhoudt, J. Huskens, *Mater. Res. Soc. Proc.* **2006,** *Vol. 901E* and P. A. Maury, M. Péter, O. Crespo-Biel, X.Y. Ling, D. N. Reinhoudt, J. Huskens, *Nanotechnology*, accepted.

The choice of anchoring to the surface involves the choice of the type of attractive interaction. The most commonly used interaction for the specific deposition and positioning of building blocks such as nanoparticles and biologic compounds is the electrostatic interaction because of its strength and the ordered structures that can be obtained.[1,2] Nevertheless, other types of interaction, such as covalent[3] and supramolecular,[4,5] are available. Some of the advantages of using supramolecular interactions are: an improved control over the linking force, higher specificity for element positioning and possibility to tune the adsorption.

The so-called molecular printboards developed by Reinhoudt et al consist of self-assembled cyclodextrin (CD) layers on gold[6] or glass substrates.[7] A large range of compounds, fluorescent molecules,[8] dendrimers,[9] particles,[10] proteins,[11] can be positioned on the molecular printboard using supramolecular interactions, provided they are functionalized with the appropriate guest functionalities, e.g. adamantyl groups. The binding interaction can be tuned in order to adsorb or desorb components. Patterning the molecular printboard allows to integrate these systems into devices.

Patterning of CD layers using nanoimprint lithography is presented in this chapter. CD layers were formed on the uncovered parts of the samples and the polymer mask was removed afterwards. The patterned CD layer was characterized with different techniques. The CD layer pattern acts as host for the attachment of a guest-functionalized dye.

5.2 Results and discussion

CD monolayers on SiO_2 substrates were formed taking into account the procedure developed by Onclin et al.[7] to attach cyclodextrins on glass substrates. It consists of a multistep covalent process. The proposed process was modified in order to use solvents that will not dissolve PMMA because here the objective is to pattern CD layers using polymer patterns as masks. The process started by forming an aminosilane from the gas phase on the SiO_2 substrate, followed by a reaction with 1,4-phenylene diisothiocyanate that reacts with the amino-groups. The reaction was performed by immersion in an ethanol solution at 40 ºC during 2 h. Samples were rinsed thoroughly with ethanol and water and dried in a N_2 flow. Attachment of per-6-amino β-CD was performed by immersion in water at 40 ºC during 2 h. Samples were rinsed thoroughly with water and dried in a N_2 flow. This procedure was characterized after each step using contact angle goniometry, ellipsometry and X-ray photoelectron spectroscopy (XPS), starting with non-patterned layers, and the results are reported in Table 1. The advancing contact angle increased after the reaction with 1,4-phenylene diisothiocyanate which is expected for an isothiocyanate-terminated SAM.[7] The small height increase measured by ellipsometry corresponds to the small size of this molecule. Sulfur was detected on the layer after the reaction with this compound as recorded by XPS, and the C/N ratio corresponds to the calculated value. After CD layer attachment, the contact angle diminished to 54° due to the hydrophilic nature of the exposed hydroxyl group of the per-6-amino β-CD. Ellipsometry showed a height of 2.8 nm that corresponds to the CD layer thickness. XPS showed an increase of the C/N ratio compared to the isothiocyanate layer according to expectation.

***Table 1**. Advancing and receding water contact angles, selected XPS data and ellipsometric thickness obtained from non-patterned SAMs; thicknesses were measured by contact mode AFM on patterned SAMs prepared by forming a SAM on a NIL-patterned substrate, followed by polymer removal in acetone using ultrasonication.*

	NH_2	**SCN**	b-**CD**
Contact angle (°) (Adv/Rec)	65/45	80/47	54/40
C/N (exp., calc.) (%) S (exp., %)	2.7/2.5 0	4.0/3.3 1.0	5.0/5.3 0
Ell. thickness (nm)	1.0	1.2	3.5
AFM height (nm)	0.85	0.85	2.80

Nanoimprint lithography was performed on silicon substrates after oxidation in piranha and spin coating of PMMA. Features of various shapes such as lines and circles were imprinted. The line width varied from 5 µm down to 200 nm in arrays of different periodicities. The circle diameter was in the range from 1 µm to 50 nm. The residual layer was removed by acetone[12] for micrometer-sized patterns and with O_2 plasma for sub-500 nm-sized patterns. The height of the polymer features with lateral dimensions from micrometer down to 700 nm was 300 nm, and for features below 200 nm it was 50 nm. Patterning SAMs on SiO_2 using NIL was previously demonstrated. A CD layer was formed on the uncovered areas of the imprinted sample following the methodology described above and schematically shown in Scheme 1. The PMMA template was removed using acetone and ultrasonication for 2 h.

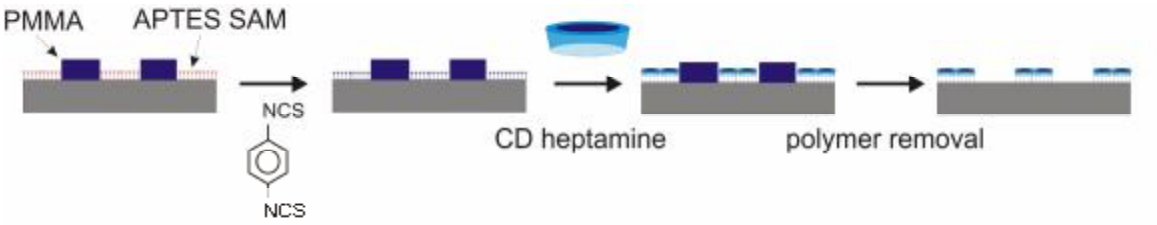

Scheme 1. *Schematic representation of the fabrication process of cyclodextrin patterned monolayers using physical polymer barriers.*

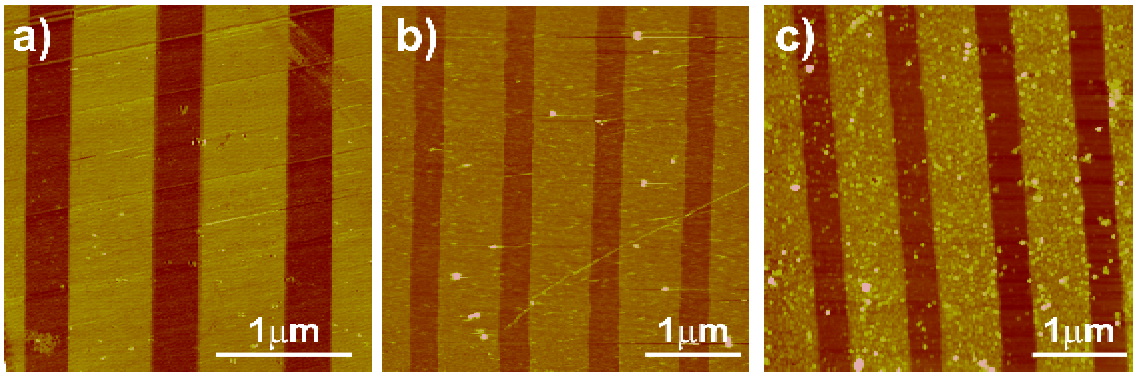

Figure 1. *Contact-mode height AFM images of 700 nm lines, 1 µm period, of (a) aminoalkyl SAM, (b) isothiocyanate SAM and (c) CD SAM on NIL patterned substrates after polymer removal.*

The patterned monolayers resulting after PMMA removal were characterized using AFM and XPS imaging. Figure 1 shows AFM images of 700 nm lines, 1 µm period of an aminoalkyl SAM, an isothiocyanate SAM and a CD SAM, respectively. The AFM height measurements are reported in Table 1. The height measured on the aminoalkyl SAM corresponds to the expected value (1 nm) and no height increase can be seen after the attachment of 1,4-phenylene diisothiocyanate. After CD attachment, an increase of 2 nm was measured.

The CD layer height of 3.2 nm corresponds to the value already measured on full SAMs.[7] An indication of the stability of the CD SAM patterns was obtained after observing that these patterns were able to withstand ultrasonication.

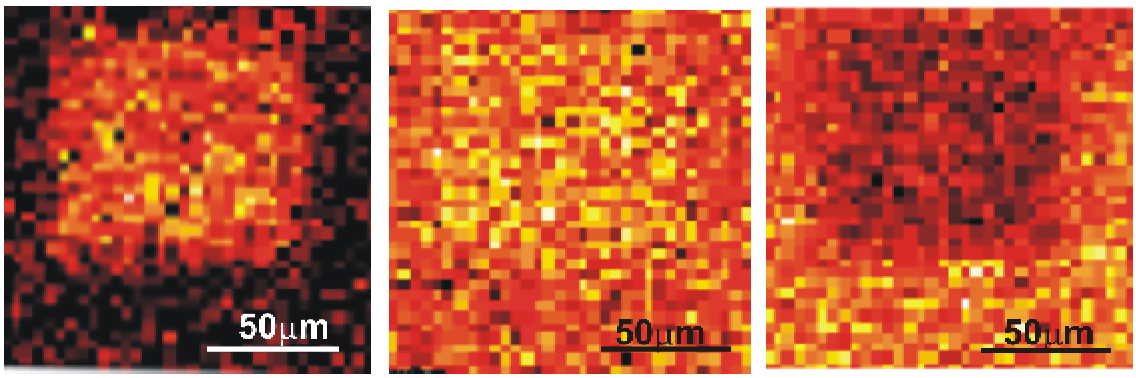

Figure 2. *XPS of 100 mm wide CD SAM squares with (a) C_{1s}, (b) N_{1s} and (c) Si_{2p} mapping.*

XPS imaging was performed on patterned samples in order to characterize the chemical elements present on the patterns. Figure 2 shows XPS mapping of 100 µm CD layer squares after polymer removal for C_{1s}, N_{1s} and Si_{2p}. The presence of C and N, that are elements present in the β-CD SAM, is confirmed in the areas corresponding to the CD layer, allowing visualization of pattern. A lower Si_{2p} signal was obtained from the CD layer regions indicating that the Si substrate is not exposed in those areas. These results confirm the presence of a patterned CD layer on the substrate.

The host behavior of the β-CD SAM patterns was studied using adamantyl-functionalized fluorescein as a guest. This molecule contains two adamantyl units for the host-guest interaction and a dye, allowing fluorescence imaging. In an earlier study, the binding behavior of this dye to CD SAMs was investigated and patterns were created using microcontact printing.[7] The specific host-guest interaction was studied both on patterned CD layers with the PMMA template still present, Scheme 2 path A, and on chemical patterns having CD and alkyl SAM areas, Scheme 2 path B.

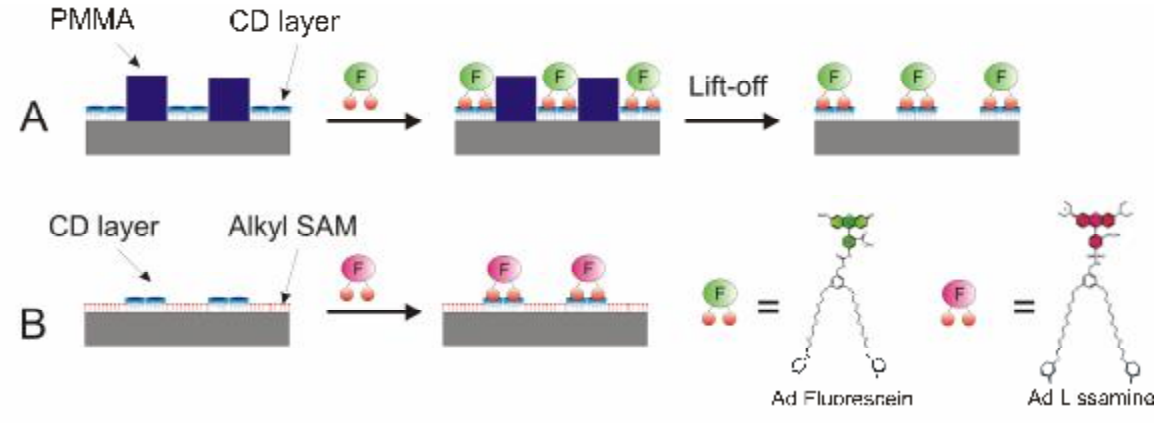

Scheme 2. *Scheme showing (A) adamantyl-functionalized fluorescein attached on a polymer template with a CD SAM and (B) adamantyl-functionalized lissamine on a chemical template consisting of patterned alkyl and CD SAMs.*

To create a chemical pattern, after imprint and residual layer removal, the uncovered parts of the sample were functionalized using an alkyl SAM. The polymer was removed and a CD layer was formed in the newly exposed areas. Adamantyl-functionalized fluorescein was attached on a patterned CD layer with the PMMA template still present and adamantyl-functionalized lissamine was attached on a chemical substrate by immersing the samples during 30 min in an aqueous 10^{-5} M dye solution. After adsorption, the samples were rinsed thoroughly with phosphate buffer to remove any physisorbed material and dried in a N_2 flow.

When using a PMMA pattern, some dye diffused into the polymer as shown in Figure 3. The PMMA pattern was removed by rinsing with warm water (50 °C) and harsh drying with N_2. The aim was to prevent the use of organic solvents that could affect the supramolecular interaction. Figure 4 depicts fluorescence microscopy images of patterned CD layers after adamantyl-functionalized fluorescein adsorption and its intensity profile on both sample types. After polymer removal, fluorescence could be observed only in the parts corresponding to the CD monolayer. The parts corresponding to the areas previously covered by PMMA were dark. Apparently, assemblies obtained through host-guest interaction stand the process of polymer removal. The intensity graph is consistent with similar experiments made using microcontact printing and shows the same long term stability as re-imaging after several weeks did not show fading.[7] For chemical patterns, adamantyl-functionalized lissamine molecules adsorbed specifically to the CD cavities and not on the alkyl SAM areas. The alkyl areas are clearly dark. The fluorescent profile is comparable to the one obtained with the polymer template.

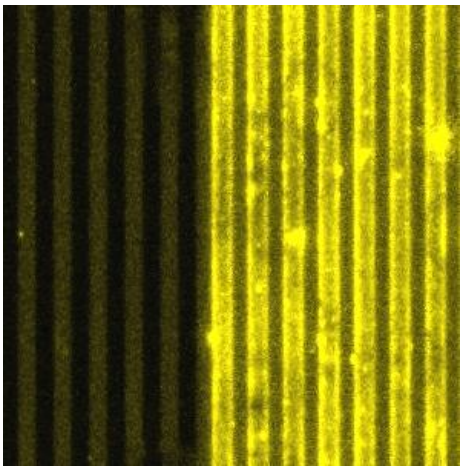

Figure 3. *Fluorescence microscopy image of patterned adamantyl-functionalized fluorescein on a polymer template, on the left side, polymer has been removed.*

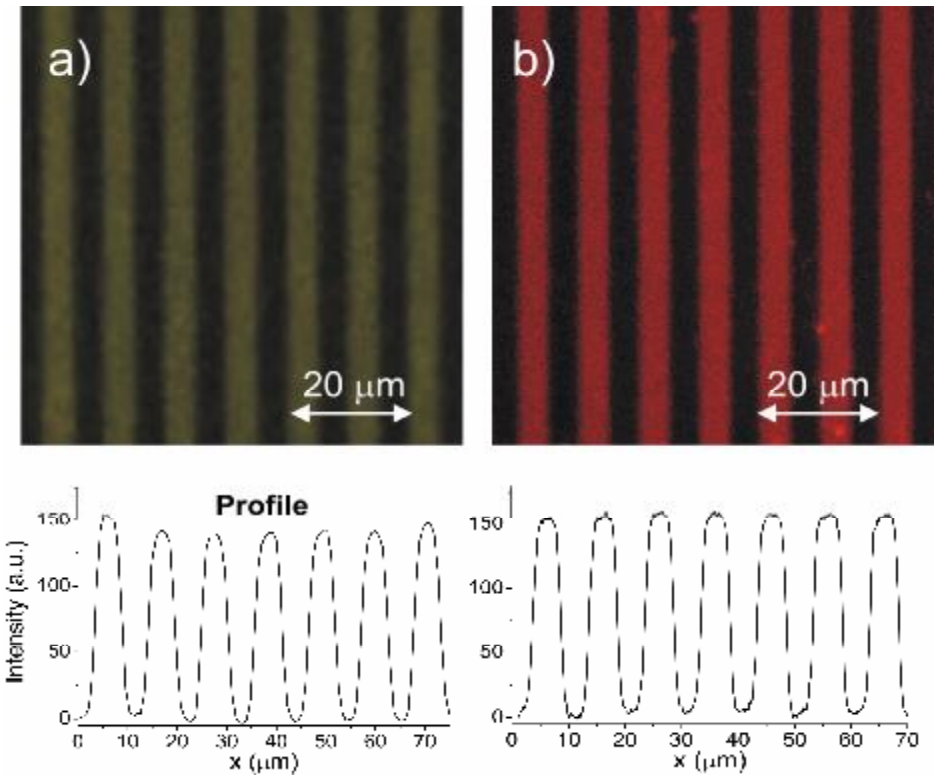

Figure 4. *Fluorescence microscopy image of patterned adamantyl-functionalized fluorescein on a polymer template (a) and its fluorescent profile. After CD SAM formation, adamantyl-functionalized fluorescein was adsorbed and finally the polymer was removed. (b) Fluorescence microscopy image of patterned adamantyl-functionalized lissamine on a chemical template. After alkyl SAM formation, the polymer template was removed and a CD SAM was formed. Adamantyl-functionalized lissamine was adsorbed on the sample followed by rinsing.*

5.3 Conclusions

In conclusion patterning of CD layers, also called molecular printboards, was demonstrated on SiO_2. For this purpose, a combination of a top-down technique, nanoimprint lithography, and bottom-up, self-assembly of monolayers, was performed. A modified process for CD layer formation was developed in order not to dissolve the polymer template. Polymer templates showed to be a good protective layer against SAM formation. AFM confirmed the expected height increase of the patterned CD layer formation and XPS confirmed the presence of elements contained in the CD layer. The patterned CD layers were used as a platform for host-guest attachment of molecules, using both topographical and chemical templates. Patterned CD layers were thus shown to be suitable for firm and well-controlled anchoring. The application in the fabrication of patterned layer-by-layer assemblies will be discussed in Chapter 6

5.4 Experimental Section

Compounds

N-[3-(trimethoxysilyl)propyl]-ethylenediamine (Aldrich), dodecyltrichlorosilane (Acros), 1,4-phenylene diisothiocyanate (Acros), 1H,1H,2H,2H-perfluorodecyltrichlorosilane (ABCR) and PMMA (MW 350 kD, Aldrich) were used as such. Adamantyl-functionalized fluorescein and adamantyl-functionalized lissamine[8] were synthesized by Alart Mulder.

Analysis

The quality and reproducibility of the monolayer formation were investigated by watercontact-angle goniometry, ellipsometry, AFM, and XPS. Contact angles were determined using a Krüss Contact Angle Measurement System G 10, and the data processed with the program Drop Shape Analysis 1.51. XPS was performed using a PHI Quantera Scanning ESCA Microprobe. Samples were investigated using an atomic force microscope AFM Nanoscope III (Veeco, Digital Instruments, USA) in contact mode equipped with a Si_3N_4 tip with a J scanner at a scan rate of 1.5 Hz.

CD layer formation

The gas-phase evaporation of aminosilanes was performed in a desiccator under vacuum. The samples were left several hours or overnight and then carefully rinsed with ethanol and Millipore water. The attachment of 1,4-phenylene diisothiocyanate was made in a 0.1 M solution in ethanol at 40 ºC during 2 h. Samples were thoroughly rinsed with ethanol and dried in a N_2 flow. The CD layer attachment was made during 2 h in an aqueous 5 mM per-6-amino-β-cyclodextrin solution (pH = 8.5) at 40 ºC. Samples were thoroughly rinsed with water and dried in a N_2 flow. The adsorption of dyes was performed by immersing the sample in a 10^{-5} M solution of adamantyl-functionalized fluorescein or adamantyl-functionalized lissamine for 20 min. The sample was rinsed thoroughly with a 10 mM phosphate buffer solution and water to remove the physisorbed material.

5.5 References

[1] S. Tzeng, K. Lin, J. Hu, L. Chen, S. Gwo, *Adv. Mater.* **2006,** *18,* 1147.
[2] F. A. Denis, A. Pallandre, B. Nysten, A. Jonas, C. Dupont-Gillain, *Small* **2005**, *10*, 984.
[3] S. Liu, R. Maoz, G. Schmidt, J. Sagiv, *Nano Lett.* **2002**, *2*, 1055.
[4] J. V. Barth, J. Weckesser, C. Cai, P. Gunter, L. Burgi, O. Jeandupeux, K. Kern, *Angew. Chem. Int. Ed.* **2000,** *39*, 1230.
[5] D. Bonifazi, H. Spillmann, A. Kiebele, M. de Wild, P. Seiler, F. Cheng, H. Guntherodt, T. Jung, F. Diederich, *Angew. Chem. Int. Ed.* **2004,** *43*, 4759.
[6] J. Huskens, M. A. Deij, D. N. Reinhoudt, *Angew. Chem. Int. Ed.* **2002,** *41*, 4467.
[7] S. Onclin, A. Mulder, J. Huskens, B. J. Ravoo, D. N. Reinhoudt, *Langmuir* **2004**, *20*, 5460.
[8] A. Mulder, S. Onclin, M. Péter, J. P. Hoogenboom, H. Beijleveld, J. ter Maat, M. F. García-Parajó, B. J. Ravoo, J. Huskens, N. F. van Hulst, D. N. Reinhoudt, *Small* **2005**, *1*, 242.
[9] C. A. Nijhuis, J. Huskens, D. N. Reinhoudt, *J. Am. Chem. Soc.* **2004**, *126*, 12266.
[10] O. Crespo-Biel, B. Dordi, D. N. Reinhoudt, J. Huskens, *J. Am. Chem. Soc.* **2005**, *127*, 7594.
[11] M. Ludden, M. Péter, D. N. Reinhoudt, J. Huskens, *Small* **2006**, *2*, 1192.
[12] P. Maury, M. Péter, V. Mahalingam, D. N. Reinhoudt, J. Huskens, *Adv. Funct. Mater.* **2005,** *15*, 451.

Chapter 6

Application of Nanoimprint Lithographically Patterned Molecular Printboards in 3D Multilayer Nanostructuring*

6.1 Introduction

A lot of research has been conducted on thin film technology that allows tailoring material properties which in turn are being exploited in applications ranging from biology to physics.[1,2] The advantage of these materials is that their physical and chemical properties can be tuned leading to new and interesting functionalities.[3] There exist several nano-manufacturing techniques that permit control over layer properties down to the molecular scale. Among these techniques, a very popular one is layer-by-layer assembly for the ease of its application, low-cost and the possibility to tune film thickness and other properties of the film.

---

* This Chapter has been in part published in: P.A. Maury, O. Crespo-Biel, M. Péter, D. N. Reinhoudt, J. Huskens *Mater. Res. Soc. Proc.* **2006,** *Vol. 901E,* O. Crespo-Biel, B. Dordi, P. Maury, M. Peter, D. N. Reinhoudt, J. Huskens, *Chem. Mater.* **2006**, *18,* 2545 and P. A. Maury, M. Péter, O. Crespo-Biel, X. Ling, D. N. Reinhoudt, J. Huskens Nanotechnology, accepted.

Layer-by-layer (LBL) assembly consists of building up multilayer films by alternatingly depositing components held together owing to attractive interactions such as electrostatics. [4] LBL assembly is considered as a candidate in order to integrate functional quantum dots in (photo)electronic devices and chemical and biological sensors.[5,6,7] Additionally, LBL photonic devices[8,9] have already been demonstrated by applying different sizes of colloids and LBL chemical and biological sensors[10] have been fabricated by using biological compounds. In order to ensure proper device operation for the previously mentioned applications, firm anchoring and accurate spatial confinement of the building blocks, as well as layer thickness control and reproducibility are crucial.

There are several ways to create functional nanostructure patterns. In the nanotransfer printing approach (nTP), a layer-by-layer film is deposited on a patterned PDMS stamp. After stamping, the material in contact with the substrate remains attached to it.[11] Another approach is to create a chemical pattern where the multilayer is built up on the patterned region with the proper functionalization.[12] In a third approach, the lift-off approach, a polymer template is used and the multilayer is non-specifically attached to the whole area. After polymer removal, only the part attached on the substrate remains.[13] In most of the cases, electrostatic interactions between polyelectrolytes with opposite charges are used.[12,13,14] On the other hand, Sagiv employs in his "constructive nanolithography" covalent interactions as a way to constructs 3D structures.[14]Most of the attempts to produce functional patterns have been made on the micrometer scale. In that respect, sub-micrometer and in particular sub-200 nm patterning has not been thoroughly studied yet, because most of the techniques are either time consuming (dip-pen)[15] and/or expensive (e-beam lithography).[16]

Nevertheless, interesting properties can be seen in this range, as the size of the pattern features start to be of the same order of magnitude as that of the molecules used.[17]

Supramolecular LBL assemblies have been developed, employing the host-guest interaction between adamantyl-functionalized dendrimers and cyclodextrin (CD)-functionalized nanoparticles[18] instead of the widely used electrostatic interaction. In Chapter 5 was demonstrated how to create patterned molecular printboards using nanoimprint lithography. Patterned LBL assemblies have been produced using chemical patterns,[19] but non-specific adsorption of the LBL assemblies occurred, which was in part solved by using nTP. Moreover, integration of the anchoring compound (CD layer) with a polymer pattern was made using lift-off to remove the non-specifically adsorbed LBL assemblies, leading to the patterned LBL structures. The attempt made in the micrometer scale showed a height increase corresponding to the number of bilayers. The lift-off process using acetone and ultrasonication did not have any effect on the thickness of the LBL assembly.

In this chapter patterning of supramolecular LBL assemblies is demonstrated in the nanometer scale to form 3D nanostructures. The patterned CD layer behaves as a host for the directed attachment of supramolecular LBL assemblies. LBL attachment of 2.8 nm CD-functionalized Au NPs was made, this time at the nanometer scale and with a large number of attached bilayers in order to construct 3D nanostructures. Investigation of supramolecular LBL assemblies with NPs of larger size and different nature, 60 nm CD-functionalized SiO_2 NPs, was made using vertical deposition to increase particle density and order of the attached NPs. Particle confinement and height increase were carefully investigated.

6.2 Results and discussion

6.2.1 Process

After imprint and CD layer formation, see Chapter 5, the substrate is used as a template for layer-by-layer assembly. The last step consists of removing the polymer which will reveal the confined LBL assemblies. The process is illustrated in Scheme 1.

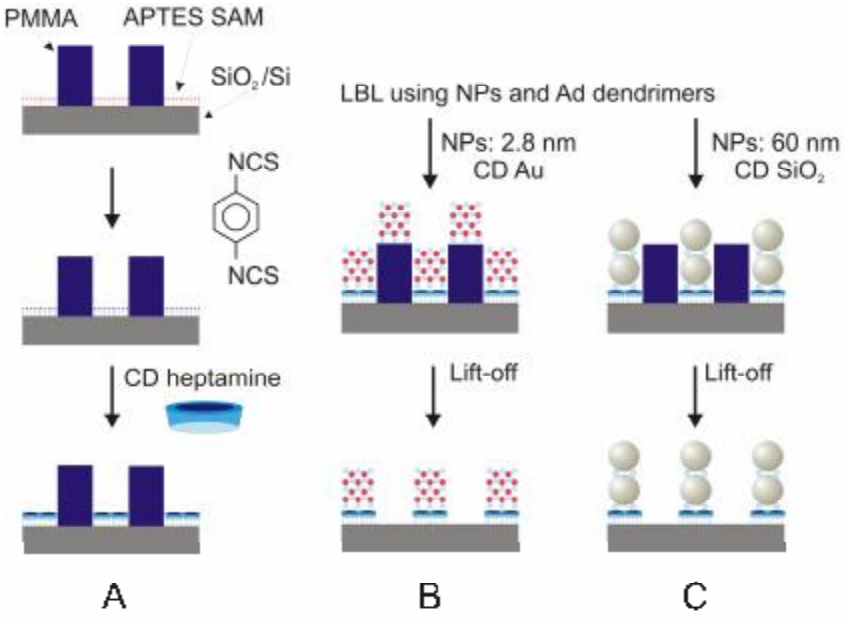

Scheme 1. *Schematic representation of the fabrication process of cyclodextrin patterned monolayers (A) and their use as templates for supramolecular layer-by-layer assembly using (B) 2.8 nm Au and (C) 60 nm silica CD-functionalized nanoparticles* .

The group of host adsorbates and nanoparticles, characterized by CD functionalization, is shown in Scheme 2, and consist of consists of CD layer,[20] CD-Au NPs[21] and CD-SiO_2 NPs.[22] The guest compound employed here is the generation-5 adamantyl -functionalized PPI dendrimer[23] (Scheme 2 shows the generation-3 derivative for clarity).

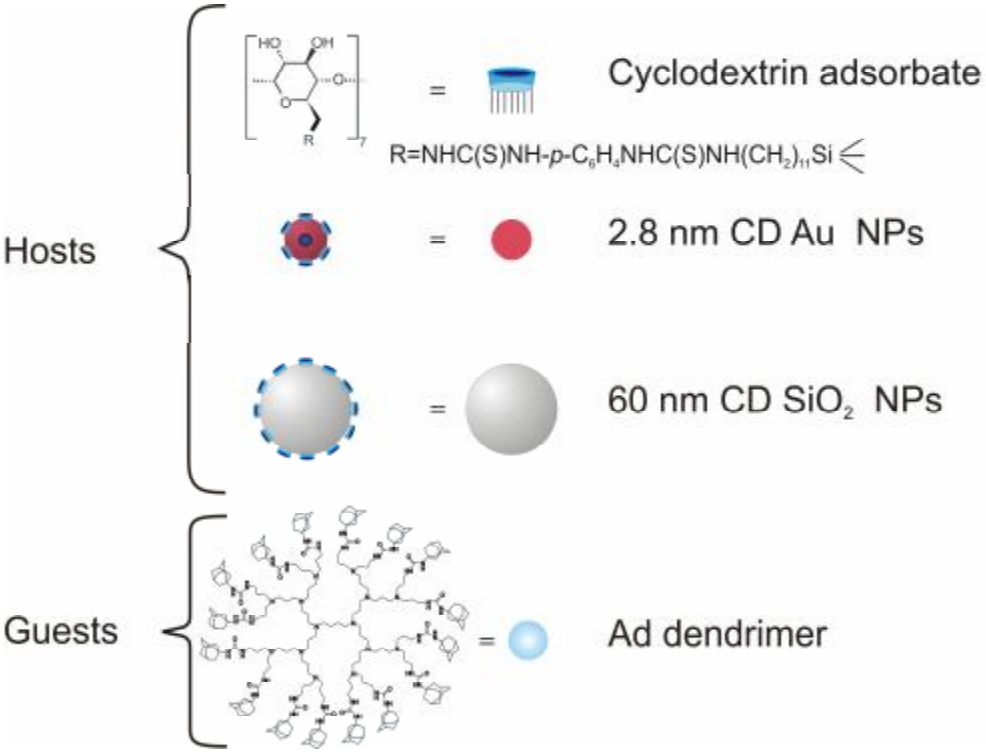

Scheme 2. *Chemical structures of the building blocks used to assemble supramolecular layer-by-layer structures.*

6.2.2 LBL assembly with 2.8 nm CD-functionalized Au NPs

In order to have an accurate control over the feature height, small CD-functionalized Au nanoparticles were used. After nanoimprint lithography and CD layer formation, the sample was immersed in an aqueous solution of Adamantyl-terminated dendrimers for 10 min then rinsed thoroughly with an aqueous CD solution (pH = 2) and water. The substrate was immersed in an aqueous solution of CD-functionalized Au nanoparticles for 10 min and then rinsed thoroughly with water. These two steps were repeated according to the desired number of bilayers, in this case 15 bilayers. The layer-by-layer film attached nonspecifically on the polymer and on the CD layer. The polymer was removed afterwards in acetone, resulting in the lift-off of the nonspecifically attached LBL assemblies, see Scheme 1 path B. Lines and dots of different sizes were made using this method. Features of 200 nm, 100 nm, and 50 nm were investigated. Figure 1 shows AFM and SEM images of lines and dots after polymer removal.

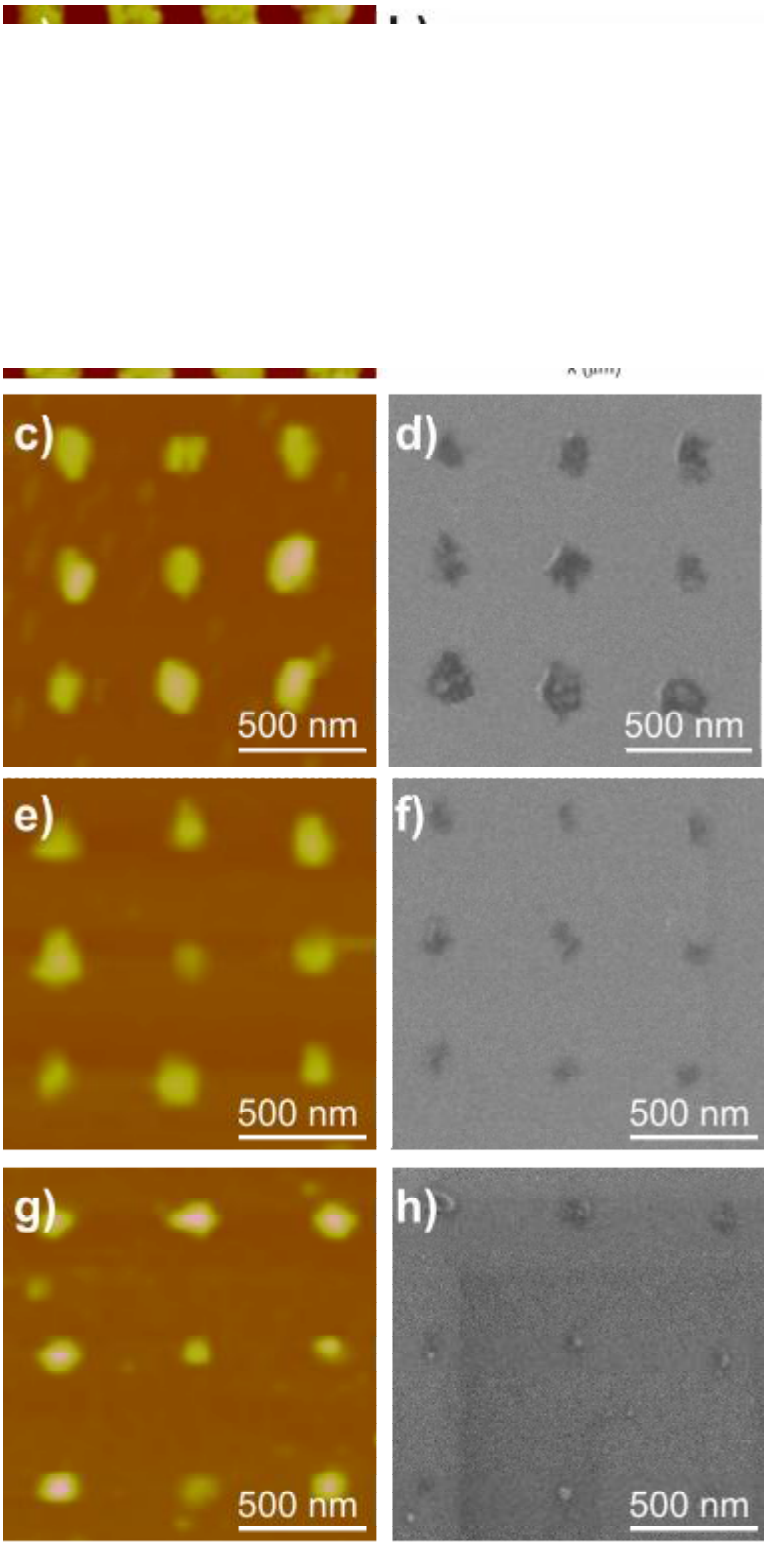

Figure 1. *AFM (a, c, e, g) and SEM (d, f, h) images of NIL-patterned CD layers followed by assembly of fifteen bilayers of adamantyl-terminated PPI dendrimers and 2.8 nm CD-functionalized Au NPs with pattern sizes going from 200 nm down to 50 nm. The profile of a multilayer assembly of 200 nm wide lines can be seen in (b).*

Figure 1a shows 200 nm lines and (1b) its height profile made on a line scan. The lateral edge roughness, measured on a 1 μm line, was 15 nm and its height was 24 nm. This value corresponds to the height measured on micrometer size patterns,[19] but it is lower compared to non-patterned LBL (30 nm). Figure 1 shows 200 nm (c, d), 100 nm (e, f) and 50 nm (g, h) features. In this case SEM could be used because the LBL assemblies contain Au NPs which are conductive. More information about the lateral dimension and the shape of the features was obtained with SEM. In the case of the 50 nm (nominal) features, AFM gave a lateral dimension of 80 nm while measured by SEM the value was 50 nm. This is probably due to the convolution of the AFM tip with the pattern. The edge roughness of the dots can be seen on the SEM images and the lateral dimensions correspond to the imprinted dimensions. The edge roughness may be caused by the usual lift-off problem that occurs when the height of the attached component is more than 1/3 of the polymer height.[24] The results could possibly be improved by using polymer templates with a higher aspect ratio but the required high aspect ratio stamps are more difficult to fabricate in the sub-200 nm scale.

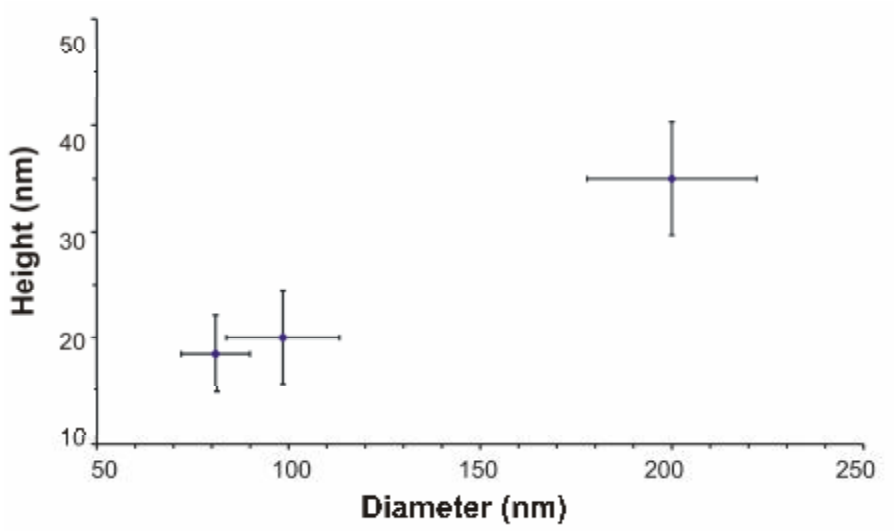

Figure 2. *Multilayer nanostructure thickness as a function of its lateral dimension. Height and lateral sizes were measured by AFM. Fifteen bilayers of adamantyl-terminated PPI dendrimers and 2.8 nm CD-functionalized Au NPs were assembled on the NIL-patterned CD areas followed by polymer lift-off.*

A decrease in height is noticed when going to sub-200 nm sizes. These results are summarized in Figure 2 where both heights and widths of the features were obtained from the AFM images. The height of the 200 nm features was 30 nm decreasing to 18 nm for the 80 nm features. This decrease in height may be due to a lower accessibility of the particles to the pattern cavities due to poor wetting by the aqueous adsorbate solutions. The aspect ratio is 0.14 for 200 nm features and 0.25 for 70 nm features.

6.2.3 LBL with 60 nm CD-functionalized SiO_2 NPs

Supramolecular LBL assemblies were also fabricated with larger NPs (60 nm) of a different nature (silica). After imprint and CD layer formation, supramolecular layer-by-layer films were prepared using adamantyl-terminated dendrimers and 60 nm CD-functionalized silica nanoparticles. After CD layer formation, samples were immersed during 10 min in an aqueous solution of adamantyl-terminated dendrimers then rinsed thoroughly with an aqueous CD solution (pH = 2) and water and dried in a N_2 flow. In a recent paper we have shown the advantage of using the vertical deposition method as a way to attach particles electrostatically with high order. [25] This method is used here to attach the CD-functionalized silica particles using supramolecular interactions, see Scheme 1 path C. To add subsequent bilayers, the above process was repeated. When the desired number of bilayers (1-3) was reached, the PMMA template was removed.

Figure 3. *SEM images of a pattern of 5 mm lines of CD-layers a) after one bilayer consisting of adamantyl-terminated PPI dendrimers and 60 nm CD-functionalized SiO_2 NPs, b) after two bilayers, c) after three bilayers, the polymer was removed afterwards. The insets show close-ups of the particle areas. d) AFM profile after one, two, and three bilayers measured on 5 mm lines. SEM images of 700 nm patterned CD layer after two bilayers formation before (e) and after (f) polymer removal and (g) of 1 mm patterned CD dots after formation of three bilayers and polymer removal. h) AFM profile of height increase after formation of two and three bilayers after polymer removal on 700 nm patterned CD layer lines.*

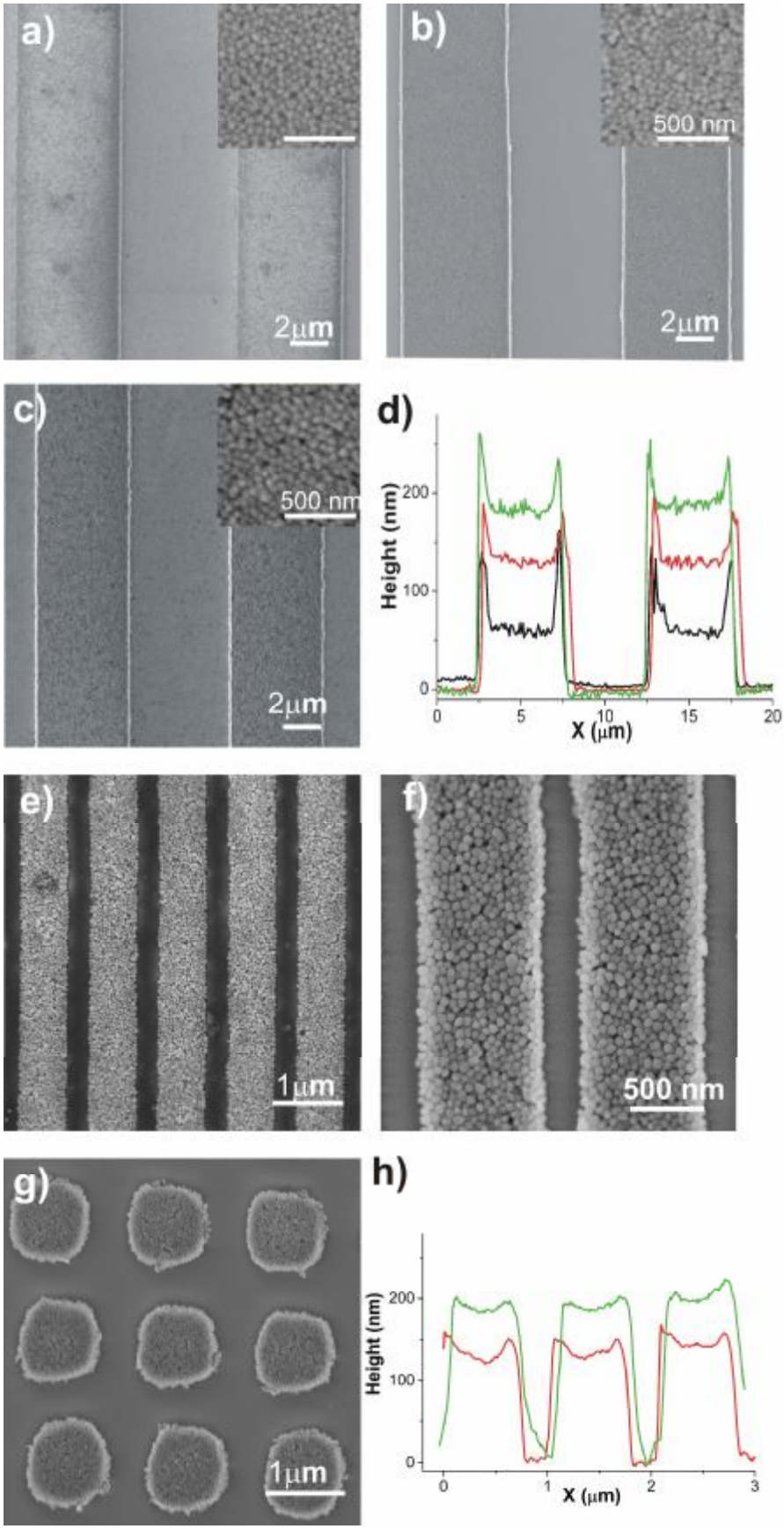
a)
2μm
b)
500 nm
2μm
c)
500 nm
2μm
d)
Height (nm)
200
100
0
0
5
10
15
20
X (μm)
e)
1μm
f)
500 nm
g)
1μm
h)
Height (nm)
200
100
0
0
1
2
3
X (μm)

Figures 3 a-c, show SEM images of CD SAMs patterned with 5 μm lines after the formation of one, two, and three bilayers followed by polymer removal. Edges are well defined laterally and particles are close packed owing to the vertical deposition of the NPs. After two and three bilayers, the same degree of order and packing can be observed, as can be seen in the inset. Immersion in the dendrimer solution while attaching bilayers does not seem to affect the packing order. Cracks appeared during SEM investigation mainly due to solvent drying and surface charging. Figures 3e and f show 700 nm lines patterned with two bilayers before and after polymer removal, respectively. No particles can be seen on the polymer pattern, which corresponds to the black lines in the figure. Polymer removal does not seem to induce disorder, as no difference in packing can be seen before and after polymer removal. Figure 3f shows SEM images of 1 μm dots patterned with PMMA and three CD bilayers after polymer removal. The results with 2D designs were comparable to the ones with 1D designs but in the 2D case the edges were not so well defined. The height measured by AFM can be seen on the profile, made on a single scan with 5 μm and 700 nm wide lines. The height increase after formation of a bilayer corresponds to the diameter of the NP. In Figure 3d, the first, second and third bilayer is one, two and three particle diameters thick respectively as can be seen from the AFM profile. The surfaces are smooth in all cases. Some extra particles remained on the edges of the features, as can be seen by the sharp peak at both edges of the lines. This effect may be due to particles sticking to the edge formed by the bilayer and the polymer template that remain after polymer removal. Nevertheless, this effect is not seen in Figure 3h, corresponding to 700 nm lines.

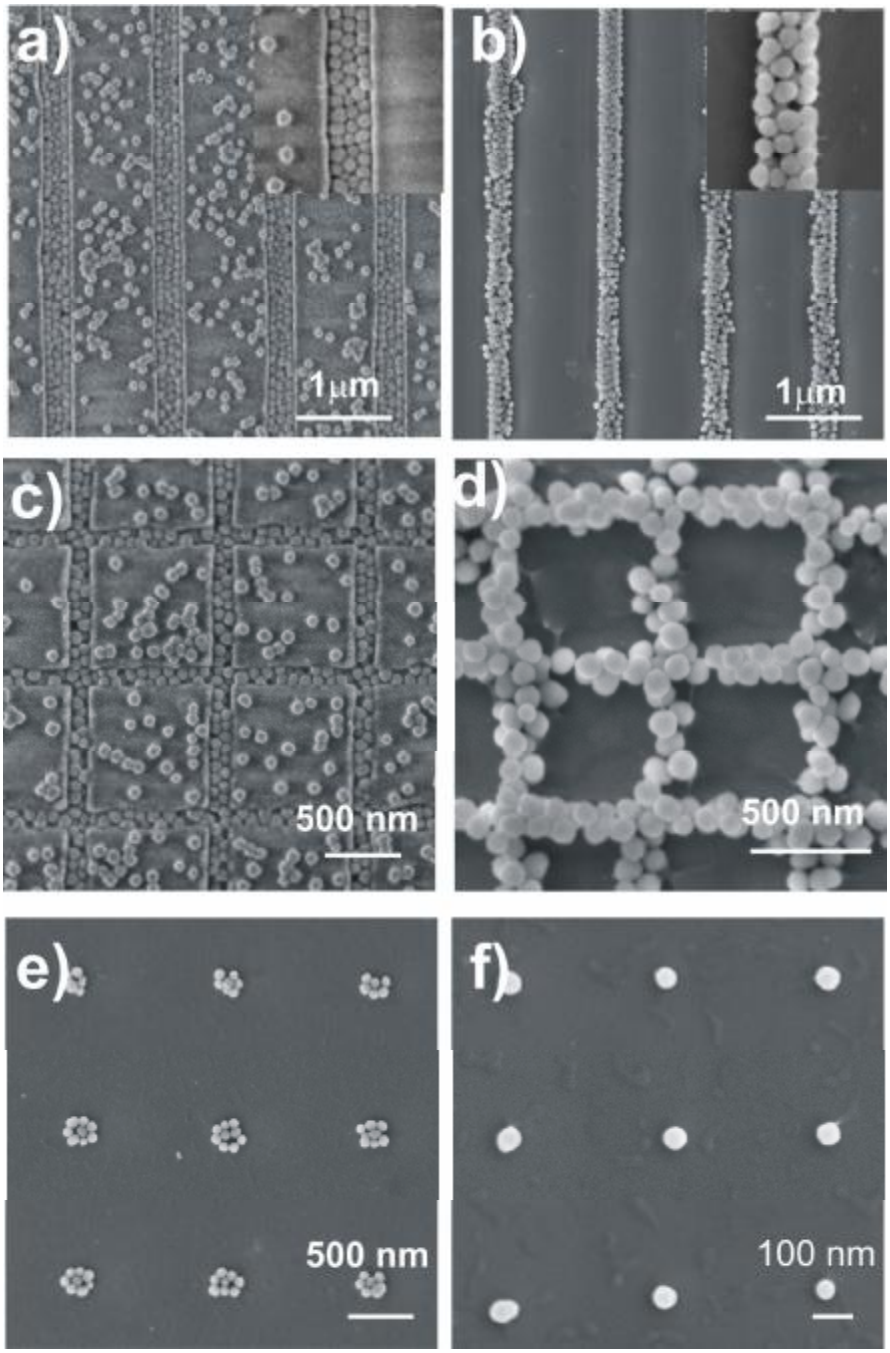

Figure 4. *SEM images of CD layer patterns in the form of (a, b) 200 nm wide lines, (c, d) 150 nm wide grids and (e, f) 200 nm and 60 nm dots, after (a, c, e, f) one bilayer formation and (b, d) 2 bilayers formation. Figures b, d, e and f were taken after polymer removal in acetone using ultrasonication. The withdrawal speed for the deposition of the NPs was 0.1 mm/s.*

Patterning on the sub-300 nm scale was investigated with a polymer height of 70 nm after residual layer removal. The withdrawal speed was lower compared to the one used in similar experiments made using electrostatic attachment,[25] 0.1 μm/s as compared to 0.5 μm/s while keeping the concentration constant. Figure 4 shows SEM images of particles attached on 200 nm imprinted lines and grids, and 200 nm and 60 nm holes, with one or two bilayers. After one bilayer, Figure 4a and c, particles arrange in order inside the lines, they are physically confined inside the pattern and take a triangular or a zigzag configuration, depending on the line width. The physical confinement is comparable to previous results with electrostatic forces[25] and as reported by Xia,[26] with the difference that here the anchoring force is supramolecular. Few disordered particles can be seen on the polymer due to non specific adsorption of dendrimers. After attachment of two bilayers, Figure 4b and d, the NPs of the second layer are physically confined on a line when the spacing between the lines is 200 nm and as a zigzag chain on top of the first one when using 150 nm lines. Physical confinement is obtained on the second layer as well. The host-guest interaction is sufficient to stand the polymer removal step in acetone. It was found that on some parts of the zigzag chain, the second layer was disordered, but this is attributed to the polymer removal step. Figure 4e and f show particles attached in holes after polymer removal. Particles were physically confined in the shape of the features as heptagons in the case of particles confined in 200 nm holes, and as single particles in 60 nm holes. The single particle attachment results in a periodic array of 60 nm particles at 500 nm period. Single particle attachment is of high importance for catalyst industry, sensing and drug screening for instance. When attaching single particles, polymer removal was a delicate step because particle shifting or detachment could be the result.

In this case some remaining polymer can be seen, as a result of a softer polymer removal step (2 s compared to 10 s when using other types of features). An attempt to attach a second bilayer inside the holes was made but did not succeed. The polymer height of the template seems to be an important factor for the number of layers that can be attached. When using sub-500 nm feature size, the polymer height after residual layer removal was approximately 70 nm. As the particle diameter was 60 nm, the height of the structure after attachment of the second bilayer was higher than the polymer height, which makes the polymer lift-off step difficult, especially in the case of a 2D pattern where the polymer surrounds the bilayer structure. A way to improve the lift-off process would be to use polymer structures with a higher thickness and a lower molecular weight polymer material (e.g. 70 kD) that dissolves easier.

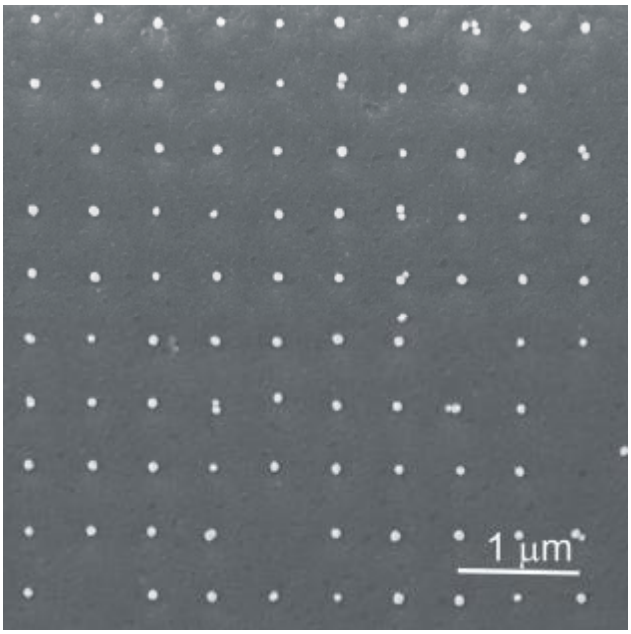

Figure 5. *Large area SEM image of the attachment of 60 nm single particles.*

Particle deposition was performed on working areas of 80 × 80 μm^2 with hole and line patterns. Figure 5 shows an overview of an area with single particle attachment. The complete patterned areas, including alignment zone, was of 1 cm × 1 cm.

The advantage of NIL compared to other methods to produce chemical patterns such as microcontact printing[27] is that, in addition to the ease to create sub-micrometer structures, the polymer protects the substrate from nonspecific adsorption or clumping.[6] It also prevents that the structures grow horizontally[6] as reported when using LBL or polymerization using a patterned precursor.

6.3 Conclusions

The patterned CD layer was used as a platform for the host-guest attachment of layer-by-layer assemblies. Owing to the high resolution of NIL, nanostructuring of layer-by-layer assemblies was demonstrated down to 60 nm and 3D nanostructures could be produced. This technique allows nanopatterning of any component having the appropriate host-functionalization. The method can be used to create various composite nano building blocks, which have a variety of application in quantum dot devices, biosensors, and particle-based sensors. Additionally, the process is highly reproducible especially taking into account of the large number of steps involved.

6.4 Experimental Section

Compounds

Fabrication of generation 5-adamantyl-terminated poly(propyleneImine) (PPI) dendrimers (with 64 adamantyl groups) by Christian Nijhuis and 2.8 nm CD-functionalized gold nanoparticles by Amela Jukovic was described elsewere.[21] The fabrication of CD-functionalized 60 nm silica particles by XingYi Ling was described elsewhere.[22]

Analysis

Samples were investigated using an atomic force microscope AFM Nanoscope III (Veeco, Digital Instruments, USA) in contact mode equipped with a Si_3N_4 tip with a J scanner at a scan rate of 1.5 Hz. SEM investigation was performed with a JEOL 5610.

Nanofabrication

Particle attachment was performed using a suspension of either 60 nm CD-functionalized silica particles or 2.8 nm CD-functionalized Au nanoparticles. In the case of Au nanoparticles, the sample is immersed in an aqueous solution of adamantyl-terminated dendrimers (1 mM in Ad groups) for 10 min, then rinsed thoroughly with an aqueous CD solution (pH = 2) and water. The substrate was then immersed in an aqueous solution of 2.8 nm CD-functionalized Au nanoparticles for 10 min and rinsed thoroughly with water. This was repeated up to 15 bilayers. There was no drying step in between. At the end of the assembly process, samples were blown dry in a N_2 flow.

In the case of silica nanoparticles, a vertical deposition set-up was used. The vertical deposition set-up consisted of a step motor (RS instruments, Code 191-8334) driven by a control card (RS instruments, GSM2 unipolar stepper motor driver). A gear box is attached to the motor to decrease the number of rpm (RS instruments 641:1). The withdrawal speed can be varied over a range of 0.1 μm/s up to several μm/s. The whole apparatus was placed in a closed box to protect the experiment from air drafts. The substrates were not rinsed afterwards. For the experiments described here, the nanoparticle concentration was kept constant (2.8 w%) and the withdrawal speed modified from 0.25 to 1 μm/s. When necessary, the PMMA template was removed in acetone and ultrasound during 10 s.

6.5 References

[1] G. M. Whitesides, B. Grzybowski, *Science* **2002**, *295*, 2418.
[2] A. Ulman, *Organic Thin Films and Surfaces: Directions for the Nineties* Volume 20 Edited Polytechnic University, Brooklyn. Academic Press: San Diego. 1995.
[3] D. Wang, A. L. Rogach, F. Caruso**,** *Nano Lett*. **2002**, *2*, 857.
[4] G. Decher, *Science* **1997**, *277*, 1232.
[5] C. Lin, C. R. Kagan, *J. Am. Chem. Soc.* **2003**, *125*, 336.
[6] S. Jaffar, K. T. Nam, A. Khademhosseini, J. Xing, R. S. Langer, A. M. Belcher, *Nano Lett*. **2004**, *4*, 1421.
[7] G. M. Lowman, S. L. Nelson, S. M. Graves, G. F. Strouse, S. K. Buratto, *Langmuir* **2004**, *20*, 2057.
[8] N. Tretreault, A. C. Arsenault, A. Mihi, S. Wong, V. Kitaev, I. Manners, H. Miguez, G. A. Ozin, *Adv. Mater.* **2005**, *17*, 1912.
[9] V. C. Sundar, H. J. Eisler, T. Deng, Y. Chan, E. L. Thomas, M. G. Bawendi, *Adv. Mater.* **2004**, *16*, 2137.
[10] J. Feng, B. Wang, C. Gao, J. Shen, *Adv. Mater.* **2004**, *16*, 1940.
[11] J. Park, P. T. Hammond, *Adv. Mater.* **2004**, *16*, 520.
[12] H. Zheng, M. F. Rubner, P. T. Hammond, *Langmuir* **2002**, *18*, 4505.
[13] F. Hua, J. Shi, Y. Lvov, T. Cui, *Nano Lett.* **2002**, *2*, 1219.
[14] S. Liu, R. Maoz, G. Schmidt, J. Sagiv, *Nano Lett*. **2002**, *2*, 1055.
[15] S. W. Lee, R. G. Sanedrin, B. K. Oh, C. A. Mirkin, *Adv. Mater.* **2005**, *17*, 2749.
[16] F. A. Denis, A. Pallandre, B. Nysten, A. Jonas, C. Dupont-Gillain, *Small* **2005**, *10*, 984.
[17] A. Pallandre, A. Moussa, B. Nysten, A. Jonas, *Adv. Mat.* **2006**, *18*, 481.
[18] O. Crespo-Biel, B. Dordi, D. N. Reinhoudt, J. Huskens, *J. Am. Chem. Soc.* **2005**, *127*, 7594.

[19] O. Crespo-Biel, B. Dordi, P. Maury, M. Peter, D. N. Reinhoudt, J. Huskens, *Chem. Mater*. **2006**, *18*, 2545.
[20] S. Onclin, A. Mulder, J. Huskens, B. J. RavooD. N. Reinhoudt, *Langmuir* **2004**, *20*, 5460.
[21] O. Crespo-Biel, A. Jukovic, M. Karlsson, D. N. Reinhoudt, J. Huskens, *Isr. J. Chem.* **2005**, *45*, 353.
[22] V. Mahalingam, S. Onclin, M. Péter, B. J. Ravoo, J. Huskens, D. N. Reinhoudt, *Langmuir* **2004**, *20*, 11756.
[23] J. J. Michels, M. W. P. L. Baars, E. W. Meijer, J. Huskens, D. N. Reinhoudt, *J. Chem. Soc.Perkin Trans.* **2000**, *2*, 1914.
[24] H. J. Whitlow, M. L. Ng, V. Auzelyte, I. Maximov, L. Montelius, J. A van Kan, A. A Bettiol, F. Watt, *Nanotechnology* **2004**, *15*, 24.
[25] P. Maury, M. Escalante, M. Péter, D. N. Reinhoudt, J. Huskens, *Adv. Mater.* **2005,** 17, 2718.
[26] Y. Xia, Y. Yin, Y. Lu, J. McLellan, *Adv. Funct. Mater*. **2003**, *13*, 907.
[27] Y. N. Xia, G. M. Whitesides, *Angew. Chem. Int. Ed.* **1998,** *37*, 551.

Chapter 7

Creating Nanopatterns of His-Tagged Proteins on Surfaces through Specific NiNTA-Histidine Interactions and Nanoimprint Lithography

7.1 Introduction

Practical technological applications of biology are being developed owing to nanotechnology.[1] For instance, integration of proteins into devices may find application in biosensors, screening tools, bio-MEMS, tissue engineering and fundamental cell biology.[2,3] The advantages added by nanotechnology are that minimal amounts of analytes and products are needed as compared to current techniques and the associated cost reduction. In addition, these techniques will lead to an increase of the throughput of protein chips and their availability, enabling to enhance analysis speed which is particularly important for genomics applications. The requirements for the production of protein arrays are accurate spatial localization, specific adsorption of the selected proteins, negligible non-specific adsorption of other components, controlled orientation of the proteins, and no denaturation of the protein.[4] This is why most of the techniques require a top-down approach to create the pattern and a bottom-up approach to enable selective anchoring of proteins.

In this type of approach, self-assembly is a popular tool to add the anchoring elements because it is easy to apply and because of the possibility to tune the functionality of the created self-assembled of monolayer (SAM) by modifying its end-group.[5]

There are different ways to obtain a SAM pattern. In microcontact printing (μCP) and dip-pen nanolithography (DPN), [6] the SAM is formed directly on a surface, typically using thiols on a gold substrate. In the molecular assembly patterning by lift-off (MAPL),[7,8] a polymer pattern is used as a mask for forming SAMs. The polymer pattern can be used directly or indirectly for attachment of proteins. In the indirect approach, the polymer is removed and a protein-resistant layer such as poly(ethylene glycol) (PEG) is formed on the areas previously covered by the polymer in order to create a chemical pattern. In general, SiO_2 substrates are employed in this method.

Several types of interactions for binding the proteins can be used such as electrostatic,[9] covalent[10] and supramolecular.[11] The advantage of the supramolecular interaction is that the proteins are attached via specific binding sites that allow control of their attachment, reversibility and orientation. For instance, the case of *N*-nitrilotriacetic acid (NTA) is particularly interesting because it allows specific and reversible binding of His-tagged proteins. This technique is widely used to purify proteins. NTA is complexed with a metal ion (Ni^{II} or Co^{II}) that allows binding of the proteins functionalized with an oligo- histidine group. Dissociation of the proteins attached by means of (M)NTA-His-tag interactions can be induced by releasing the chelate complex using EDTA or by using a competitive agent such as histidine or imidazole. Tampé et al. have developed this approach on gold surfaces via μCP.[12] The advantages of this approach are control over the protein orientation, prevention of non-specific binding of other proteins, and substrate regeneration by reversing the interaction.

Nevertheless, this method is limited to NTA thiols on Au substrates that are not compatible with semiconductor industry processing. Moreover, μCP is limited to micrometer patterns.In the approach presented in this chapter, His-tagged protein arrays are produced using a new process to form NTA layers covalently attached on SiO_2 and patterned using nanoimprint lithography (NIL). NIL is a high resolution (5 nm has been reported), high throughput and low-cost nanolithography technique.[13] The polymer pattern can be kept until protein attachment or removed before in order to create a chemical pattern with a protein-resisting layer such as PEG. The chemical patterning method is very useful in the case the desired protein cannot stand organic solvents required for lift-off. The firm covalent attachment of NTA on the substrate permits easier regeneration. This process allows integration of proteins into devices, since it can be performed on e.g. the native oxide of Si as well.

As described in this chapter, proteins were attached to topographical and chemical patterns using electrostatic interactions in order to study the behavior of the proteins under the processing conditions required for attachment. Protein patterns were characterized by AFM and fluorescence microscopy. A new method to form NTA SAMs on SiO_2 using a multistep covalent process is described as well as patterning of the NTA SAM using NIL. Resulting layers have been characterized using contact angle goniometry, ellipsometry, XPS, and AFM. Topographical templates with NTA patterns and chemical templates functionalized with resisting-protein fluoroalkyl or PEG SAM and an NTA SAM have been prepared. They were both used as templates for His-tagged DsRed protein attachment. The specific attachment was revealed by AFM and fluorescence microscopy. Reattachment of a different type of protein after regeneration of the substrates using imidazole was shown by fluorescence microscopy.

7.2 Results and discussion

7.2.1 Patterning DsRed using electrostatic interactions

The DsRed protein is a derivative of the green fluorescent protein (GFP) from the jelly fish *Aequorea Victoria*. As all the GFPs, DsRed is a popular protein label and marker of gene expression owing to its fluorescent properties and robustness. DsRed is a relatively small protein of 25-30 kDa mass and a size of 5 × 6 nm. The DsRed derivative used here has a histidine tag and its surface is negatively charged.

Polymer templates were created by NIL on PMMA/SiO_2 substrates followed by residual layer removal. An aminoalkyl SAM was chosen to form a positively charged area in order to attach electrostatically the DsRed protein. The polymer template was used as a mask for formation of the patterned aminoalkyl SAM. Two configurations were investigated: (i) a polymer template with an aminoalkyl SAM in the vacant areas, see Scheme 1 path A, and (ii) a chemical template with an aminoalkyl SAM pattern, the other part of the pattern being filled with a protein-resistant, fluoroalkyl or PEG SAM, see Scheme 1 path B1 and B2. The two types of chemical patterns used here were produced in the following way: (i) a fluoroalkyl SAM was formed, then the polymer was removed, and an aminoalkyl SAM was formed (B2), (ii) an aminoalkyl SAM was formed, then the polymer was removed, and a PEG layer was formed (B1). The PEG layer was formed after the aminoalkyl SAM to prevent reaction of the methoxysilyl group with the oxygen group from the PEG in the case when the order of the steps is inverted.

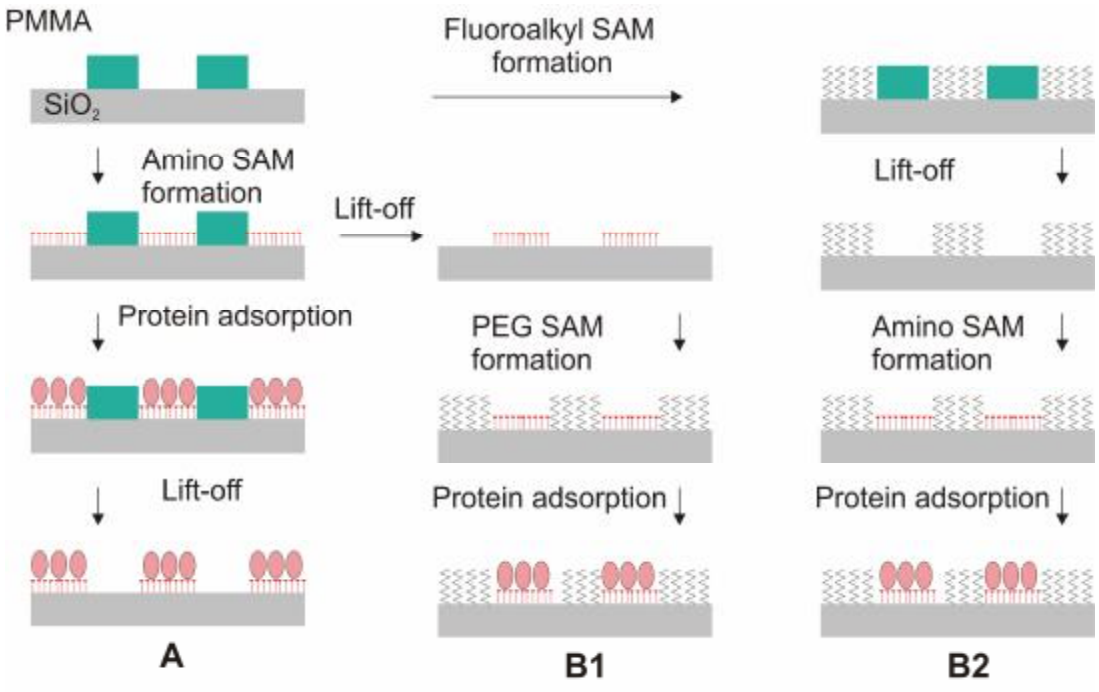

Scheme 1. *Schematic representation of protein attachment on (A) a topographical template with an aminoalkyl SAM functionalization and (B) chemical templates formed by amino alkyl and protein-resistant SAMs (PEG, B1 or fluoroalkyl SAMs, B2).*

Protonation of the aminoalkyl monolayer was performed by rinsing the sample with a MES buffer (pH = 5.6). DsRed proteins were adsorbed on the various types of substrates, topographical and chemical templates, by immersion for 20 min in an aqueous solution of DsRed (100 mM tris-HCl, pH=7.5). Samples were rinsed with 100 mM Tris buffer and dried in a N_2 flow. In the case of topographical templates, PMMA was removed by rinsing with acetone and drying in a N_2 flow.

Figures 1a and b show AFM images of DsRed attached on an aminoalkyl SAM formed on a NIL-patterned substrate on 5 μm and on 700 nm lines and their profiles after subsequent removal of the polymer. The height measured on the 5 μm and 700 nm lines is 6 nm.

This value corresponds to the size of the DsRed protein (5 nm diameter, 6 nm height), taking into account the 0.9 nm of the aminoalkyl SAM. The proteins seem to attach to the aminoalkyl SAM areas with some inhomogeneities. Nevertheless, the areas corresponding to the areas previously covered by the polymer appear free from protein and the edges are well defined.

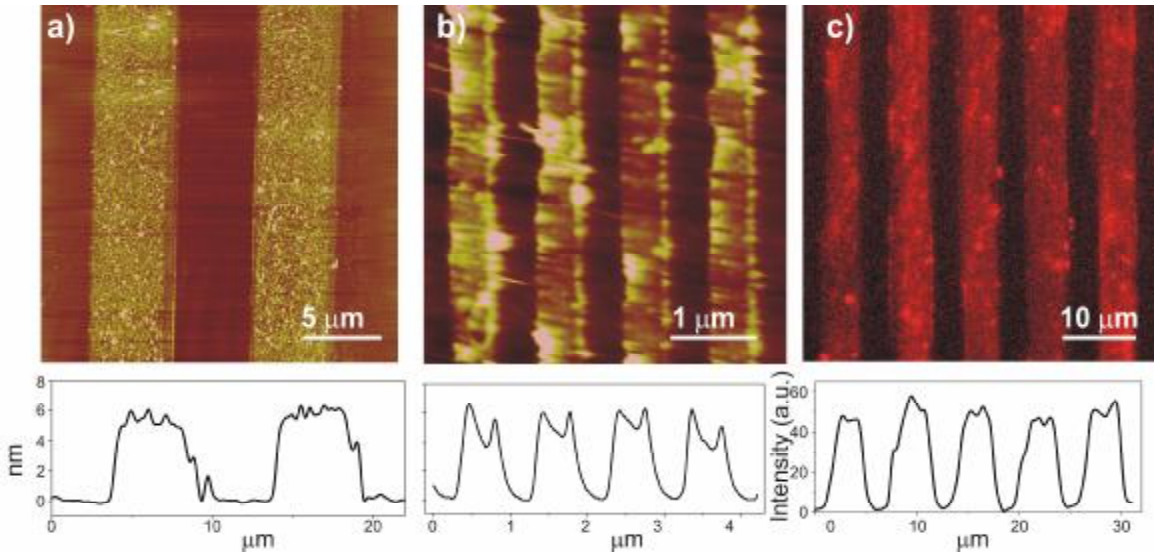

Figure 1. *AFM (a,b) and fluorescence microscopy (c) images of DsRed proteins attached on 5 mm (a,c) and (b) 700 nm aminoalkyl SAM lines patterned using NIL. The polymer was removed after protein attachment by lift-off in acetone.*

Figure 1c depicts a fluorescence micrograph on 5 μm patterned aminoalkyl SAM lines after DsRed protein adsorption and polymer removal, and its intensity profile. After polymer removal, fluorescence was observed only on the parts corresponding to the aminoalkyl SAM. The parts corresponding to the areas previously covered by PMMA were dark. Apparently, the proteins stand the process of polymer removal as they are still fluorescent. The profile shows the intensity corresponding to one layer of proteins as deducted from the AFM profile. Again, some homogeneities are observed, in line with the AFM data.

Alternatively, DsRed adsorption was performed on substrates patterned with two adsorbates (Scheme 1, path B). For the first configuration, a fluoroalkyl and an aminoalkyl SAM were patterned (path B2).

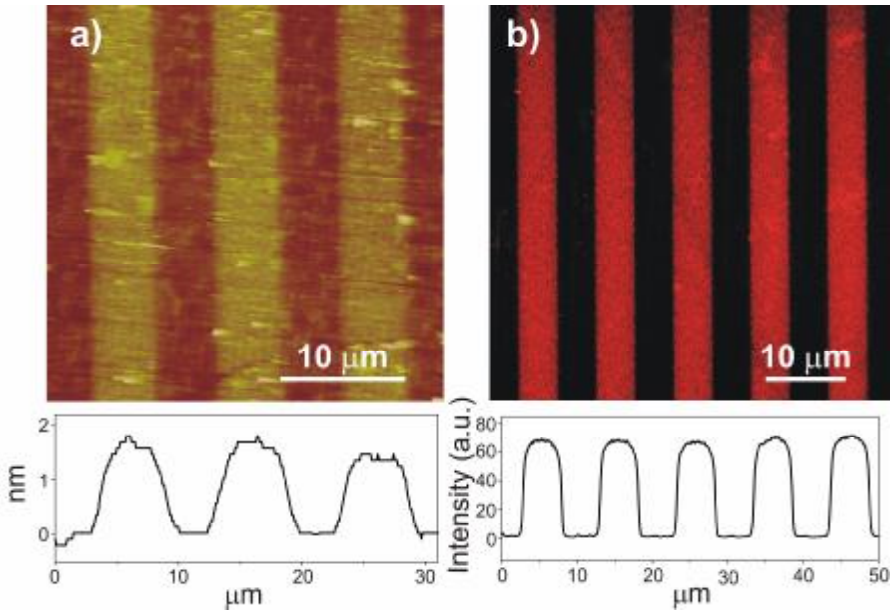

Figure 2. *AFM (a) and fluorescence microscopy (b) images of DsRed protein attached on chemical templates formed by 5mm aminoalkyl and 5mm fluoroalkyl SAM lines patterned using NIL.*

Figure 2 shows AFM and fluorescence microscopy images of DsRed adsorbed on 5 μm aminoalkyl and 5 μm fluoroalkyl SAM lines. The height difference beween the amino and fluoroalkyl SAMs is 2.3 nm. After protein adsorption, the height difference between the lines is 1.9 nm. This value corresponds to an adsorbed layer of 4.2 nm which is of the same order of magnitude as the height of the protein layer. The pattern can be clearly seen by AFM. Fluorescence can be detected only on the areas corresponding to the aminoalkyl SAM. Proteins apparently attached with high selectivity on the aminoalkyl SAM while the parts corresponding to the fluoroalkyl SAM appear dark and free from proteins.

For the second configuration of a chemical pattern (scheme 1 path B), a PEG SAM was formed from solution onto an amino-patterned SAM substrate during two hours. The sample was thoroughly rinsed with toluene, ethanol and water to remove the physisorbed components. Figure 3 shows AFM images of (a) a chemical pattern formed by 5 μm aminoalkyl SAM and 5 μm PEG SAM lines, (b) DsRed attached on the chemical substrate and their profiles, and (c) a fluorescence microscopy image of the chemical template after DsRed protein attachment and its profile. The PEG SAM is 1.3 nm higher than the amino SAM due to its longer chain. After DsRed protein attachment, the height difference is 2.7 nm, which indicates to a height increase of 4 nm on the amino areas, which corresponds to the height of a single layer of proteins. In the fluorescence image, the parts corresponding to the PEG SAM appear clean of DsRed. DsRed protein matched closely the dimensions of the aminoalkyl SAM areas, as can be noticed because the line edges are well defined. DsRed attached with high selectivity on the aminoalkyl SAM with respect to the PEG SAM. The fluorescence was measured on the same sample as the one measured by AFM, having a thickness of the same order of magnitude as one protein.

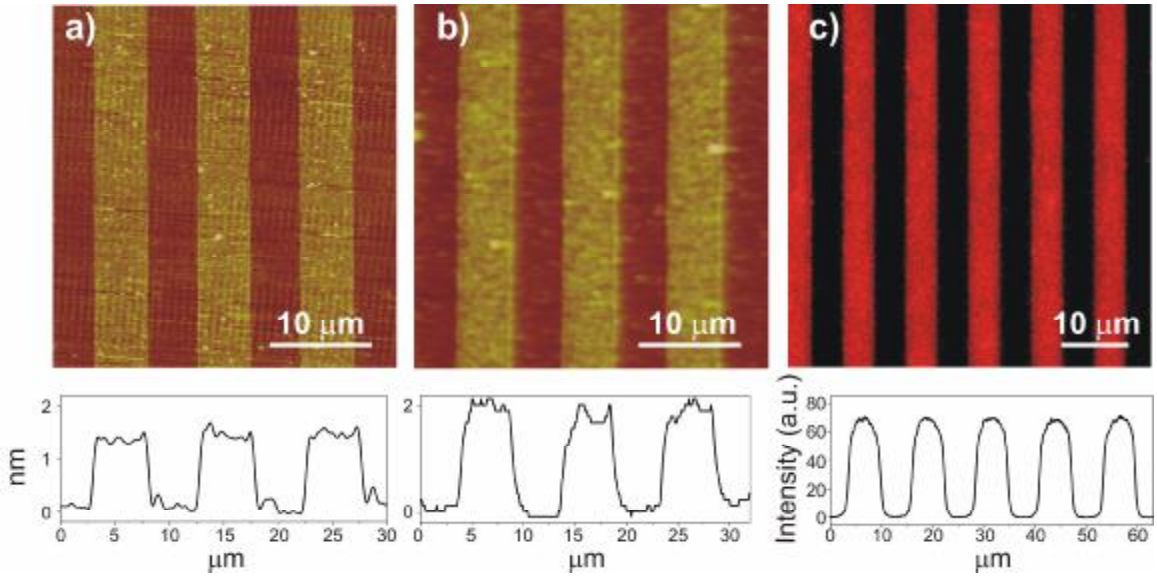

Figure 3. *AFM (a,b) and fluorescence microscopy (c) images of (a) a chemical template formed by 5 mm aminoalkyl and 5 mm PEG SAM lines patterned using NIL, and (b,c) the same sample after DsRed attachment*.

The fluoroalkyl and PEG SAMs showed equal protein-resistant properties. DsRed attached with high selectivity on the aminoalkyl SAM areas with respect to the protein-resistant SAMs, as can be seen from the fluorescence images. The main advantages of chemical patterning over the topographical template patterning of protein is that no organic solvent is needed that could denature the proteins. Probably this is the reason why the images obtained for the chemical templates look more homogeneous than the one obtained for the topographical templates, as shown above by AFM as well as fluorescence microscopy.

7.2.2 Patterned proteins using NTA-His-tagged protein interactions

NiNTA monolayers on SiO_2 substrates were fabricated in order to immobilize DsRed via its His-tag functionalization. SAMs were formed using a similar procedure as described for CD SAMs in Chapter 5 consisting of a multistep covalent process. The process is depicted in Scheme 2A. An aminosilane formed from the gas phase on the SiO_2 substrate was reacted with 1,4-phenylene diisothiocyanate (DITC). The reaction was performed by immersion in an ethanol solution at 40 ºC for 2 h. Samples were rinsed thoroughly with ethanol and water and dried in a N_2 flow. Attachment of *N,N*-bis(carboxymethyl)-L-lysine was performed by immersion in a aqueous solution for 30 min. Samples were rinsed thoroughly with water and dried in a N_2 flow. Finally the samples were immersed for 20 min in an aqueous $NiCl_2$ solution.

Samples were characterized after each step of the procedure using contact angle goniometry, ellipsometry and X-ray photoelectron spectroscopy (XPS), starting with non-patterned layers. The results are reported in Table 1.

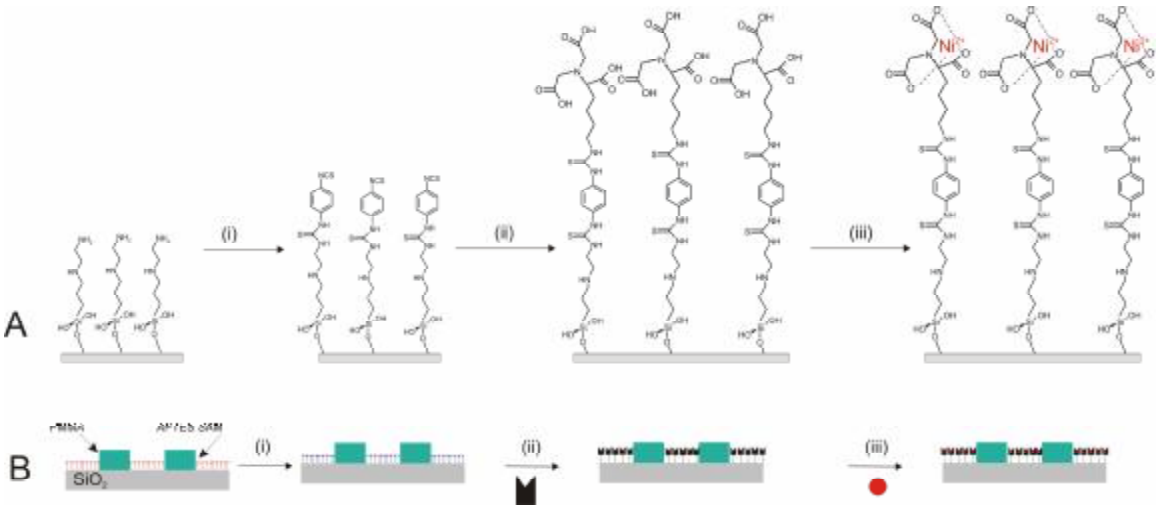

Scheme 2. *Schematic representation of the preparation of (A) NiNTA monolayer on SiO_2: (i) DITC, ethanol, 40ºC (ii) N,N-bis(Carboxymethyl)-l-lysine , water (iii) $Ni^{2+}Cl_2$, water and (B) patterned NTA SAM using NIL-patterned PMMA as a template.*

The advancing contact angle increased after the reaction with DITC which is expected for an isothiocyanate-terminated SAM.[26] After attachment of N,N-bis(Carboxymethyl)-l-lysine, the contact angle diminished to 50°. This reduction of the contact angle is a result of the hydrophilic nature of the carboxylic acid groups present at the NTA layer. The height of the assembly increased after each step, as recorded by ellipsometry because of the covalent attachment of 1,4-phenylene diisothiocyanate and N,N-bis(Carboxymethyl)-l-lysine. Ellipsometry measurements gave a final height of 3.2 nm that corresponds to a NTA layer thickness. Sulfur was detected on the layer after the reaction with DITC as recorded by XPS. XPS also showed an increase of the C/N ratio after each reaction, in qualitative agreement with the theoretically expected trends.

Table 1. *Advancing and receding water contact angles, selected XPS data and ellipsometric thicknesses obtained from non-patterned SAMs;AFM thicknesses were measured by contact mode AFM on patterned SAMs.*

	NH_2	**SCN**	**Ni**NTA
Contact angle (Adv/Rec)	65/45	80/47	50/38
C/N (calc.) C/N (exp.) S Ni	2.5 2.7 0 Not meas.	3.3 4.0 1.0 Not meas.	4.0 5.2 0 1.3
Ell. thickness (nm)	1.0	1.2	3.2
AFM height (nm)	0.85	0.85	2.1

Nanoimprint lithography was performed on silicon substrates after cleaning and oxidation in piranha and spin coating of PMMA. Patterning SAMs on SiO_2 using NIL was previously demonstrated.[14] An NTA layer was formed on the uncovered areas of the imprinted sample following the methodology described above and schematically shown in Scheme 2 B. The PMMA template was removed using acetone and ultrasonication for 2 h.

The patterned monolayers resulting after PMMA removal were characterized using AFM and XPS imaging. Figures 4 a and b show AFM images of 400 nm lines, 1 µm period of isothiocyanate and NTA SAMs, respectively. The AFM height measurements are reported in Table 1. The height measured on the isothiocyanate layer corresponds to the expected value. After NTA attachment, an increase of 1.25 nm was measured. The total NTA layer height of 2.1 nm corresponds to the theoretical value, taking the structure into account. An indication of the stability of the NTA SAM patterns was obtained after observing that these patterns were able to withstand ultrasonication. XPS elemental spectra were made inside and outside the patterned NTA layer, see Figure 5. C and N element are visible inside the pattern, indicating the formation of the NTA layer. The presence of Ni was detected in the patterns as well.

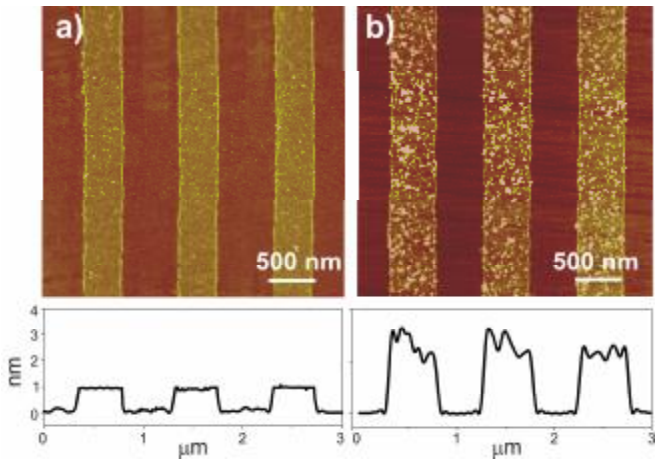

Figure 4. *AFM images of patterned isothiocyanate and NTA SAMs.The polymer was removed afterwards.*

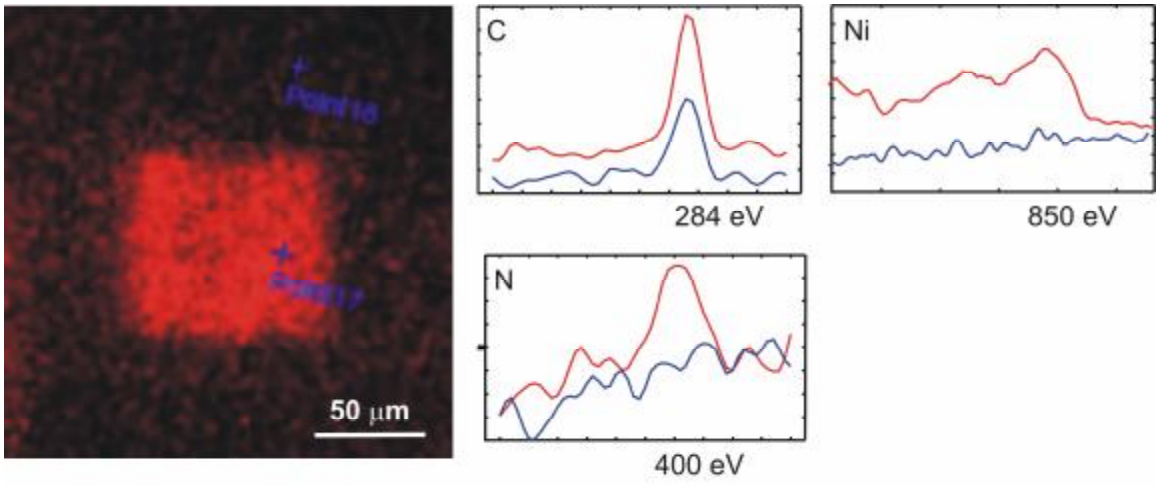

Figure 5. *XPS mapping of a 100 mm square with an NTA layer inside, as prepared by NIL, NTA SAM formation and lift-off, and three partial spectra (C, N and Ni) made inside (red) and outside (blue) the square.*

7.2.3 Directed assembly of His-tagged proteins using specific NiNTA-Histidine interactions

Two types of sample were used for the directed assembly of His-tagged proteins: i) a topographical template with a NiNTA functionalization, and ii) a chemical template with patterned fluoroalkyl and NiNTA SAMs, see Scheme 3. The His-tagged protein DsRed was attached to the substrates by immersing the samples for 20 min in an aqueous 10^{-5} M DsRed solution (Tris buffer, pH=8.5). After adsorption, the samples were rinsed thoroughly with 100 mM Tris buffer to remove any physisorbed material and dried in a N_2 flow. The PMMA was removed by rinsing with hot water (50 °C) and harsh drying with N_2. This method was chosen in order to prevent the use of organic solvents that could affect the NiNTA-His-tagged protein interaction.

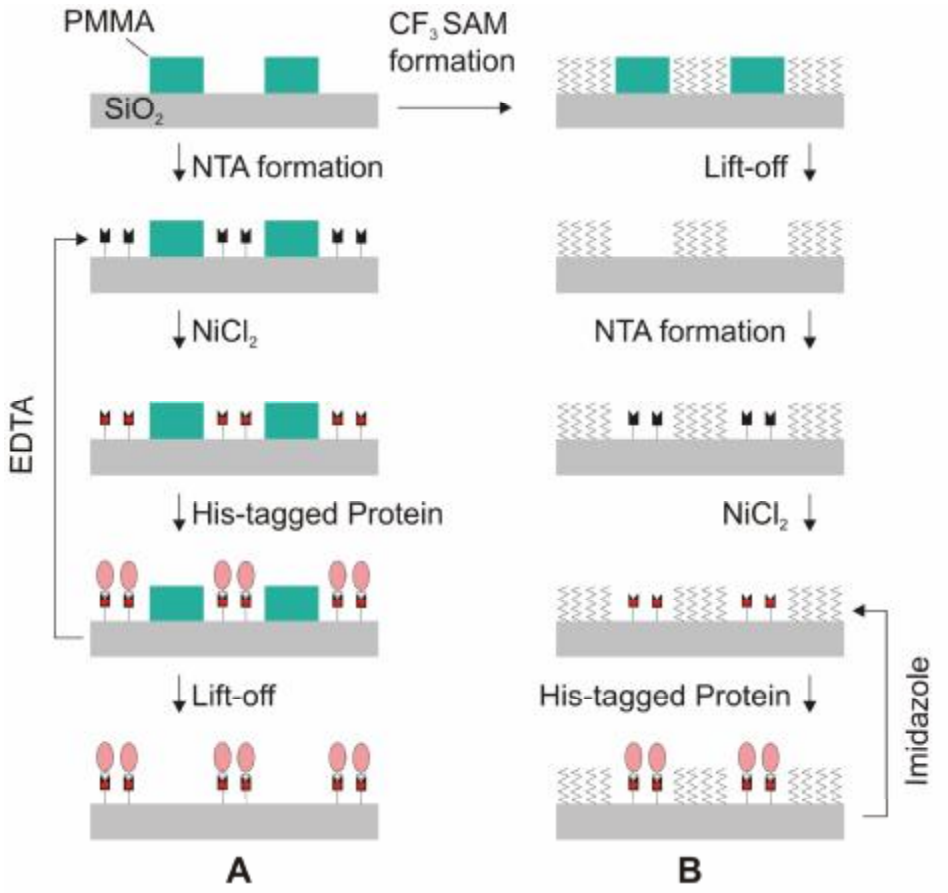

Scheme 3. *Schematic representation of the (A) topographically and (B) chemically patterned NTA and its application to immobilize His-tagged proteins.*

Figures 6a and b depict AFM and fluorescence microscopy images of patterned NTA layers after DsRed adsorption and polymer removal as well as their height and intensity profiles. The measured height is on average 10 nm and it is approximately equal to the size of a DsRed protein attached onto an NTA layer. The height corresponds again to attachment of a single layer of proteins. The edges of the lines are well defined. Fluorescence is observed only in the parts corresponding to the NTA monolayer. The parts corresponding to the areas previously covered by PMMA are clean and appear dark.

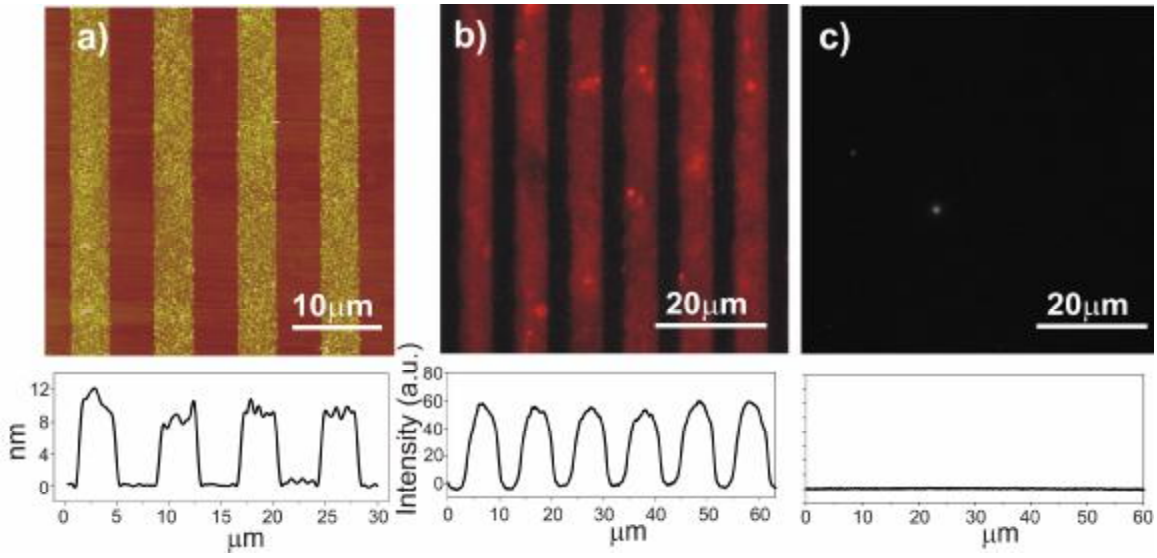

Figure 6. *AFM (a) and fluorescence microscopy (b,c) images of (a,b) His-tagged DsRed attached to patterned NiNTA followed by polymer lift-off, and of (c) the substrate after His-tagged DsRed attachment followed by, rinsing of the sample with EDTA and polymer lift-off.*

After protein adsorption, a sample was immersed in 1 mM EDTA solution (pH=8) in order to desorb the Ni^{2+} and the protein from the NTA layer, followed by the removal of the polymer (Figure 6c). No fluorescence was detected which indicates the absence of proteins on the sample. This result shows that the binding of the proteins is reversible, and thus results from the specific NiNTA-His-tag binding.

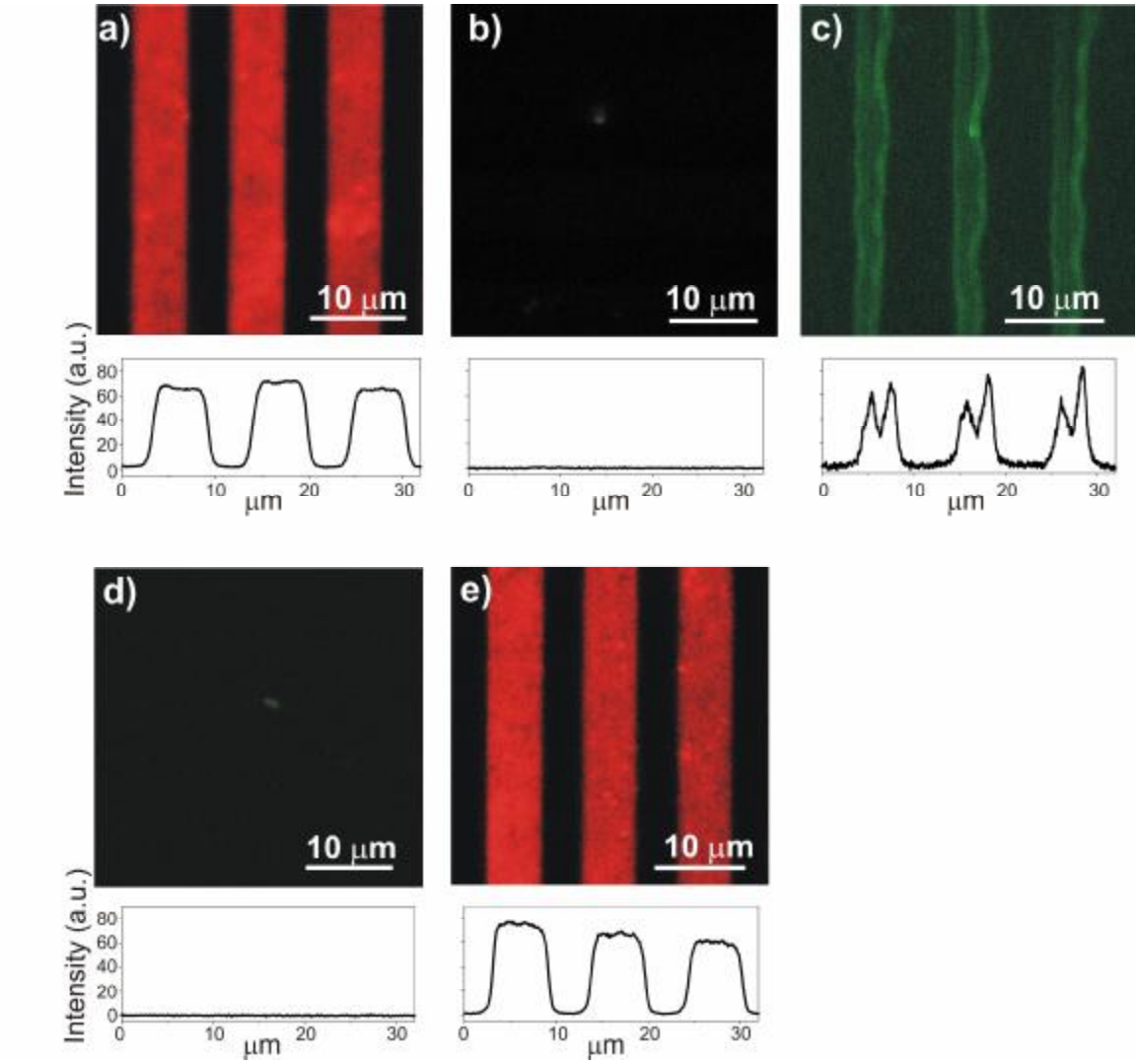

Figure 7. *Consecutive fluorescence microscopy images of His-tagged proteins successively attached on a chemical pattern made of NiNTA and fluoroalkyl SAMs after rinsing the substrate to regenerate the NTA arrays. (a, e) substrate after DsRed attachment, (c) after EGFP attachment, (b, d) sample after rinsing with imidazole.*

Another experiment was performed using a chemical pattern formed by (Ni) NTA and fluoroalkyl SAMs to test the regeneration of the NTA array. First DsRed was immobilized on the sample. The sample was then rinsed with imidazole (300mM) which is commonly used to compete with the NiNTA-His-tag interaction to strip the selectively bound protein from NiNTA surface.

The substrate was used to attach another His-tagged protein (EGFP), from the same family than DsRED, eg Green Fluorescent Protein (GFP), but with another emission spectrum. EGFP protein was subsequently immobilized onto the same sample. This protein was removed as well using imidazole. Finally, DsRed was immobilized again on the sample. Figure 7 shows the consecutive fluorescence microscopy images of the sample after three successive steps of protein immobilization (a, c, e) as well as after protein removal using imidazole. Both DsRed and EGFP attached selectively on the NiNTA layers with respect to the fluoroalkyl SAM, where no proteins can be seen by fluorescence imaging. After rinsing with imidazole, no fluorescence was observed on the entire surface, showing complete removal of the His-tagged proteins from the sample in both cases.

This series of experiments shows: (i) the excellent specificity for binding His-tagged proteins to Ni-NTA SAMs, and (ii) the convenient regeneration of the NiNTA SAM. The latter is confirmed by the equal fluorescence intensities observed for the adsorption of DsRED (Figures 7 a and e), which shows that the Ni^{2+} is retained on the NTA SAMs after rinsing with imidazole.

7.3 Conclusions

Directing proteins attachment on topographical templates with a chemical functionalization and on chemical patterns through electrostatic interactions was demonstrated. Proteins attached with high selectivity on the positively charged areas of the samples. The protein layer was one protein thick. Nevertheless control over the interaction strength and the protein orientation is rather poor. Formation of an NTA SAM on SiO_2 has been demonstrated using a multistep covalent process. The NTA was successfully patterned using nanoimprint lithography. Two types of substrates were made, one keeping the topographical template and another creating a chemical template with a protein-resistant SAM and an NTA functionalization. Both substrates were shown to be adequate for His-tagged protein attachment. The protein was immobilized specifically through the Histidine tag. Regeneration of the chemical substrate was demonstrated by attaching a different His-tagged protein. This approach is very promising for protein chip fabrication. It allows to integrate proteins using semiconductor technology and to control their positioning via a supramolecular interaction. Owing to regeneration such chips can be reused.

7.4 Experimental Section

Compounds

N-[3-(trimethoxysilyl)propyl]-ethylenediamine (Aldrich), 1,4-phenylene diisothiocyanate (Acros), 1H,1H,2H,2H-perfluorodecyltrichlorosilane (ABCR), *N,N*-bis(carboxymethyl)-L-Lysine (Aldrich) and PMMA (MW 350 kD, Aldrich) were used as such. Ethylene diaminotetraacid was provided by Acros and nickel chloride by Aldrich. Imidazole is a commercial product, from FLUKA, 99.5%

The Fluorescent Timer mutant of DsRed was produced by standard site-directed mutagenesis approaches as reported previously.[15] The PCR product was cloned into pQE-30/BamHI/Hind III vector. Escherichia coli JM101 cells were transformed with the plasmid. The expression of 6His-tagged Fluorescent Timer was induced by 1 mM IPTG for various lengths of time (3–24 h). To purify Fluorescent Timer-6His the clarified cell lysate was adsorbed on Nickel-NTA agarose (Qiagen, Hilden, Germany) overnight at 4 °C, and the protein was eluted with 250 mM imidazole. The eluted fractions were dialyzed against 100 mM Tris-HCl, pH 8.5, 100 mM NaCl overnight.

EGFP mutants were produced by standard procedure. Briefly, recombinant protein expression in E.coli was induced by IPTG, after which the collected cells were lysed. For purification of the clarified cell extract successively a Heparin-Sepharose, a Phosphocellulose and a Ni-NTA column were used. Protein fractions at each stage during production and purification were analyzed by standard SDS-PAGE.

Analysis

The quality and reproducibility of the monolayer formation were investigated by water contact-angle goniometry, ellipsometry, AFM, and XPS. Contact angles were determined using a Krüss Contact Angle Measurement System G 10, and the data processed with the program Drop Shape Analysis 1.51. XPS was performed using a PHI Quantera Scanning ESCA Microprobe. Samples were investigated using an atomic force microscope AFM Nanoscope III (Veeco, Digital Instruments, USA) in contact mode equipped with a Si_3N_4 tip with a J scanner at a scan rate of 1.5 Hz.

NTA layer formation and protein immobilization

Fabrication of patterned sample using nanoimprint is made following same process explained in Chapter 3. The gas-phase evaporation of aminosilanes was performed in a desiccator under vacuum. The samples were left several hours or overnight and then carefully rinsed with ethanol and Millipore water. The attachment of 1,4-phenylene diisothiocyanate was made in a 0.1 M solution in ethanol at 40 ºC during 2 h. Samples were thoroughly rinsed with ethanol and dried in a N_2 flow. The NTA layer attachment was made during 30 min in an aqueous 0.5 mM N,N-Bis(Carboxymethyl)-L-Lysine solution (pH = 8). Samples were thoroughly rinsed with water and dried in a N_2 flow. Samples were immersed in a 1 mM solution (pH = 5) to allow absorption of Ni^{2+} on the NTA SAM, during 20 min and dried in a N_2 flow. The adsorption of the proteins was performed by immersing the sample in a 0.4 μM solution in Tris-HCl buffer of DsRed or EGFP for 20 min. The sample was rinsed thoroughly with a 100 mM tris-HCl buffer solution (pH = 8.5) to remove the physisorbed material. The regeneration of the sample was made by two ways: the sample was immersed in a 1 mM EDTA solution (pH = 8) to remove the Ni from the NTA, during 20 min. The samples are dried in a N_2 flow afterwards. Another way was to remove the proteins from the substrate by rinsing with 300 mM imidazole (pH = 8) that behaves as a competitive agent. The samples are dried in a N_2 flow afterwards.

7.5 References

[1] H. Klefenz, *Eng. Life. Sci.* **2004**, *4*, 211.
[2] G. M. Whitesides, E. Ostuni, S. Takayama, X. Y. Jiang, D. E. Ingber, *Annu. Rev. Biomed. Eng.* **2001,** *3*, 335.
[3] T. H. Park, M. L. Shuler, *Biotechnol. Prog.* **2003,** *29*, 243.
[4] Y. Ito, *Biotechnol. Prog.* **2006,** *22*, 924.
[5] R. G. Chapman, E. Ostuni, S. Takayama, R.E. Homlin, L. Yan, G. M. Whitesides, *J. Am. Chem. Soc.* **2000,** *122*, 8030.
[6] S. F. Kingsmore, *Nat. Rev. Drug Discov.* **2006,** *5*, 310 .
[7] D. Falconner, A. Koenig, F. Assi, M. Textor, *Adv. Funct. Mater.* **2004,** *14*, 749.
[8] J. D. Hoff, L. Cheng, E. Meyhofer, L. J. Guo, A. J. Hunt, *Nano Lett.* **2004**, *4*, 853.
[9] G. MacBeath, S. L. Schreiber, *Science* **2000**, *289*, 1760.
[10] S. Lofas, B. Johnson, *Chem. Commun.* **1990,** 1526.
[11] R. N. Orth, T. G. Clark, H. G. Craighead, *Biomed. Microdev.* **2003,** *5*, 29.
[12] G. Klenkar, R. Valiokas, I. Lundstrom, A. Tinazli, R. Tampe, J. Piehler, B. Liedberg, *Anal. Chem.* **2006**, *78*, 3643.
[13] S. Y. Chou, P. R. Krauss, P. J. Renstrom, *Science* **1996**, *272*, 85.
[14] P. Maury, M. Péter, V. Mahalingam, D. N. Reinhoudt, J. Huskens, *Adv. Funct. Mater.* **2005,** *15*, 451.
[15] A. Terskikh, A. Fradkov, G. Ermakova, A. Zaraisky, P. Tan, A. Kajava, X. Zhao, S. Lukyanov, M. Matz, S. Kim, I. Weissman, P. Siebert, S*cience*, **2000**, *290,* 1585.

Summary

Nanoimprint lithography (NIL) was used as a tool to pattern self-assembled monolayers (SAMs) on silicon substrates because of its ability to pattern in the micrometer and nanometer ranges. The resulting polymer template behaved as a physical barrier preventing the formation of a SAM in the covered areas of the substrate. After polymer removal, patterned SAM were obtained. The versatility of the method was shown in various nanofabrication schemes. Substrates were functionalized with a second type of silane adsorbate. Two types of substrates were thus made (i) topographical templates with a chemical functionalization and (ii) chemically patterned, topographically flat, substrates. Nano-objects such as molecules, nanoparticles and proteins were directed onto these two types of substrates. Two types of interactions were used to direct the assembly of these nano-objects namely electrostatic and supramolecular interactions. The advantage of supramolecular interactions is that the binding strength between the host and guest is known, the interaction is reversible and the attachment of the nano-object is made through a specific site, allowing control over the position of the nano-objects.

A literature survey was presented in Chapter 2 that described the different types of top-down and bottom-up techniques. The review focused on the combination of top-down and bottom-up techniques applied to the production of high-resolution features.

Functional devices that can be fabricated by a combination of top-down and bottom-up techniques were reviewed. Special attention was given to 3D photonic devices and protein arrays. The structures of these two types of devices are closely related to the structures fabricated in this thesis.

Chapter 3 described the preparation of patterned SAMs with different end group functionalities on SiO_2 using nanoimprint lithography. The patterned monolayer was characterized by AFM and XPS. SAM patterns with features down to 125 nm lines were produced. Chemically patterned substrates were prepared and characterized by AFM. Carboxylate-functionalized nanoparticles were attached by drop casting on topographical and chemically patterned substrates directed by the SAM end-group functionality. Characterization was performed by SEM. Attachment of particles on features down to 700 nm lines using a topographical template and 300 nm lines using chemically patterned templates was shown. Nevertheless, the packing was not satisfactory due to lack of control of the drying process.

In Chapter 4, the use of vertical deposition in order to attach particles with high order was demonstrated. The moving meniscus principle was employed by means of vertical deposition to control the drying rate of the solvent of the suspension. On topographical templates, nanoparticles attached with hexagonal close packing on the μm-sized features and with typical confined particle geometries on nm-sized features. The polymer template could be removed afterwards when using the silica nanoparticles. On chemically patterned substrates, nanoparticles attached with high density. Confined geometries were obtained as well. Patterned nanoparticles were used as shadow masks for further processes such as metal lift-off and Si etching.

Chapter 5 dealt with patterning of CD layers in a multistep process using nanoimprint lithography to create the polymer pattern. Patterned CD layers were characterized by AFM and XPS. After each step, AFM showed a height increase. XPS confirmed the presence of the elements contained in cyclodextrins. Fluorescence microscopy showed selective attachment of adamantyl-functionalized fluorescent molecules on patterned CD layers, using topographical templates and chemically patterned substrates.

In Chapter 6, patterning of supramolecular LBL assemblies making use of the patterned CD layers as a host was reported. Supramolecular LBL assemblies consisting of adamantyl-functionalized dendrimers and 2.8 nm Au CD-functionalized nanoparticles were directed onto CD patterned SAMs keeping the polymer template fabricated by nanoimprint lithography. Up to 15 bilayers were assembled and followed by polymer lift-off to reveal the LBL nanostructures. Features with lateral sizes down to 50 nm and a height of 20 nm were thus made. Supramolecular LBL assemblies consisting of adamantyl-functionalized dendrimers and 60 nm CD-functionalized SiO_2 nanoparticle were directed using vertical deposition in order to increase ordering and nanoparticles density. SEM was used to check the order and AFM to measure the increase in height after each bilayer. Up to three bilayers were formed using micrometer scale lateral feature sizes, with each layer of nanoparticles being densely packed. On the nm-scale, confined geometries were obtained for the first and second bilayers in lines down to 150 nm width. Single particle attachment was obtained in this way as well.

In addition to nanoparticles, proteins can also be assembled onto topographical and chemically patterned substrates. In Chapter 7, the directed assembly of DsRed using electrostatic interactions was shown.

The use of supramolecular interactions to direct DsRed employed the histidine functionalization of the DsRed protein and its specific interaction with NiNTA. To achieve this, NTA SAMs were patterned using NIL in a multistep process and characterized using AFM and XPS. Fluorescence microscopy was used to check the specific attachment of the proteins on the patterned NiNTA SAMs. The substrate could be regenerated by removing the Ni^{2+} ions using EDTA or a competitive agent. The regeneration of the patterned NTA was shown by three successive attachments of different proteins on the same substrate, rinsing the substrate with a competitive agent between the protein adsorption steps.

In conclusion, nanoimprint lithography and self-assembly of monolayers have been combined to produce SAM patterns with a resolution down to 50 nm. These patterns were employed as templates for the attachment of different nano-objects such as nanoparticles, LBL assemblies and proteins. Patterning of these nano-objects may serve potential applications such as photonic crystals, molecular electronics and protein chips. The process developed in this thesis indicates a promising route for the fabrication of such devices. Another extension of this research would be to study the behavior of the nano-objects patterns below 50 nm, where the size of the nano-object is commensurate to the one of the pattern and study its properties as compared to bulk material.

Abbreviations List

AFM: Atomic Force Microscop

EBL:electron-beam lithography

FIB: Focused Ion Beam

SEM: Scanning Electron Microscop

µCP: Microcontact Printing

NIL: Nanoimprint Lithography

PDMS: Poly(dimethylsiloxane)

PMMA: Poly(methylmethacrylate)

SAM: Self-assembly of Monolayers

LBL: Layer-by-Layer assembly

XPS: X-ray Photoelectronic spectroscopy

DPN: dip-pen nanolithography

CD: β-Cyclodextrin

Ni-NTA: Nickel N-nitrilotriacetic acid

NP: nanoparticle

His-Tag protein: Histidine tagged protein

RIE: Reactive Ion Etching

1D, 2D, 3D: one dimensional, two-dimensional.

PS: polystyrene

PEG: Polyethylene glycol

NSL: Nanosphere lithography